

CAPITAL UNIVERSITY OF SCIENCE AND  
TECHNOLOGY, ISLAMABAD



# Bandpass Sampling Methodology for Uniformly Spaced Multiband Energy-Sparse Spectrum

by

Tauqeer Ahmed

A thesis submitted in partial fulfillment for the  
degree of Doctor of Philosophy

in the

Faculty of Engineering

Department of Electrical Engineering

2019

# Bandpass Sampling Methodology for Uniformly Spaced, Multiband, Energy-Sparse Spectrum

By

Tauqeer Ahmed

(PE113003)

Prof. Dr. Muhammad Imran

Glasgow College UESTC, University of Glasgow, UK

Associate Professor Dr. Raheel Nawaz

Manchester Metropolitan University, All Saints, Manchester, UK

Dr. Noor Muhammad Khan

(Thesis Supervisor)

Dr. Noor Muhammad Khan

(Head, Department of Electrical Engineering)

Dr. Imtiaz Ahmed Taj

(Dean, Faculty of Engineering)

DEPARTMENT OF ELECTRICAL ENGINEERING  
CAPITAL UNIVERSITY OF SCIENCE AND TECHNOLOGY  
ISLAMABAD

2019

Copyright © 2019 by Tauqeer Ahmed

All rights reserved. No part of this thesis may be reproduced, distributed, or transmitted in any form or by any means, including photocopying, recording, or other electronic or mechanical methods, by any information storage and retrieval system without the prior written permission of the author.

This thesis work is dedicated:

To my beloved wife and children for their gracious cooperation to accomplish  
this uphill task.

To my brothers and sisters, who encouraged and supported me in countless ways;

To Dr. Atta-ur-Rehman former Chairman HEC, Pakistan who promoted the  
higher education culture in my beloved country Pakistan.



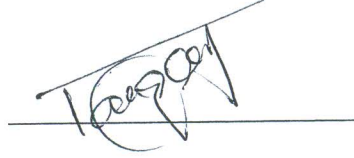
**CAPITAL UNIVERSITY OF SCIENCE & TECHNOLOGY  
ISLAMABAD**

Expressway, Kahuta Road, Zone-V, Islamabad  
Phone: +92-51-111-555-666 Fax: +92-51-4486705  
Email: [info@cust.edu.pk](mailto:info@cust.edu.pk) Website: <https://www.cust.edu.pk>

**CERTIFICATE OF APPROVAL**

This is to certify that the research work presented in the thesis, entitled “**Bandpass Sampling Methodology for Uniformly Spaced Multiband Energy-Sparse Spectrum**” was conducted under the supervision of **Dr. Noor Muhammad Khan**. No part of this thesis has been submitted anywhere else for any other degree. This thesis is submitted to the **Department of Electrical Engineering, Capital University of Science and Technology** in partial fulfillment of the requirements for the degree of Doctor in Philosophy in the field of **Electrical Engineering**. The open defence of the thesis was conducted on **February 08, 2019**.


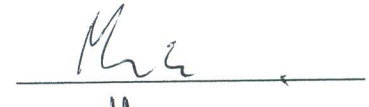

Student Name: Mr. Tauqeer Ahmed (PE113003)



The Examining Committee unanimously agrees to award PhD degree in the mentioned field.

**Examination Committee :**

- (a) External Examiner 1: Dr. Shahid Khattak  
Professor  
COMSATS University,  
Abbottabad Campus
- (b) External Examiner 2: Dr. Mukhtar Ullah  
Associate Professor  
FAST-NU, Islamabad
- (c) Internal Examiner : Dr. Imtiaz Ahmad Taj  
Professor  
CUST, Islamabad



**Supervisor Name :**

Dr. Noor Muhammad Khan  
Professor  
CUST, Islamabad



**Name of HoD :**

Dr. Noor Muhammad Khan  
Professor  
CUST, Islamabad



**Name of Dean :**

Dr. Imtiaz Ahmad Taj  
Professor  
CUST, Islamabad



## AUTHOR'S DECLARATION

I, **Mr. Tauqeer Ahmed (Registration No. PE-113003)**, hereby state that my PhD thesis titled, '**Bandpass Sampling Methodology for Uniformly Spaced Multiband Energy-Sparse Spectrum**' is my own work and has not been submitted previously by me for taking any degree from Capital University of Science and Technology, Islamabad or anywhere else in the country/ world.

At any time, if my statement is found to be incorrect even after my graduation, the University has the right to withdraw my PhD Degree.



(**Mr. Tauqeer Ahmed**)

Dated:



February, 2019

Registration No : PE113003

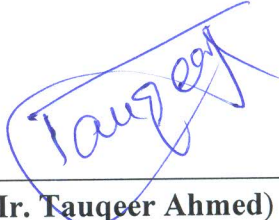
## PLAGIARISM UNDERTAKING

I solemnly declare that research work presented in the thesis titled “**Bandpass Sampling Methodology for Uniformly Spaced Multiband Energy-Sparse Spectrum**” is solely my research work with no significant contribution from any other person. Small contribution/ help wherever taken has been duly acknowledged and that complete thesis has been written by me.

I understand the zero tolerance policy of the HEC and Capital University of Science and Technology towards plagiarism. Therefore, I as an author of the above titled thesis declare that no portion of my thesis has been plagiarized and any material used as reference is properly referred/ cited.

I undertake that if I am found guilty of any formal plagiarism in the above titled thesis even after award of PhD Degree, the University reserves the right to withdraw/ revoke my PhD degree and that HEC and the University have the right to publish my name on the HEC/ University Website on which names of students are placed who submitted plagiarized thesis.

Dated: 8 February, 2019

  
\_\_\_\_\_  
(Mr. Tauqeer Ahmed)  
Registration No. PE113003

---

## *List of Publications*

It is certified that following publication(s) have been made out of the research work that has been carried out for this thesis:-

1. Tauqeer Ahmed, Noor. M. Khan, “Direct radio frequency sampling methodology for multiple signals in an energy-sparse spectrum” *Turkish Journal of Electrical Engineering & Computer Sciences*, vol. 24 no. 6, pp.4637-4647, 2016.

**Status:** Published.

2. Muhammad Muzzammil, Tauqeer Ahmed, Noor Muhammad Khan, Lei Wan, “Low Cost, Faster Detection of Cognitive Radio through Filter Banks with Bandpass Sampling” *Physical Communication* vol. 33 no. 2 , pp. 1-8, 2019.

**Status:** Published on line.

3. Tauqeer Ahmed, Noor Muhammad Khan, “A Simple and Low cost LMR Design for Interoperability Among Radio Networks in a Public Safety Scenario.” *ComTech 2019: International conference on Communication Technologies 2019*.

**Status:** Accepted.

**Tauqeer Ahmed**

(PE113003)



## *Acknowledgements*

First and foremost, I bow my head in gratitude and thank to Allah for giving me the strength to complete this dissertation.

I owe a deep debt of gratitude to my university for giving me the opportunity to complete this work.

I am obliged to some people, who have been consistently a source of inspiration and encouragement for me from the beginning till the completion of this research work. In particular, I am extremely thankful to my research supervisor Dr. Noor Muhammad Khan, who has been always generous during all phases of this research work, for his motivation and support over the last five years, and especially in the last few months. I am grateful for his encouragement to join the Ph.D. programme under his supervision, and for taking me on as a member of ARWiC. He has done a great deal for me over the years. I particularly enjoyed the research atmosphere in the group and our discussions on various academic and non-academic topics.

I would also to take this opportunity so say warm thanks to every member of ARWiC, especially Mirza Yasir and Hassan for their cooperation.

I am also obliged to all my family members, especially to my mother, for always showing her concern to keep me in touch with my studies and for her unconditional love and prayers. To my brother Hassan Quraishi for his generous support.

Finally, I wish to express my sincere appreciation to my wife for her endless cooperation, assistance, and encouragement throughout my studies.

# *Abstract*

In this dissertation, a novel methodology for direct down-conversion of radio frequency (RF) is proposed, which in return is useful to minimize sampling frequency for an evenly spaced spectrum comprising multiband RF signals. The proposed methodology describes a set of rules to achieve the lowest possible sampling frequency without any compromise of spectrum folding or overlap of aliases in base-band after down conversion. It is shown that the minimum sampling rate has a unique relation with the layout of the spectrum of interest (SOI). For instance, if there are  $N$  number of information bands of equal bandwidth  $B$  in the SOI, then it is possible to down-convert the complete SOI using the sampling rate,  $2NB$ , which is twice of the total information bandwidth only if all bands are evenly spaced in the SOI. Another factor introduced to the achieve the minimum sampling rate is the sparseness-nature in the SOI, which is the ratio of null bandwidth to information bandwidth. The proposed methodology is general in nature and is flexible to the number of input signals or bands as well as to their positions in the desired spectrum. In the proposed research work, simulations are carried out that verify that by using the recommended minimum sampling rates, the desired signal is extractable without any additional computational complexity due to spectrum folding or aliasing-overlap. Our proposed methodology has a vast scope in the design of general-purpose receivers, global navigational satellite system (GNSS) receiver and cognitive radios (CR) because of the use of a low speed ADC. Moreover, the same can be efficiently used to monitor a wide band spectrum in military communications especially for electronic warfare receivers, where reduction of the complexity, size and cost has significant importance.

As a model application of our proposed work, we present a composite design for the multiband-multistandard GNSS receiver. The design efficacy is based on the proposed bandpass sampling methodology that transforms the sparse-spectrum electromagnetic environment into a quasi-uniformly spaced spectrum of compact bandwidth, which is more appropriate and useful for simultaneous digitization and down-conversion of analogue signals. In this method, only a part of SOI is transformed to an intermediate frequency. In this way, the desired frequency bands of

information that are widely spread, are grouped to form a contiguous-spectrum which is quasi-uniformly spaced. There on, a sub-sampling is carried out for simultaneous digitization and translation of input signals to the first-Nyquist zone. The proposed composite architecture is also helpful to circumvent the higher-order intermodulation components. The proposed design is validated for conventional Global Positioning System L1 and L2 bands and also for new L5 band used in GNSS (GLONASS, Galileo and Beidou) receivers. The presented results show considerable reduction in the sampling rates, and improvement in signal-to-noise and distortion ratio, which can be easily managed by a low sampling analogue to digital conversion.

# Contents

<b>Author's Declaration</b>	<b>v</b>
<b>Plagiarism Undertaking</b>	<b>vi</b>
<b>List of Publications</b>	<b>vii</b>
<b>Acknowledgements</b>	<b>viii</b>
<b>Abstract</b>	<b>ix</b>
<b>List of Figures</b>	<b>xiv</b>
<b>List of Tables</b>	<b>xvii</b>
<b>Abbreviations</b>	<b>xviii</b>
<b>Symbols</b>	<b>xix</b>
<b>1 Introduction</b>	<b>1</b>
1.1 Overview . . . . .	1
1.2 Objective and Significance of the Research . . . . .	3
1.3 Research Methodology . . . . .	6
1.4 Thesis Organization . . . . .	7
<b>2 Fundamentals of Sampling Theory</b>	<b>8</b>
2.1 Overview . . . . .	8
2.2 Sampling . . . . .	9
2.2.1 Practical Sampling Methods. . . . .	9
2.2.1.1 Voltage Sampling. . . . .	9
2.2.1.2 Charge Sampling. . . . .	10
2.2.2 Sampling Model . . . . .	12
2.2.3 Lowpass sampling theorem . . . . .	13
2.2.4 Analytical reconstruction of analogue signal . . . . .	14
2.2.5 Bandpass sampling theorem . . . . .	16
2.3 The Concept of Aliasing-ambiguity . . . . .	26

---

2.4	Receivers Architectures . . . . .	32
2.5	Bandpass Sampling for Multiple RF Signals . . . . .	36
2.5.1	Boundary constraint. . . . .	37
2.5.2	Neighborhood constraint. . . . .	38
<b>3</b>	<b>Literature Review and Problem Formulation</b>	<b>40</b>
3.1	Literature Survey. . . . .	40
3.1.1	Evolution of the Sampling Techniques . . . . .	40
3.1.2	Bandpass Sampling for Multiband Sparse Spectrum . . . . .	43
3.1.3	Bandpass Sampling Application . . . . .	47
3.1.3.1	General Purpose Communication Receiver . . . . .	47
3.1.3.2	Software Defined Radio. . . . .	48
3.1.3.3	Bandpass Sampling and GNSS Receivers . . . . .	50
3.2	Gap Analysis . . . . .	51
3.3	Research Motivation . . . . .	52
3.4	Problem Statement . . . . .	53
3.5	Thesis Contributions . . . . .	54
<b>4</b>	<b>System Model and Proposed Sampling Theory</b>	<b>55</b>
4.1	Overview . . . . .	55
4.2	System Model . . . . .	56
4.3	Technical Details . . . . .	57
4.4	The Proposed BPS Methodology . . . . .	61
4.4.1	Sparsity ratio . . . . .	61
4.4.2	Lowest Center-frequency . . . . .	62
4.4.2.1	When $\text{mod}((f_j - f_i), 2NB) \neq 0$ . . . . .	64
4.4.2.2	When $\text{mod}((f_j - f_i), 2NB) = 0$ . . . . .	68
<b>5</b>	<b>Test Set up and Simulation Results</b>	<b>71</b>
5.1	Overview . . . . .	71
5.2	Analysis Parameters . . . . .	72
5.2.1	Sparsity Ratio . . . . .	72
5.2.2	Number of Bands in the SOI . . . . .	72
5.2.3	Minimum Frequency for SOI . . . . .	73
5.2.4	Sampling Frequency . . . . .	73
5.3	General Assumptions . . . . .	73
5.3.1	Guard-band Inclusion . . . . .	73
5.3.2	Post Folding Order of Signals . . . . .	74
5.4	Simulation Tools . . . . .	74
5.4.1	Multisim . . . . .	74
5.4.2	Matlab . . . . .	75
5.5	Validation of Results . . . . .	75
5.5.1	Scenario-I . . . . .	75
5.5.2	Scenario-II. . . . .	80
5.5.3	Scenario-III. . . . .	85

---

5.5.4	Scenario-IV. . . . .	92
5.5.5	Conclusion. . . . .	94
<b>6</b>	<b>A Composite GNSS Receiver Design</b>	<b>97</b>
6.1	Overview . . . . .	97
6.2	GNSS Receiver Evolution . . . . .	99
6.3	Receiver Architectures . . . . .	102
6.3.1	GNSS Receiver . . . . .	102
6.3.2	Proposed Design . . . . .	103
6.4	Design Methodology. . . . .	105
6.4.1	Sampling rate viz-a-viz spectrum layout . . . . .	105
6.4.2	Intermodulation Distortion (IMD) Components. . . . .	111
6.5	Results and Simulations . . . . .	119
<b>7</b>	<b>Conclusion and Future work</b>	<b>124</b>
	<b>Bibliography</b>	<b>128</b>

# List of Figures

2.1	Voltage sampling using switched capacitor circuit . . . . .	10
2.2	An ideal charge sampling process . . . . .	11
2.3	Charge sampling in SC-circuit, representing three phase; holding/read-out, charge integral and reset. . . . .	12
2.4	A simple sampling operation model. (a) Sampling operation. (b) Sampling function. . . . .	13
2.5	An illustration of lowpass sampling theorem . . . . .	16
2.6	Allowable sampling frequency laying in the range $2B \leq f_s \leq 4B$ . .	17
2.7	A passband signal of bandwidth $B$ Hz, located at frequency $f_c$ . .	18
2.8	Bandpass sampling frequency limits: (a) Bandpass sample rate $f_s = f_{s'} = (2f_c - B)/m$ by taking $m = 6$ ; (b) Bandpass sampling rate is less than $f_{s'}$ ; (c) Lowest possible sampling rate $f_{s''} < f_{s'}$ . . . . .	18
2.9	Permissible sampling-frequency ranges of a dual-tone passband signal comprising of 21 kHz and 27 kHz tones: (a) $f_s = 42$ kHz produces inverted spectrum alongwith $N_{OB}$ ; (b) $f_s = 27$ kHz produces inverted spectrum; (c) $f_s = 21$ kHz is optimized;(d) $f_s = 18$ kHz but produces $N_{OB}$ (e) $f_s = 13.5$ kHz produces inverted spectrum . .	20
2.10	The minimum normalized sampling frequency $f_s$ as a function of the normalized highest frequency. . . . .	22
2.11	Useable sampling rates for BPS, normalized to the signal bandwidth ( $f_s/B$ ). . . . .	24
2.12	Useable sample rates for the bandpass signal of bandwidth 6 kHz and bandwidth-normalized frequency to $R = 4.5$ . . . . .	25
2.13	BPS with aliasing occurring only in the filter guard bands. (a) A typical BPS setup. (b) Spectrum of original continuous time signal showing bandpass filter response. (c) Spectrum of filtered continuous signal showing parts of in-band noise. (d) Spectrum of digital samples after A/D conversion. . . . .	26
2.14	Typical operating point for $f_s$ to compensate for nonideal hardware. . . . .	27
2.15	Intermediate $f_{s_i}$ and $f_{s,ctr}$ operating points, to evade operating beside the gray-shaded regions for the signal of bandwidth, $B = 6$ kHz and bandwidth-normalized frequency $R = 4.5$ . . . . .	28
2.16	Discrete-time sequence of values . . . . .	28
2.17	Different sinusoids created from same set of discrete values . . . . .	29
2.18	sampling process of two sinusoid . . . . .	30
2.19	FFT spectrum showing energy at 2kHz only . . . . .	30

2.20	A conventional dual IF superhysterdyne receiver with second IF as zero . . . . .	33
2.21	Homodyne receiver architecture with reduced discrete components . . . . .	34
2.22	Low-IF receiver architecture . . . . .	35
2.23	Wideband IF receiver architecture . . . . .	35
2.24	A sub-sampling SDR architecture . . . . .	35
2.25	Subsampling receiver architecture . . . . .	36
2.26	Passband spectrum of multiple RF bandpass signal . . . . .	37
2.27	Spectrum of single bandpass signal (a) Prior to sampling (b) After sampling at $f_s$ . . . . .	38
2.28	Downconverted spectrum of multiple RF signal using bandpass sampling . . . . .	39
4.1	A spectrum comprising N number of RF signals . . . . .	56
4.2	The front end of a receiver architecture with the functionality of digitizing multiband input signals . . . . .	57
4.3	Direct down conversion of a tri-band RF spectrum . . . . .	63
4.4	Flow chart to calculate sampling frequency and carrier positions in passband . . . . .	65
4.5	(a) Signal $X(f)$ positioned at $f_c$ . (b) Down-conversion of $X(f)$ in the first-Nyquist zone. (c) Shift of $\sigma$ Hz in the position of $X(f)$ . (d) A boundary constraint overlap of $X(f)$ after down-conversion . . . . .	67
4.6	A down-conversion of quad-channel spectrum using a sample rate of 200 ksps, resulted in complete aliasing-overlap at 12.5 kHz . . . . .	69
4.7	A down-conversion of quad-channel spectrum without any aliasing-overlap for a sample rate of 225 ksps . . . . .	69
5.1	A Multisim based test set up for simultaneous downconversion and digitization of Multiband SOI . . . . .	76
5.2	Down-conversion of a tri-band sparse-spectrum using $f_s = 12$ ksps. The input bands are sinusoidal-tones generated at 5, 15, 25 kHz and down-converted into the First-Nyquist zone, where these are positioned at a frequency gap of 2 kHz from the adjacent band. This separation of 2 kHz between their peaks shows that there is no aliaing-overlap for a bandwidth of 2 kHz. . . . .	78
5.3	Downconversion of 13, 39, 65 kHz sinusoids using $f_s = 12$ ksps and $\Delta f/B = 13$ . . . . .	79
5.4	Downconversion of 1, 81, 161 kHz sinusoids using $f_s = 12$ ksps and $\Delta f/B = 40$ . . . . .	79
5.5	Downconversion of 51, 153, 255 kHz sinusoids using $f_s = 12$ ksps and $\Delta f/B = 51$ . . . . .	80
5.6	Direct down-conversion of three sinusoids for $\gamma$ equal to 5, 14, 40 and 51 using proposed methodology . . . . .	81
5.7	Direct down-conversion of three sinusoids using Munoz et al. shows a frequency overlap for $\gamma$ equal to 5 and 51 . . . . .	82
5.8	Baseband spectrum of a uniformly spaced quad-signal environment. . . . .	83



---

5.9	$\gamma = 10$ . $N=5$ , $B=4000$ . . . . .	84
5.10	$\gamma = 12$ . $N=6$ , $B=4000$ . . . . .	84
5.11	Down-conversion of a six-band sparse-spectrum with sparsity of 1:83	85
5.12	Triband downconversion using four different values of gamma . . . . .	90
5.13	Welch power density estimate for 24 kHz bandwidth . . . . .	91
5.14	Welch power density of tri-band radio spectrum . . . . .	92
5.15	An RF output of a filters bank, comprised of L filters of equal bandwidth being sampled in a sequential order. . . . .	94
5.16	Detection time comparison for the heterodyne receiver, non-uniform sampler, random pre-integrator, bandpass sampling receiver, homo- dyne receiver and the proposed filters bank based receiver with BPS architecture. . . . .	95
6.1	The architecture of a conventional analogue GPS receiver. . . . .	101
6.2	A scenario comprising a combination of GNSS signals of GPS, GLONASS, Galileo and Compass. . . . .	102
6.3	A composite receiver design for Global Navigational Satellite Sys- tem signals. . . . .	104
6.4	A $m$ -bands spectrum with a total bandwidth of $mB$ Hz.(a) All bands are equally spaced. (b) An equally spaced sparse-spectrum. (c) Band-II is shifted right at $21B/2 + \delta$ . . . . .	107
6.5	Sampling rate increases in a non-linear fashion for a non-uniform spectrum, when there is any frequency shift, $ \delta $ in the positions of B-II and B-III. . . . .	110
6.6	TOI product formation in the first-Nyquist zone of the dual-band LMR. . . . .	115
6.7	TOI and spurious-noise components for a dual-band LMR (using dual tones at centre-frequencies) in the case of direct RF sub-sampling.	116
6.8	Reduction of spurious components using composite receiver method- ology. . . . .	117
6.9	An illustration of TOI-component at 82.994 MHz alongwith other spurious-noise components causing distortion. . . . .	118
6.10	A simplified circuit of composite receiver using a sampling rate of 9.18 MHz. . . . .	120
6.11	Down conversion of L1, L2 to 1.243 MHz and 3.54 MHz using a sampling rate of 9.18 MHz. . . . .	121
6.12	Down conversion of L1/E1, B1 to 2.6 MHz and 7.42 MHz using a sampling rate of 19.6 MHz. . . . .	122

# List of Tables

2.1	Selection of upper bound and lower bound sampling frequency in kHz and optimum sampling frequency, $f_{opt}$ in kHz, for BPS . . . . .	19
4.1	A comparison of proposed methodology with [65] . . . . .	60
4.2	Down-conversion of a quad-channel spectrum of 100 kHz bandwidth using a sample rate 200 kHz resulted in a complete aliasing-overlap in the first-Nyquist zone. . . . .	70
4.3	Down-conversion of a quad-channel spectrum of 100 kHz bandwidth using a sample rate 225 kHz proved useful to circumvent aliasing-overlap. . . . .	70
5.1	Some possible values for $\Delta f/B$ , which avoid aliasing when using the minimum sampling frequency ( $N = 2, 3, \dots, 12$ ) . . . . .	80
5.2	A spectrum comprising three sinusoids with sparsity ratio 5, 13, 40 and 51. . . . .	81
5.3	Passband positions of six-band system . . . . .	83
5.4	Suitable values of lowest frequency $f_{L1}$ to avoid aliases overlap. . . . .	85
5.5	Set of useable frequencies for a multi-band radio design in a sparse electromagnetic environment . . . . .	91
5.6	A spectrum of nonzero energy contents with sparsity ratio 1 to 6. The last column lists values of normalized sparsity to avoid aliasing for given minimum sampling frequencies. . . . .	93
6.1	B-II and B-III positions are shifted from 35 MHz and 51 MHz to 42 MHz and 44 MHz respectively, in steps of 500 kHz. Last column shows that minimum sampling rate is required if the bands are equi-distant. . . . .	109
6.2	Regions of acceptable bandpass sampling rates for down-conversion of L1/L5a and L1/E1/B1 signals and location of third-order inter-modulation component . . . . .	118
6.3	Group-formation of GNSS signals and the minimum sampling rates for their down-conversion. . . . .	119
6.4	A comparison of sampling rate, useable for Global Navigational Satellite Signals receiver . . . . .	123

# Abbreviations

<b>ADC</b>	Analogue to Digital Converter
<b>BPS</b>	Band-pass Sampling
<b>BPF</b>	Band-pass Filter
<b>CW</b>	Continuous Wave
<b>DAC</b>	Digital to Analogue Converter
<b>DSP</b>	Digital Signal Processing
<b>FE</b>	Front End
<b>FT</b>	Fourier Transform
<b>GNSS</b>	Global Navigation Satellite System
<b>GPS</b>	Global Positioning System
<b>IF</b>	Intermediate Frequency
<b>IMD3</b>	Intermodulation of Third Order
<b>LNA</b>	Low Noise Amplifier
<b>LMR</b>	Land Mobile Radio
<b>LPF</b>	Low-pass Filter
<b>NF</b>	Noise Figure
<b>NUS</b>	Non-uniform Sampling
<b>QAM</b>	Quarter Amplitude Modulation
<b>RF</b>	Radio Frequency
<b>SDR</b>	Software Defined Radio
<b>SNR</b>	Signal-to- Noise Ratio
<b>SOI</b>	Spectrum of Interest
<b>SINAD</b>	Signal-to-Interference and Noise Distortion
<b>TOI</b>	Third Order Intermodulation

# Symbols

$B$	Bandwidth
$\Delta f$	Channel separation
$\delta$	Dirac delta function
$\sigma$	Small deviation
$\epsilon$	Variation
$f_c$	Carrier frequency
$f_l$	Lower frequency for a specific band or channel
$f_h$	Higher frequency for a specific band or channel
$f_s$	Sampling frequency
$f_{s,min}$	Minimum sampling frequency
$G$	Gain
$N$	Number of signals/bands
$N_i$	Number of samples for integration
$N_{in}$	Input noise
$N_{out}$	Output noise
$S_{in}$	Input signal strength
$S_{out}$	Output signal strength
$SNR_{in}$	SNR at the input
$T_{aq}$	Acquisition time
$T_i$	Integration time
$T_{sw}$	Switching time
$W_c$	Bandwidth of a single channel

# Chapter 1

## Introduction

### 1.1 Overview

Bandpass sampling is a well established process that downconverts an analogue pass-band signal either directly to base-band or to an intermediate frequency (IF) signal without involving analog mixers [1]. As a matter of fact, this process makes signal processing very simple and efficient, where the sampling process is accomplished by applying an analogue signal to an analog-to-digital (A/D) converter whose output is a sequence of discrete values. What we are calling bandpass sampling (BPS) is also goes by a number of alternative terms in the literature, such as intermediate frequency sampling, harmonic sampling [2], sub-Nyquist sampling, under-sampling [3], first-order bandpass sampling and sub-sampling [4]. As BPS is a type of periodic sampling of real signals, the Nyquist-Shannon criterion must still be satisfied.

The Nyquist- Shannon sampling theorem sets a necessary and sufficient condition, not only for the sampling of a band-limited signal but also for the reconstruction of an original analogue signal. When the reconstruction of an analogue signal is accomplished through the Whittaker-Shannon interpolation formula, then to avoid aliasing, the Nyquist criterion also becomes a necessary condition. This implies that if sampling rate is slower than twice the bandwidth, then there are chances

that a part of the signal will be destructed, resulting in loss of information. Nevertheless, if additional constraints, like position, bandwidth, sparseness etc are imposed on the signal, then the Nyquist criterion may no longer be a mandatory restriction. An imperative example that takes advantage of additional suppositions about the signal is provided by the latest field of compressed sensing, which permits the complete reconstruction of input signal sampled at a sub-Nyquist rate. Specially, this is pertinent to the signals that are sparse in frequency domain. As we know that compressed sensing is performed for a spectrum that has a little non-zero energy content (the information bandwidth), over indefinite frequency locations, rather than being composed of a contiguous single band. In other words, the frequency spectrum is sparse and under such constraints the pass-band methodology doesn't remain applicable in a classical sense. Fundamentally, the indispensable sampling rate is thus twice of the information bandwidth. On the contrary, compressed sensing techniques provide an alternative that the information signal could be reconstructed in a perfect manner even if it is sampled at a rate slightly lesser than twice of the information bandwidth. The drawback of this technique is that reconstruction is not given in closed form by a formula. Consequently, it is dependent on the solution to a convex optimization program which requires well-calculated but nonlinear methods [5].

In connection to the sampling theory, the elementary point of concern, which needs attention is just how quick a given signal that is continuous in the time domain must be sampled so that its information contents may be recovered in the reconstruction process without any loss. Of course, we can sample a time-continuous signal at an appropriate sample rate suitable to our application, and get a series of discrete values but here we need to answer three basic questions. How close do the remitted discrete values represent the actual signal? What are the optimum sampling rates and what price in terms of complexity, power dissipation, cost, size etc we are paying for the remitted sampling rates?

## 1.2 Objective and Significance of the Research

In wireless communication particularly in software defined radio (SDR) systems, it is desirable to down convert multiple RF signals simultaneously by placing the analogue-to-digital converter (ADC) as near to the antenna as possible [6]. However, this requires very large sampling rates using high speed analogue to digital converters. Resultantly, such type of solution poses two major disadvantages. The first is the large power dissipation and the second is the cost effect. In this connection, radio frequency (RF) sub-sampling generally known as bandpass sampling is considered to be the alternative established methodology that is used in radio receivers to directly down-convert and digitize RF signals.

In our proposed research work, we intend to explore the bandpass sampling theory in order to reduce the sampling rates. Analytical methods that exist in the literature permit minimum bandpass sampling frequencies to be computed in case of single-band spectrum. However, BPS has its issues for multiband signal spectrum due to its non-linear nature. This includes constraints like aliasing, spectral folding, reconstruction of information band etc. Also there is no analogous set of equations available for a multiband bandpass system, consisting of signals with arbitrary center frequencies and bandwidths. In the last decade, BPS for multiband signals gained significant attention and efforts have been made to find out valid bandpass sampling frequency ranges for direct down-conversion of multiband RF signals. However, formulation for the minimum sampling frequency cannot be acquired in a closed form due to the nonlinear nature of spectrum folding in the process of sampling. In order to find out the minimum useable sampling frequency, the literature highlights the need to address certain BPS limitations like sparse spectrum, fixed bandwidth (BW) and non-availability of a universal rule. In this connection, various sampling methods, DSP techniques and hardware, and reconstruction algorithms have their role to define the bounds. Another alternative term, which is used in literature to understand and solve the above mentioned problem and realize the solution is Digital Aliasing-free Signal Processing (DASP)[7].

To exemplify the significance of the digital aliasing-free signal processing, upper-bound of the application array of analogue-to-digital convertor practicable in a large number of cases may be considered on the basis of this DASP techniques. Taking into account the conventional digital signal processing (DSP) approach, the upper limit of the sampling rates of the existing analogue-to-digital convertor characterize their application extension in the frequency domain. In the field of DSP it is possible to implement processing of a desired signal in the digital domain only if the available analogue-to-digital convertor could be used at a higher enough sampling frequency. In this way the useable highest sampling frequency of the particular type of analogue-to-digital convertor might be considered as a yardstick defining the application matrix. A significant amount of effort and money have been expended on evolving the expertise for manufacturing state of the art microelectronic devices. This includes but is not limited to manufacturing of wide-band, high speed and more precise ADC, FPGAs and DSP kits etc. Consequently, superior analogue-to-digital convertor chips, appropriate for a broader frequency range, were developed and made available in the market. As a result, the application range of DSP skills begin to widen uninterruptedly. Nonetheless, the progression that took place followed a long path and is considered evolutionary, somewhat time-consuming and considerably overpriced. On the other hand digital aliasing free signal processing shows the way to the requisite outcomes in a much economical fashion for a large variety of applications. Nevertheless, in DASP broadening, the ADC applications array is accomplished by means of unconventional signal processing techniques and methods instead of refining the existing manufacturing technologies in the field of semiconductor physics. In a traditional approach founded on DSP, a desired input signal that could be managed by an ADC rests on two pertinent parameters: the analogue bandwidth of the input signal and the highest sampling rate. The prescribed analogue bandwidth then has to be equal to or greater than at least half of the highest sampling rate. However, practically in a number of cases it is wider enough to be handled by an ordinary ADC. Typically it is often 4 to 8 times wider than the corresponding half of the sampling rate [7]. Consequently the worthy foundation of ADC technology could



not be best utilized in a large number of applications based on traditional DSP techniques. Thus it is the DASP technology, whose induction into system design changes the situation drastically. Here, appropriate bandpass sampling and compatible DSP techniques can be applied to circumvent aliasing. Eventually, the requisite sampling frequency does not exclusively rest on the upper frequency of the input signal. Only the other stated ADC feature, viz. the analogue bandwidth of the input signal, limits this upper frequency. Conversely, as in majority cases, this bandwidth is significantly broader for a given ADC than half of the acceptable sampling rate. Using the DASP methodology classically enhances the frequency bound to a point that is more than a many times higher. The area of bandpass sampling is thus a facet of DSP which finds applications in diverse disciplines including, but not limited to communication, optics, radar, power measurements, biomedical signals, and instrumentation such as oscilloscope, spectrum analyzer etc. The only thing, which requires attention is how to use this technology in an efficient manner. **The objective of our research is to establish necessary conditions to find minimum sampling rates for a uniformly-spaced sparse spectrum with any sparse ratio.** The intended research has a number of applications in radio receivers, global navigational receiver systems, cognitive radios for spectrum sensing and other wireless applications, where reduction in complexity, size and cost etc has significant importance. However, case of the multiband or multistandard radio receiver, system-nonlinearities, specifically due to low-noise amplifiers and down-conversion circuits can produce a series of output spectra with varying amplitude components. Bandpass sampling of such a spectrum, in the presence of other non-idealities such as jitter noise and thermal folded noise, without aliasing-overlap is not the perview of this research. We intend to remain restricted to find out the necessary and sufficient conditions which ensure minimum sampling rates. Conversely, our endeavour is to describe the nature and layout of the electromagnetic spectra when it best suits the Nyquist sampling rates for direct down-conversion to an intermediate frequency that is less than or equal to half of the sampling rate.

### 1.3 Research Methodology

Our research methodology is based on both analytical and empirical methods. It may be broadly divided into two parts: Part-I and Part-II. Part-I further consists of three stages. In the first stage, a comprehensive survey is conducted. The survey mainly reveals and exploits two areas. First area pertains to the contemporary sampling techniques, their strong point and their weaknesses. In the second area, applications of these sampling techniques are evaluated. A special emphasis is given to the the field of radio receivers specially software defined radios (SDRs) and viz-a-viz bandpass sampling. In the second stage, a theory is developed in order to ascertain the ideal conditions, where minimum sampling rate could be achieved with out any aliasing-overlap or loss of information. Then necessary conditions are established so that the desired results can be achieved with full reliability. Finally, these conditions are incorporated in to an algorithm. In the third and final stage, simulations are carried out using Matlab<sup>®</sup> and it is confirmed that the proposed theory is valid for simultaneous down-conversion and digitization of multiple bands or signals in spectrum of interest. Firstly, the proposed theory along with achieved result is published in [8].

In the part-II, after ascertaining the theoretical part, an emphasis is given to its practical applications. In this context a composite receiver design is simulated to set up scenario for the application of the proposed work. This design is later used for a composite receiver for Global Navigational Satellite System (GNSS). As the various bands used by the conventional positioning systems (GPS, GLONASS, Galileo and Beidou) are not uniformly spaced, therefore the proposed theory is not directly applicable. Consequently, some modification are made in terms of radio spectrum management to achieve a quasi-uniformly spaced spectrum. The target is to acquire minimum possible sampling rate without any aliasing in the base-band. The results are compared with those already obtained by [9–12] and a significant reduction is achieved. Besides Matlab<sup>®</sup>, simulations are also carried out using Multisim<sup>©</sup>, of National Instruments (NI) and the achieved results are found same as that of Matlab<sup>®</sup>.

## 1.4 Thesis Organization

Chapter 2 gives a brief description of bandpass sampling theory. In chapter 3 the literature survey is presented and we formulated the problem statement, keeping in view the previous work carried out by researchers. Chapter 4 pertains to the analytical description and research methodology that we intend to adopt in the light of the basics of sampling theory. Chapter 5 pertains to the test set up and simulations to verify the proposed methodology. In chapter 6 we presented a composite receiver design as an application of our work and applied the methodology to a non-uniform sparse-spectrum . A case of GNSS-spectrum is studied and then by carrying spectrum-management planning, where the spectrum of interest (SOI) is transformed into a quasi uniform. There on the proposed sampling methodology is applied. In chapter 7 we conclude our research work and suggest its extension to future work.

# Chapter 2

## Fundamentals of Sampling

### Theory

#### 2.1 Overview

The widespread usage of digital devices for data processing has increased the significance of various techniques used in digital signal processing (DSP). A continuous signal in time domain can not be directly processed by digital devices. To process an analogue signal in time domain, it is first mandatory to convert it into sequences of discrete values by sampling. A digital computer can process only binary numbers in form of ones and zeros. For this objective, sampling rate must be selected in such a way that characteristics of analogue signal are not changed, while reconstructing it from the sequences obtained during sampling.

In this chapter we explain the fundamental terms and concepts used in sampling theory. After developing a clear understanding of the terminology, we explore further and introduce famous theorems used in sampling schemes. Both lowpass sampling and bandpass sampling theorems are still very much used in the area of digital signal processing (DSP) and have their own advantages and disadvantages.

## 2.2 Sampling

In digital signal processing, sampling can be described as a simple process used for conversion of analogue or continuous-time signal,  $x(t)$  to discrete sequence of values. In this way, we obtain a series of points in time to produce the sample values,  $x_s(t) = x(nT_s) = x[n]$ . Normally it is followed by operations like quantization and encoding to acquire a digital signal. This is carried out in a fashion so as, we can reconstruct the original signal without loss of information.

### 2.2.1 Practical Sampling Methods.

In electrical circuits, sampling methods are based on voltage sampling and charge sampling. Voltage sampling is realized by the sample-and-hold (S/H) circuit, which tracks an analogue signal and stores the sampled value as a voltage across a sampling-capacitor for some duration of time. On the contrary to the voltage sampling, charge sampling does not track the signal level but integrates the signal current within a given interval of time [13]. The analogue signal to be sampled (in its voltage mode) is first converted to current mode by a trans-conductance cell before carrying out charge sampling. As compared to voltage sampling, charge sampling has the advantage that the bandwidth of the charge sampling device only relies on the sampling duration but not on the switch-on resistance so that a wide-band sampler design is more feasible [14]. Bandpass sampling can also be performed by both charge sampling and voltage sampling [15].

#### 2.2.1.1 Voltage Sampling.

An ideal voltage sampling process can be demonstrated as an input voltage signal  $x(t)$  sampled by a periodic pulse  $p(t) = \sum_{n=-\infty}^{\infty} \delta(t - t_s(n))$  (see Fig. 2.1). However, in practice, voltage sampling is implemented straightaway by an Sample-and-Hold (S/H) circuit as shown in Fig. 2.1 along with the suitable clock scheme. Consider the sampling function is not a series of Dirac delta functions but the convolution

of the Dirac delta functions with a pulse shape  $t_n = nT_s$  (where  $f_s = 1/T_s$ ), is the discrete time and  $\tau$  is the duty cycle of sampling clock  $\phi$  ( $0 < \tau < 1$ ). The output voltage  $V_{out}(t)$  by Sample-and-Hold is a convolution of  $x_s(t)$  and  $h(t)$ , given by

$$V_{out}(t) = x_s(t) * h(t), \quad (2.1)$$

where  $x_s(t)$  is defined as

$$x_s(t) = x(t)p(t) = x(t) \sum_{n=-\infty}^{\infty} \delta(t - t_s(n)) \quad (2.2)$$

consequently,  $h(t) = 1$  for  $nT_s \leq t \leq (n + \tau)T_s$  and equal to zero, otherwise.

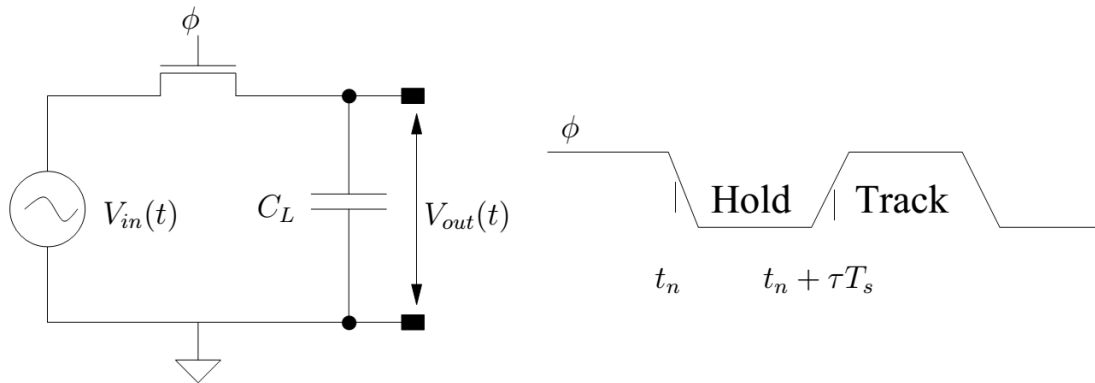


FIGURE 2.1: Voltage sampling using switched capacitor circuit

In the frequency domain output voltage will be

$$\tilde{V}_{out} = X_s(f)H(f), = \tau e^{j\pi \frac{f}{f_s} \tau} \text{sinc}\left(\frac{f}{f_s} \tau\right) \cdot \sum_{n=-\infty}^{\infty} X(f - kf_s) \quad (2.3)$$

### 2.2.1.2 Charge Sampling.

Charge sampling is different from the voltage sampling in the way that, instead of storing the voltage value across a sampling capacitor, charge sampling integrates charge within a time window  $[t_n, t_n + t]$ . This process can be modeled as illustrated in Fig. 2.2, where  $s(t) = \sum_{n=-\infty}^{\infty} \delta(t - (t_n + \Delta t))$  represents a mathematical equivalent

of an ideal sampling process and  $t_n$  represents the instant when the integration process gets starts. The sampled output data-signal  $x_s(t) = x'(t)s(t)$  is expressed by

$$\begin{aligned} x_s(t) &= x'(t)s(t) \\ &= \sum_{n=-\infty}^{\infty} \left( \int_{t_n}^{t_n+\Delta t} x(\xi)d\xi \right) \delta(t - t_n - \Delta t). \end{aligned} \quad (2.4)$$

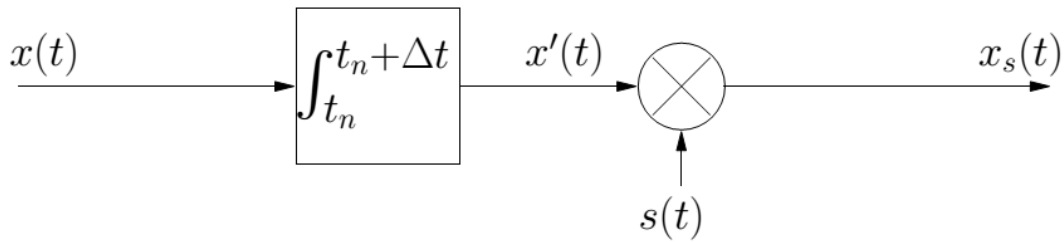


FIGURE 2.2: An ideal charge sampling process

However, in practice, charge sampling is modeled as a switched capacitor circuit with  $I_{in}(t)$  as an input current signal, alongwith an appropriate clock scheme as shown in Fig. 2.3. Assuming that  $t_n = nT_s$  and starting from Eq. 2.4 , the output voltage of charge sampling and the corresponding Fourier transform spectrum are given as

$$V_{out}(t) = \frac{1}{C_L} \left( \int_{t_n}^{t_n+\Delta t} I_{in}(\xi)d\xi \right) \sum_{n=-\infty}^{\infty} \delta(t - t_n - \Delta t). \quad (2.5)$$

and

$$V_{out}(f) = \frac{\Delta t}{C_L \cdot T_s} \sum_{k=-\infty}^{\infty} I_{in}(f - kf_s) \text{sinc}[(f - kf_s)\Delta t] e^{-j\pi(f+kf_s)\Delta t} \quad (2.6)$$

respectively, without considering the zero-order sample and hold function at the hold phase, where  $\text{sinc}(x) = \sin(\pi x)/(\pi x)$ .

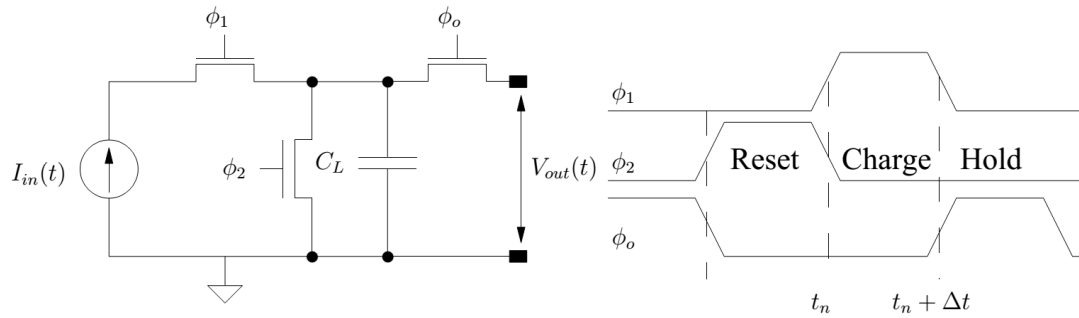


FIGURE 2.3: Charge sampling in SC-circuit, representing three phase; holding/readout, charge integral and reset.

## 2.2.2 Sampling Model

The primary step to reconstruct a digital signal,  $x[n]$  from a continuous-time signal,  $x(t)$ , is to sample  $x(t)$  at uniformly spaced intervals in time domain to produce discrete sample values, such that  $x_s(t) = x(nT_s)$ , where parameter  $T_s = 1/f_s$  is known as the sampling period.

A basic model as shown in Fig. 2.4 illustrates the sampling operation, where the input continuous-time signal  $x(t)$  is multiplied by a periodic pulse  $p(t)$  to form the sampled signal  $x_s(t)$ . Mathematically,

$$x_s(t) = x(t)p(t) \quad (2.7)$$

where  $p(t)$  is the sampling function, which in practice is a periodic narrow pulse having an amplitude either 0 zero or 1. Being periodic in nature  $p(t)$  can be represented by the Fourier series as given by

$$p(t) = \sum_{n=-\infty}^{\infty} C_n \exp(j2\pi n f_s t) \quad (2.8)$$



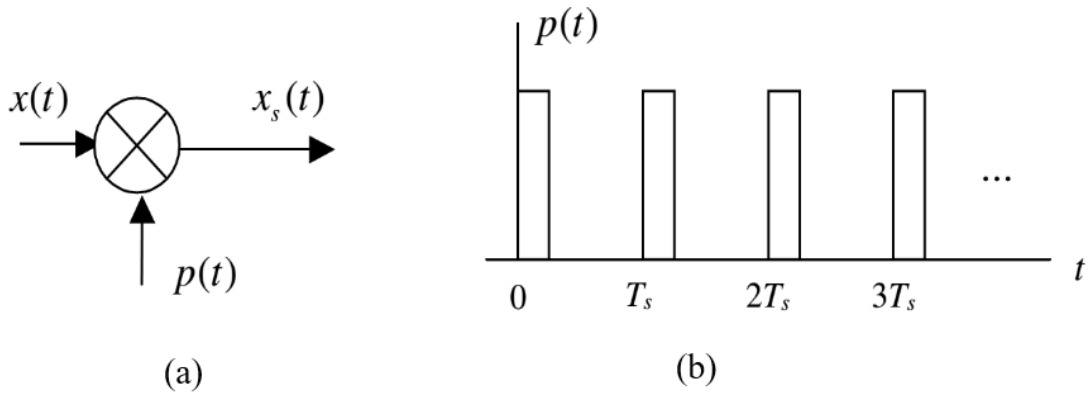


FIGURE 2.4: A simple sampling operation model. (a) Sampling operation. (b) Sampling function.

in which  $C_n$  are known as the Fourier coefficients and can be defined by

$$C_n = 1/T_s \int_{-T_s/2}^{T_s/2} p(t) \exp(-j2\pi n f_s t) dt \quad (2.9)$$

Substituting value of  $p(t)$  from Eq. 2.8 into Eq. 2.7 results

$$x_s(t) = x(t) \sum_{n=-\infty}^{\infty} C_n \exp(j2\pi n f_s t) \quad (2.10)$$

for the sampled signal.

### 2.2.3 Lowpass sampling theorem

*A band-limited signal  $x(t)$  can be reconstructed without any loss of information or error from sample values of the signal provided the sampling frequency  $f_s \geq 2f_h$ , where  $f_h$  is the highest frequency component present in the signal under sampling operation.*

In literature this theorem is also known by many other names, like, Nyquist sampling theorem or lowpass sampling theorem.

### 2.2.4 Analytical reconstruction of analogue signal

Consider a discrete signal  $x_d(n)$  such that  $x(nT_s)$  denotes the  $n$ th sample of the original continuous in time signal,  $x(t)$ , where  $t$  represents time in seconds. Thus,  $T_s$  is the sampling period in seconds and  $n$  ranges over integers. The sampling frequency in Hertz (Hz) is just the reciprocal of the sampling period, i.e.,  $f_s = 1/T_s$ . To avoid losing any information as a result of sampling, we must assume  $x(t)$  is band-limited to less than half the sampling frequency. This means there can be no energy in  $x(t)$  at frequency  $f_s/2$  or above.

Let  $X(f)$  denote the Fourier transform of  $x(t)$ , i.e.,

$$X(f) = \int_{-\infty}^{\infty} x(t)\exp(-j2\pi f)t dt. \quad (2.11)$$

In order to prove that under given constraint  $x(t)$  can be completely reconstructed by the samples  $x(nT_s)$ . In this regard, we have to derive the spectrum of  $x_s(t)$  and show that  $x(t)$  can be reliably reconstructed from  $x_s(t)$ . Taking Fourier transform of sampled signal in Eq. 2.10 gives

$$X_s(f) = \int_{-\infty}^{\infty} x(t) \sum_{n=-\infty}^{\infty} C_n \exp(j2\pi n f_s t) \exp(-j2\pi f)t dt \quad (2.12)$$

which, after a little manipulation becomes

$$X_s(f) = \sum_{n=-\infty}^{\infty} C_n \int_{-\infty}^{\infty} x(t) \exp[-j2\pi(f - n f_s)t] dt \quad (2.13)$$

Using Fourier transform theory and equation Eq. 2.13 the Fourier transform (FT) of the sampled signal can be obtained as

$$X_s(f) = \sum_{n=-\infty}^{\infty} C_n X(f - n f_s) \quad (2.14)$$

It is therefore evident from Eq. 2.14 that a continuous-time signal sampled at an appropriate rate can be reproduced around  $f = 0$  Hz and its harmonics are translated to the integer multiple of the sampling frequency, i.e, ( $f = nf_s$ ). However, these translated spectra are weighted by the respective  $C_n$  of the narrow sampling pulse  $p(t)$ .

The last step, in the derivation of the lowpass sampling theorem is to define  $p(t)$ . As we know that all the samples are taken instantaneously, an appropriate definition of  $p(t)$  is

$$p(t) = \sum_{n=-\infty}^{\infty} \delta(t - nT_s) \quad (2.15)$$

This is called as impulse function sampling. It is to be noticed that, in this, the sample values are represented by the weights of the impulse functions already mentioned in Eq. 2.9. Substituting Eq. 2.15 into Eq. 2.9 gives

$$C_n = 1/T_s \int_{-T_s/2}^{T_s/2} \delta(t) \exp(-j2\pi n f_s t) dt \quad (2.16)$$

Again applying sifting property of the  $\delta(t)$  function gives us the results

$$C_n = 1/T_s = f_s \quad (2.17)$$

Using this result in Eq. 2.8 shows that the Fourier transform of  $p(t)$  can be represented by

$$P(f) = f_s \sum_{n=-\infty}^{\infty} \delta(f - nf_s) \quad (2.18)$$

Since for impulse function sampling and also from Eq. 2.17 we see that  $C_n = f_s$  for all  $n$ . Thus, Eq. 2.14 the spectrum of the sampled signal becomes

$$X_s(f) = f_s \sum_{n=-\infty}^{\infty} X(f - nf_s) \quad (2.19)$$

Note that this result could have also been obtained from the expression

$$X_s(f) = X(f) \otimes P(f) \quad (2.20)$$

where  $\otimes$  denotes convolution.  $X_s(f)$  the Fourier transform of sampled signal  $x(t)$  using Eq. 2.20 is illustrated in Eq. 2.5. This is in fact an illustration of lowpass sampling theorem.

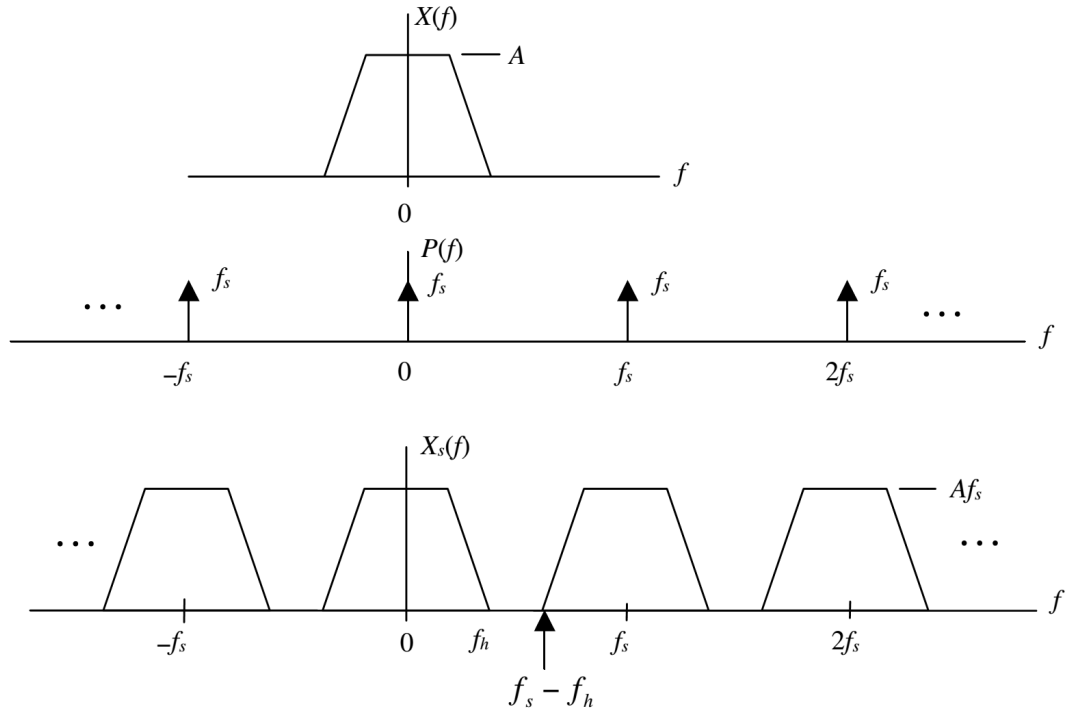


FIGURE 2.5: An illustration of lowpass sampling theorem

### 2.2.5 Bandpass sampling theorem

Bandpass sampling is a technique that performs simultaneous digitization and frequency translation of single or multiple bands in the first Nyquist zone in a single process. In the literature, bandpass sampling is also known by other names, such as undersampling, sub-Nyquist sampling, sub-sampling, intermediate frequency sampling and harmonic sampling [16], [17]. Bandpass sub-sampling provides us two major advantages. First, it reduces the requirement of high speed of A/D converters as required for conventional direct RF sampling. Secondly, it requires very less amount of digital memory necessary for storage of a continuous signal of the same time interval.

The bandpass sampling theorem may be stated as follows [18]:

*If a bandpass signal has bandwidth  $B$  and highest frequency  $f_h$ , the signal can be sampled and reconstructed using a sampling frequency of  $f_s = 2f_h/m$ , where  $m$  is the largest integer not exceeding  $f_h/B$ . All higher sampling frequencies are not necessarily usable unless they exceed  $2f_h$ , which is the value of  $f_s$  dictated by the lowpass sampling theorem.*

A plot of the normalized sampling frequency  $f_s/B$  as a function of the normalized center frequency  $f_c/B$  is illustrated in Fig. 2.6, where  $f_c$  and  $f_h$  are related by  $f_h = f_c + B/2$ . As described in [19] the allowable sampling frequency always lies in the range  $2B \leq f_s \leq 4B$ . However, we see that the theoretically achieved minimum sampling rate  $f_s = 2B$ , corresponding to integer band positioning lies at the tips of the wedges and these points are not feasible from implementation point of view, because any hardware imperfection will move the sampling rate into disallowed area causing aliases overlaps.

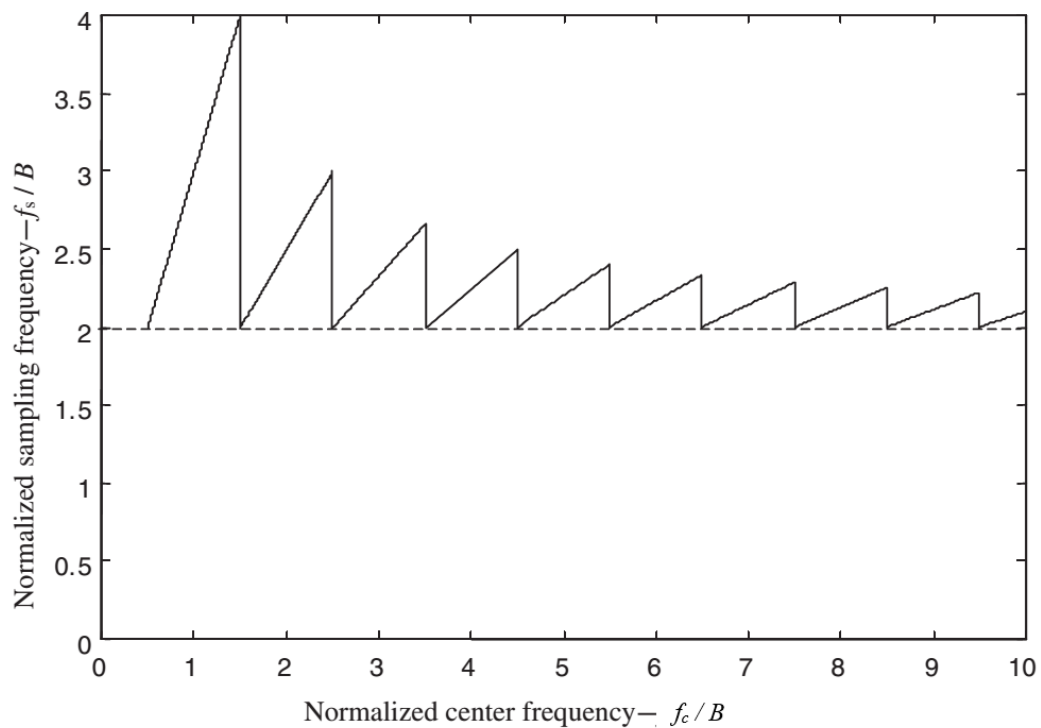


FIGURE 2.6: Allowable sampling frequency laying in the range  $2B \leq f_s \leq 4B$

Let us consider a continuous-time input signal of bandwidth  $B$  with its carrier frequency centered at  $f_c$  Hz as shown in Fig. 2.7. It is possible for us to sample

the continuous signal at a rate,  $f_s = f_{s'}$  Hz, such that spectral replicas of the positive and negative bands, just come up against each other exactly at the origin, i.e, zero Hz as shown in the Fig. 2.8(a). If  $m$  is an arbitrary number of replications, with upper bound less than  $2f_c - B$ , we can realize that,

$$mf_{s'} = 2f_c - B \tag{2.21}$$

This implies that

$$f_{s'} = (2f_c - B)/m \tag{2.22}$$

where  $m$  is a positive integer such that  $f_{s'} \geq 2B$

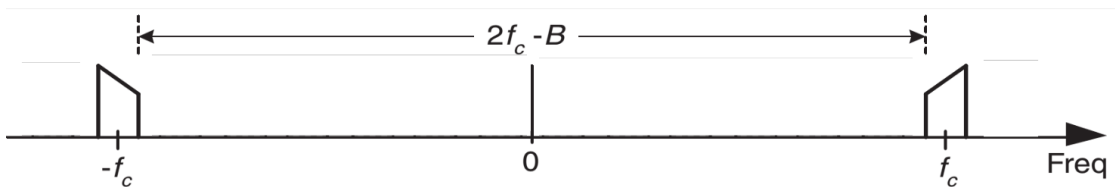


FIGURE 2.7: A passband signal of bandwidth  $B$  Hz, located at frequency  $f_c$

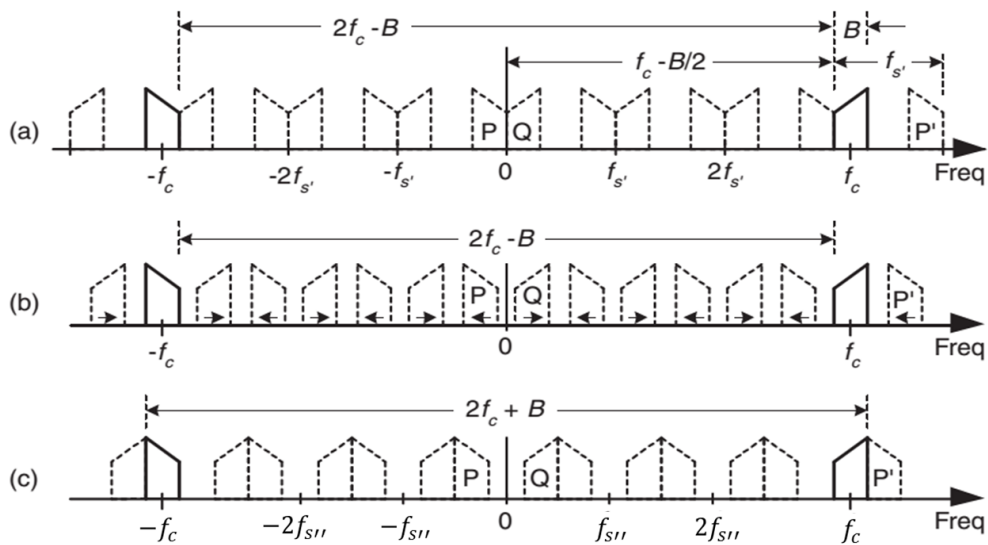


FIGURE 2.8: Bandpass sampling frequency limits: (a) Bandpass sample rate  $f_s = f_{s'} = (2f_c - B)/m$  by taking  $m = 6$ ; (b) Bandpass sampling rate is less than  $f_{s'}$ ; (c) Lowest possible sampling rate  $f_{s''} < f_{s'}$ .

TABLE 2.1: Selection of upper bound and lower bound sampling frequency in kHz and optimum sampling frequency,  $f_{opt}$  in kHz, for BPS

$m$	$f_{s'} = (2f_c - B)/m$	$f_{s''} = (2f_c + B)/(m + 1)$	$f_{opt}$
1	42	27	27
2	21	18	21
3	14	13.5	13.5
4	10.5	10.8	-
5	8.4	9.0	-

If the sampling rate  $f_s$  is increased further beyond  $f_{s'}$ , the already butt up replications, i.e, P and Q tend to overlap with each other. However, the original signal does not shift. This shows that  $f_{s'}$  is in fact upper limit prescribed in Eq. 2.22, therefore, for an arbitrary  $m$ , upper bound of the sampling rate  $f_s$  can be given as

$$f_{s'} \leq (2f_c - B)/m \quad (2.23)$$

Similarly, as we can see in Fig. 2.8 (b) when we start reducing the sampling rate from  $f_{s'}$ , the inter replications gaps starts decreasing without any effect on the original spectra. Again we notice that at some sampling rate  $f_{s''} \leq f_{s'}$ , a situation arises when the replication P' will just come up against the original signal centered at  $f_c$  as shown in Fig. 2.8(c). At this stage any reduction in sampling rate will cause aliasing overlap. We may consider this  $f_{s''}$  as the lower sampling bound, i.e, the sampling rate must always exceed this to circumvent any aliasing-overlap. This lower bound of  $f_s$  may be expressed as

$$f_{s''} \geq (2f_c + B)/(m + 1) \quad (2.24)$$

Finally, combining Eqs. 2.23 and 2.24 we can choose  $f_s$  anywhere in between  $f_{s''}$  and  $f_{s'}$  to avoid any overlaps resulting in loss of information

$$(2f_c + B)/(m + 1) \geq f_s \leq (2f_c - B)/(m) \quad (2.25)$$

To explore further the significance of frequently-referred relationships in Eq. 2.25, in literature [20], we need to explain with an example of a bandpass signal. Let us

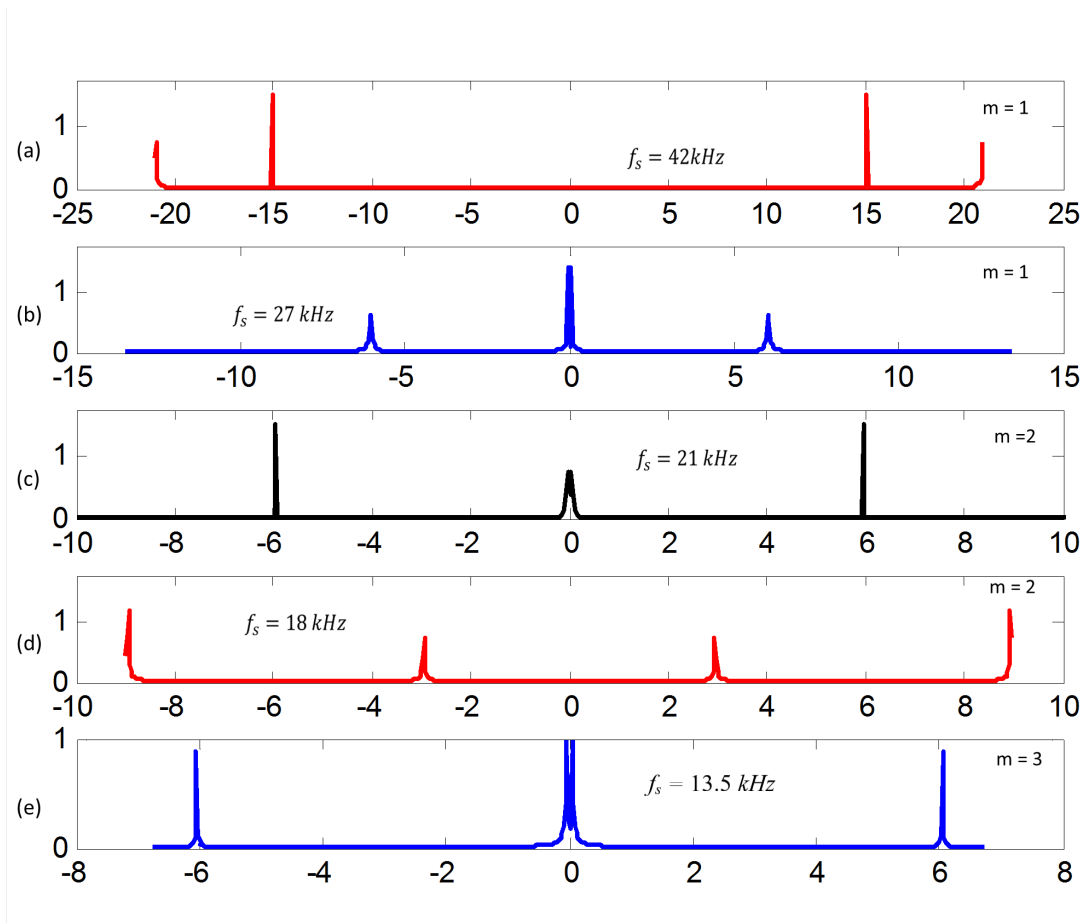


FIGURE 2.9: Permissible sampling-frequency ranges of a dual-tone passband signal comprising of 21 kHz and 27 kHz tones: (a)  $f_s = 42$  kHz produces inverted spectrum alongwith  $N_{OB}$ ; (b)  $f_s = 27$  kHz produces inverted spectrum; (c)  $f_s = 21$  kHz is optimized; (d)  $f_s = 18$  kHz but produces  $N_{OB}$  (e)  $f_s = 13.5$  kHz produces inverted spectrum

have a signal comprising of two tones only, i.e, 21 kHz and 27 kHz such that there is no other information signal between these two tones. The central frequency  $f_c$  of our signal will be 24 kHz. In other word bandwidth of our signal is 6 kHz. Using Eq. 2.25, we can calculate various sampling rates shown in Table 2.1, which tells us that permissible sample rate may vary in between of 13.5 and 42 kHz. However, the complete range is not suitable or allowable and is further split in three sub-ranges, i.e, from 27-42 kHz, 18-21 kHz and 13.5- 14 kHz. Any sample rate below 13.5 kHz is unacceptable because that does not satisfy Eq. 2.25 as well as the basic Nyquist criterion of  $f_s \geq 2B$ . The aliases frequency or replica signals resulting from permissible sampling rates given in Table 2.1 are illustrated in Fig. 2.9. In Table 2.1, values of  $f_{s'}$  and  $f_{s''}$  are listed for m ranging from 1 to 5. It can



be noticed that we can select optimum values for  $m = 1, 2$  and  $3$  and for higher values of  $m$ , the signal will suffer aliasing-overlap because conditions imposed in Eq. 2.25 are violated. Similarly, spectra for sampling rates below  $2B$  is not shown because of guaranteed aliasing.

Finally, after determining permissible sampling ranges, we are able to select optimal frequency for each value of  $m$  as shown in the last column of Table 2.1. Here we refer to the term optimum sampling frequency in the same way as defined in [20]. It is the frequency where spectral replications do not butt up against each other except at zero Hz. As we see in Fig. 2.9(a), if the signal is sampled at the rate of 42 KHz it would certainly suffer out-of band noise (0- 15 kHz while using LPF), while the permissible sampling frequency of 27 kHz; makes the sampled signal to undergo subsequent digital signal processing like filtering operations and other processing much easier. This is because, our lowpass filter is designed for 0-  $f_s/2$  and may give more gain to the components below  $f_s/2 - B$  and starts attenuating the original signal closer to  $f_s/2$ . Also notice that for other two optimal frequencies, we observe spectral inversion. This spectral inversion occurs for all odd values of  $m$  as illustrated in Fig. 2.9(a), 2.9(b) and 2.9(e). For all even values of  $m$  the original positive spectral components of are symmetrical about the  $f = f_c$  or  $f = 0$ , no spectral inversion is possible. Thus any non-aliasing value for  $f_s$  from Eq. 2.25 can be selected.

Another method of illustrating the behaviour of Eq. (210) is to plot the normalized minimum sampling rate,  $(2fc + B)/(m + 1)$ , for values of  $m$ , as a function of newly introduced term bandwidth-normalized frequency component, ' $R$ ' defined as

$$R = (f_c + B/2)/B \quad (2.26)$$

and normalized sampling rate may be obtained from Eq. 2.25 by dividing  $f_s$  by the signal-bandwidth  $B$ . As a result, we acquire a curve whose axes are normalized to the bandwidth  $B$  marked as the solid-curve in Fig. 2.10. This figure presents the minimum normalized sampling frequency  $f_s$  as a function of the normalized highest frequency component present in the bandpass signal. It can also be witnessed that,

irrespective of the value of  $R$ , the minimum sampling frequency is always less than  $4B$  and tends towards  $2B$  with increase in the carrier frequency. Ironically, the minimum acceptable sample rate approaches towards  $2B$ , i.e, decreases as the carrier frequency increases.

In the light of our above discussion and observing the bold-gray line at  $f_s/B = 2.25$  in Fig. 2.10 we can infer by reviewing example depicted in Fig. 2.9 where  $R = 27/6 = 4.5$ . This  $R$  value is indicated by the gray line in Fig. 2.10 showing that for  $m = 3$  the ratio  $f_s/B$  is 2.25. With  $B = 6$  kHz, then, the minimum  $f_s = 13.5$  kHz in agreement with Table 2.4. The leftmost line in Fig. 2.10 shows the low-pass sampling case, where the sample rate  $f_s$  must be twice the signals highest frequency component. So the normalized sample rate  $f_s/B$  is twice the highest frequency component over  $B$  or  $2R$ .

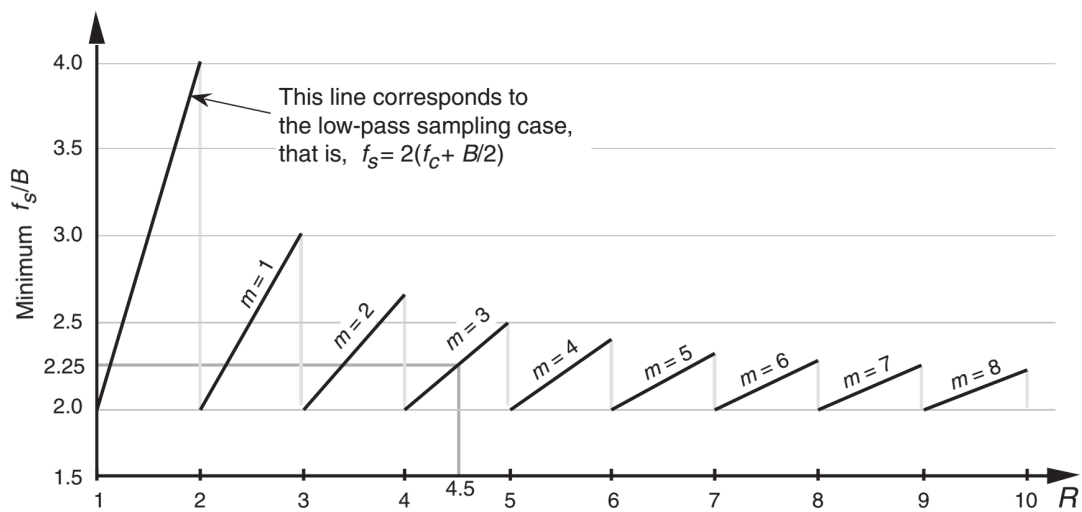


FIGURE 2.10: The minimum normalized sampling frequency  $f_s$  as a function of the normalized highest frequency.

Fig. 2.10 has been frequently referred in the literature, but at times it is possible that the viewer may jump to the false deduction, that all sample rates above the minimum rates as shown in the figure are acceptable.[21], [22], [23], [24], [25]. In order to avoid any such confusion, if we plot the permissible ranges of BPS frequencies as given in Eq. 2.25 as functions of  $R$ , we get the illustration shown in Fig. 2.11. As we notice from Eq. 2.25, Table 2.1, and Fig. 2.9, permissible BPS rates are the sequences of frequency ranges with gaps of undesirable sampling frequencies rates. It means a permissible BPS frequency has to be above the

minimum sampling frequency as depicted in Fig. 2.10, but it cannot be any random frequency of own choice above the minimum sampling frequency other than the defined range. The gray areas in Fig. 2.11 show the normalized BPS rates, which will be a root cause of spectral aliasing. Sample rates within the white areas of Fig. 2.11 are permissible. Therefore, in the case of BPS, we want our sample rate must be in the white regions linked with some value of  $m$  as prescribed by Eq. 2.25. The importance of Fig. 2.11 can be emphasized once again by considering bandpass signal example illustrated in Fig. 2.9. As shown in Fig. 2.12,  $R$  being the ratio of the highest frequency component and bandwidth  $B$  is 4.5, denoted by vertical line in gray colour. The gray line intersects the three acceptable sample frequency ranges alongwith the undesired sample rates (shown in gray shaded region). The same results can also be verified from the already calculated sample rates presented in Table 2.4. So we can claim that Fig. 2.11 gives a more clear illustration of bandpass sampling constraints as compared to that given in Fig. 2.10.

Although, Fig. 2.11 and 2.12 permit the use of sample rates those are set on the edges of white and gray-shaded regions; however, such sample rates should be avoided for all practical purposes. The major reasons for this is the non-ideal response of analogue bandpass filters (BPF), instabilities in sample rate clock-generator and the imperfections in A/D converters, which do not permit to achieve the exact cut off frequencies. It is, therefore, wise to keep  $f_s$  somewhat in the middle of the extreme limits.

Consider the BPS setup shown in Fig. 2.13a. The frequency response of typical analogue bandpass filter (BPF) is indicated by the gray colour line. Under such circumstances, it is wise to consider the filters bandwidth a little plus than the desired bandwidth  $B$  as shown in Fig 2.13b. The additional bandwidth, called as guard bandwidth is in fact used to compensate the shortcomings of our BPF due to its nonideal behaviour. This means that if we keep an additional bandwidth (based on roll off factor of BPF and other component limitations) on either side of the filter we can avoid any aliasing by a careful calculation as shown in Fig. 2.13d. This is just a brief description for the selection of sampling frequency.

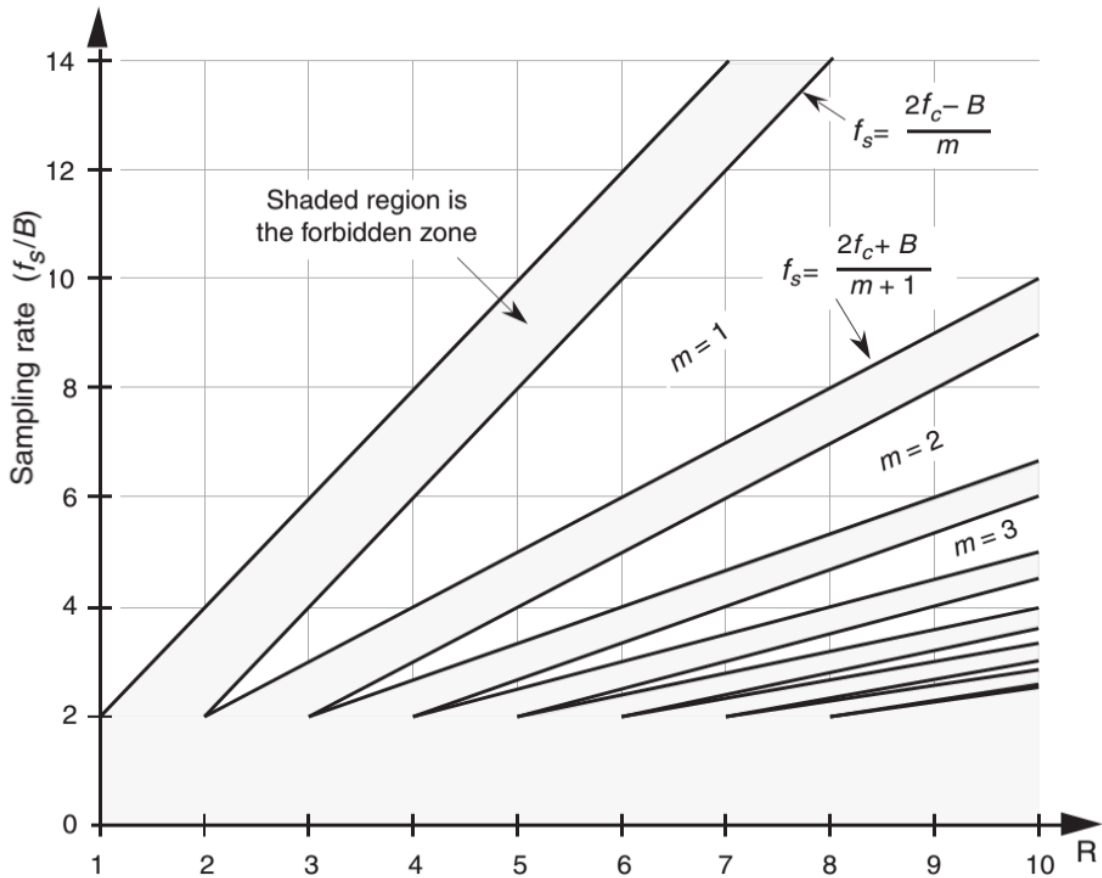


FIGURE 2.11: Useable sampling rates for BPS, normalized to the signal bandwidth ( $f_s/B$ ).

A comprehensive analysis, of how guard bandwidths and A/D clock parameters relate to the geometry of Figure 2.11 is available in [19].

Now let us see, how this guard band idea is applicable to Fig. 2.11. Examine one of the white wedges of it, for example, the one related to  $m = 1$ . The closer we select our sampling rate to the vertex of it, the more strict are the requirements of BPF design and vice versa. A more clear depiction is illustrated in Fig. 2.15. It can be noticed that if we set our sampling rate down towards the vertex of the white area we are more successful in acquiring a low sampling rate. Nonetheless, the closer we set our operating point to the boundary of a gray-shaded area, the lesser the margin we will have for the guard band, demanding a steeper analogue BPF. In addition, it needs strict compliance to the stability and accuracy of the analogue-to-digital clock generator. This implies, as a safety measure, we select some intermediate point, which is fairly optimized with reference to the sampling

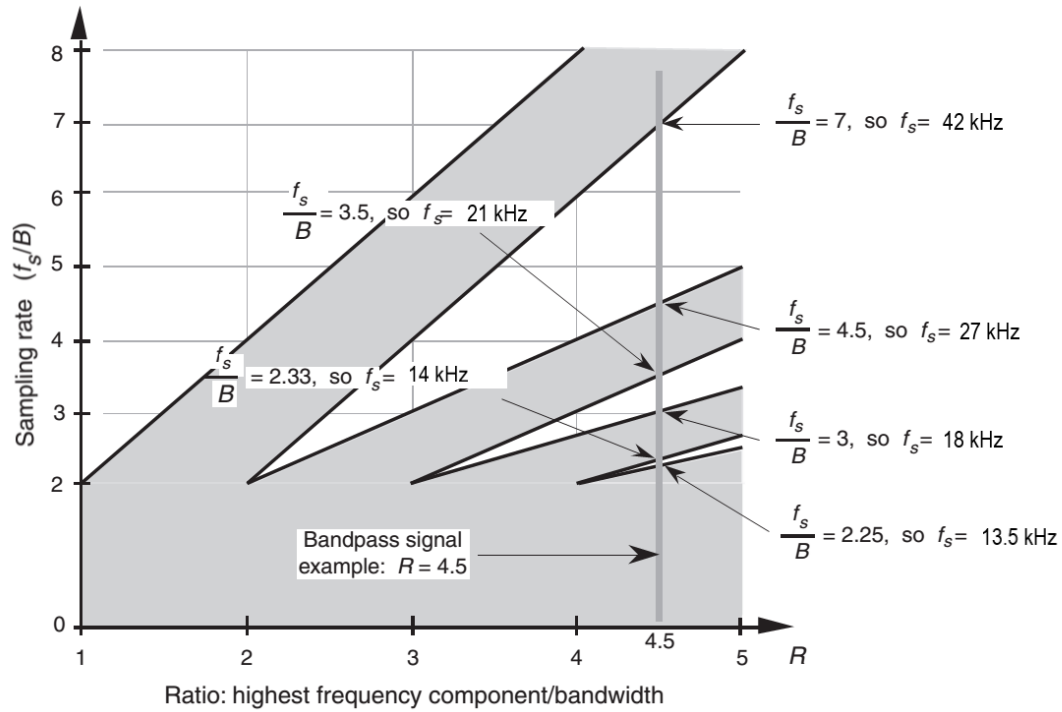


FIGURE 2.12: Useable sample rates for the bandpass signal of bandwidth 6 kHz and bandwidth-normalized frequency to  $R = 4.5$ .

rates and hardware constraints, away from the gray-shaded regions as shown in Fig. 2.14.

In order to ensure that we are not operating closer to the boundary, we have two options. Option one is to select the sampling rate in the center of the respective white-region for a given value of  $R$ . This can be accomplished by taking the mean value of the maximum and minimum sampling rates for a specific value of  $m$ , using Eq. 2.25, we get a sampling rate given as

$$f_{s,\text{cntr}} = \frac{1}{2} \left[ \frac{2f_c - B}{m} + \frac{2f_c + B}{m+1} \right] = \frac{2f_c - B/2}{m} + \frac{2f_c + B/2}{m+1} \quad (2.27)$$

The other option is that we evade the boundaries of Fig. 2.14 and by using the expression given below and find an intermediate  $f_{si}$  operating point:

$$f_{si} = 4f_c/m_{\text{odd}} \quad (2.28)$$

where  $m_{\text{odd}}$  is an odd integer [26]. Using Eq. 2.28 leads to an interesting conclusion

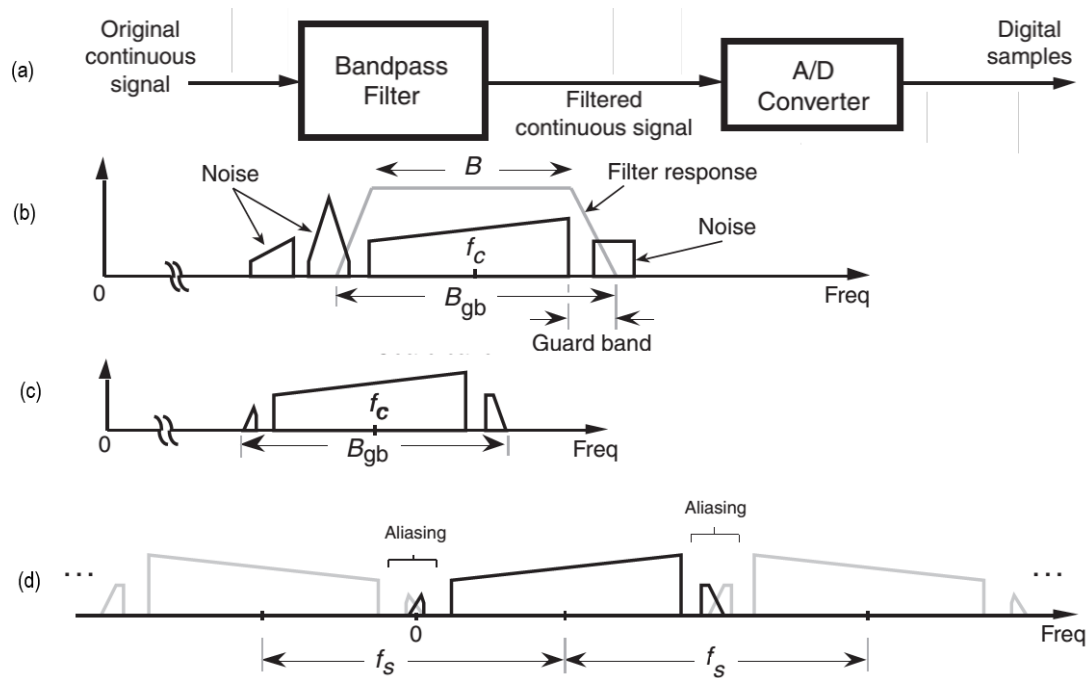


FIGURE 2.13: BPS with aliasing occurring only in the filter guard bands. (a) A typical BPS setup. (b) Spectrum of original continuous time signal showing bandpass filter response. (c) Spectrum of filtered continuous signal showing parts of in-band noise. (d) Spectrum of digital samples after A/D conversion.

that the spectrum of the sampled signal will be centered at one-fourth of the sample rate, i.e.,  $(f_{si}/4)$ . This situation is attractive because it greatly simplifies follow-on complex frequency translation down to the first Nyquist zone and is of great use in a number of applications pertaining to digital communications. However, the constraint of  $m_{\text{odd}}$  must ensure that the Nyquist restriction of  $f_{si} > 2B$  be satisfied.

## 2.3 The Concept of Aliasing-ambiguity

Aliasing is considered as a frequency-domain ambiguity that does not exist in time domain. The phenomenon occurs when a continuous signal  $x(t)$  is sampled at a uniform rate, then there exists a set of equally spaced values in the sequence obtained, which are a sub set of some other discrete sequence obtained by sampling some signal  $y(t)$ . To appreciate the effects of this ambiguity, we require some understanding pertaining to the nature of discrete sequences obtained as a result

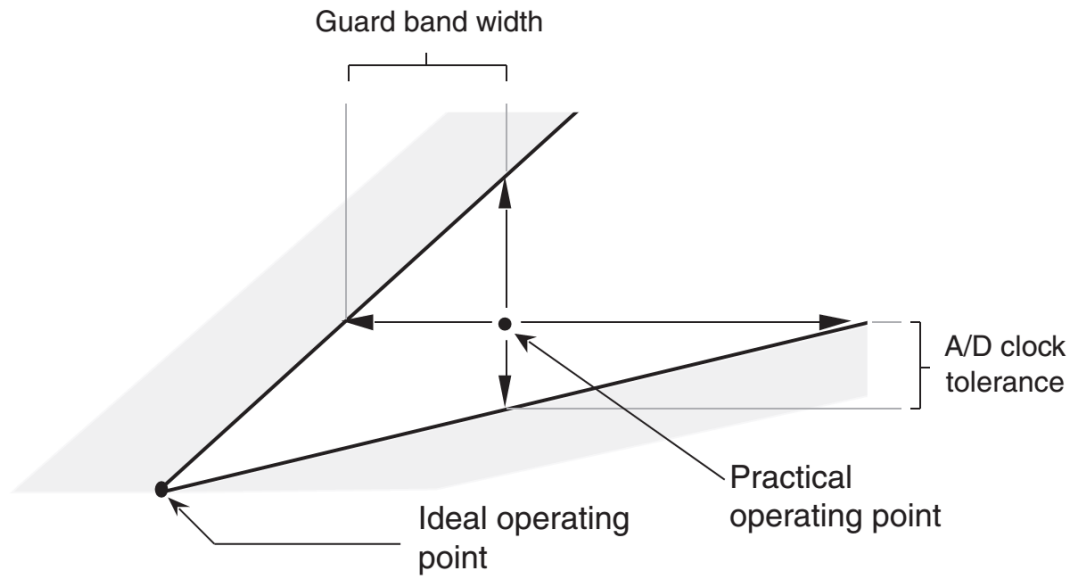


FIGURE 2.14: Typical operating point for  $f_s$  to compensate for nonideal hardware.

of sampling. Consider the following sequence of values obtained by sampling a sinewave at uniform periodic-intervals:-

$$\begin{aligned} \mathbf{x}[n] &= [x(0) \quad x(1) \quad x(2) \quad x(3) \quad x(4) \quad x(5) \quad x(6)] \\ &= [0 \quad 0.6695 \quad 0.6695 \quad 0 \quad -0.6695 \quad -0.6695 \quad 0] \end{aligned} \quad (2.29)$$

Now if we draw the sinewave by plotting the above mentioned sequence of discrete values shown with the help of stems in Fig. 2.16, it is not necessary that there exists only one sinewave of given frequency. In otherword, it is not mandatory that, the achieved sinewave is necessarily formed by using the above given sequence of values. In Fig. 2.17 we can see two sinusoids of frequency 2-kHz and 8-kHz, both are constructed from the same sequence of discrete values.

In order to have an analytical review, we derive an expression for this frequency-domain ambiguity. Let us have a continuous time-domain signal defined as

$$x(t) = \sin(2\pi f_0 t) = \sin(w_o t) \quad (2.30)$$

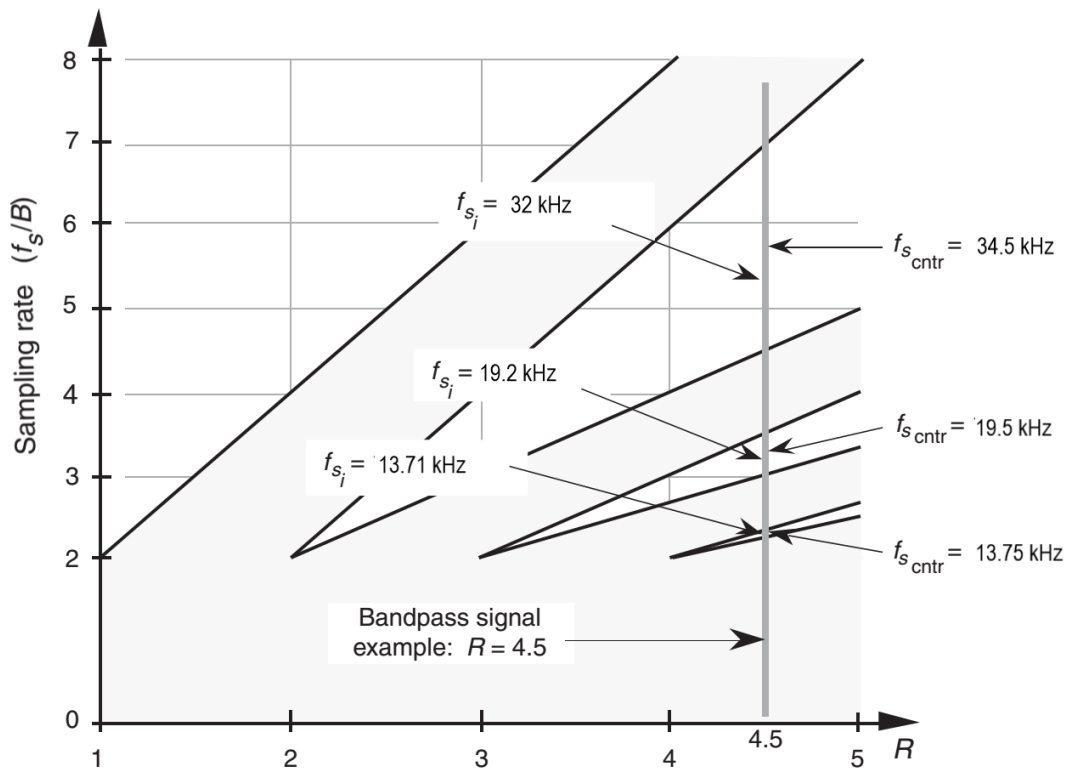


FIGURE 2.15: Intermediate  $f_{s_i}$  and  $f_{s,ctr}$  operating points, to evade operating beside the gray-shaded regions for the signal of bandwidth,  $B = 6$  kHz and bandwidth-normalized frequency  $R = 4.5$

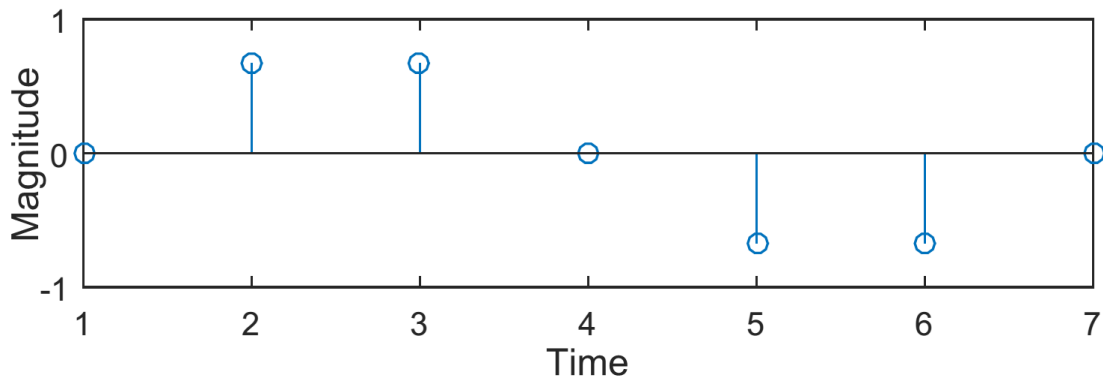


FIGURE 2.16: Discrete-time sequence of values

Now if we sample  $x(t)$  at a rate of  $f_s$  samples/s, that is, at uniform intervals of  $t_s$  seconds where  $t_s = 1/f_s$ . we obtain:

$$x(n) = \sin(2\pi f_0 n t_s) \tag{2.31}$$



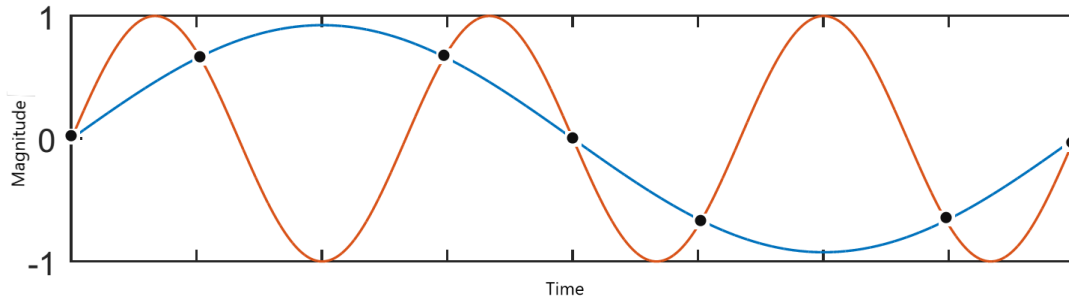


FIGURE 2.17: Different sinusoids created from same set of discrete values

Using the trigonometric identity,  $\sin(\theta) = \sin(\theta + 2\pi m)$  where  $m$  is any integer, we can write Eq. 2.31 as

$$x(n) = \sin(2\pi f_0 n t_s + 2\pi m) = \sin(2\pi(f_0 + m/n t_s) n t_s) \quad (2.32)$$

Now if we consider  $m$  as an integer multiple of  $n$ , so that  $m = kn$  and  $1/t_s = f_s$ , it is possible to replace the ratio  $m/n$  in Eq. 2.32 with  $k$  such that

$$x(n) = \sin(2\pi f_0 n t_s + 2\pi m) = \sin(2\pi(f_0 + k f_s) n t_s) \quad (2.33)$$

This shows that, factors  $f_0$  and  $(f_0 + k f_s)$  in Eq 2.33 are equal. This also implies that,  $x(n)$  sequence of equally spaced discrete samples values, present in a sinewave of  $f_0$  Hz, also exactly produces sinewaves at some other frequencies, namely,  $f_0 \pm k f_s$ . This relationship is of a paramount significance in the field of DSP and forms basis of sampling theory. In words, Eq. 2.33 states that

***When sampling at a rate of  $f_s$  samples/s, it is not possible to distinguish between the sampled values obtained from a sinusoid having a fundamental frequency  $f_0$  Hz and a sinewave of  $(f_0 \pm k f_s)$  Hz where  $k$  is any positive or negative integer.***

To illustrate further the impact of Eq. 2.33, we may use Fig. 2.17 and consider the sampling of a 6-kHz sinusoid at a sample rate of 8 kHz. A new set of samples is obtained, equally spaced at an interval of 125 microseconds. Their values are shown at intersection points alongwith another sinewave in Fig. 2.17. Now if we replace

6 kHz sinusoid with 2 kHz and sample it at the same rate, i.e, 8 kps kHz we notice that the discrete values remains same, i.e, intersection points of both sinusoid.

Comparing it with Eq. 2.33  $f_0 = 6$  kHz,  $f_s = 8$  kps, and  $k = -1$ , we notice that  $|f_0 \pm kf_s| = |[6 - 1(8)]| = 2$  kHz. This implies that 2 kHz is an alias of 6-kHz when sampled at the rate of 8 kps. In reality there is no processing scheme that can determine if the discrete values of given sequence, are output of 6 kHz or a 2 kHz sinusoid. If these amplitude values are applied to a DSP system that is capable of detecting energy at 2 kHz, the detector response would be positive, i.e., showing energy at 2 kHz.

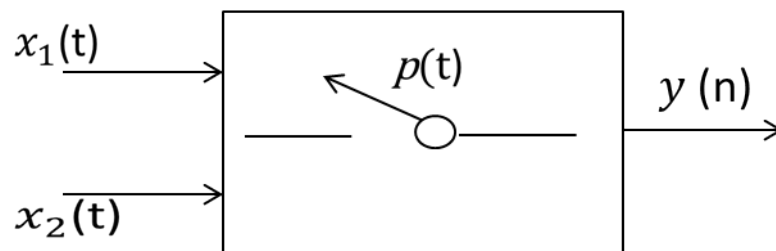


FIGURE 2.18: sampling process of two sinusoid

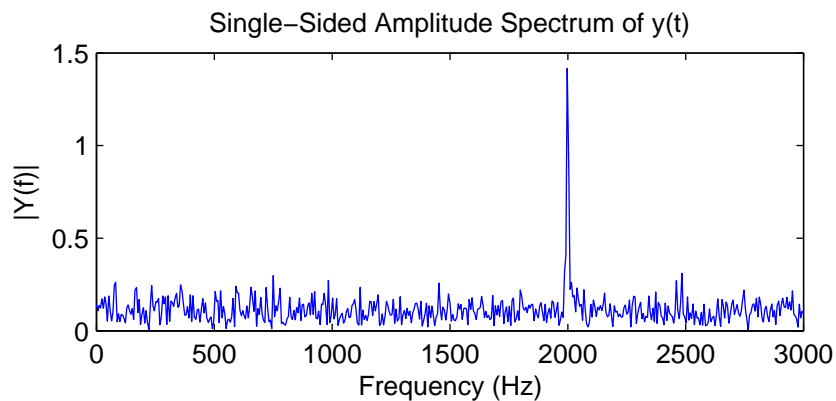


FIGURE 2.19: FFT spectrum showing energy at 2kHz only

Now let us apply both sinusoid to a processing system, which can determine spectrum of the given input. If  $p(t)$  is the sampling pulse and  $x_1(t)$  and  $x_2(t)$  are inputs to the system, we can find out the sampling sequence  $y(n)$  as shown in Fig. 2.18. Using the same sampling rate of 8 kps kHz and input sinusoid of 2 kHz and 6 kHz, we see that there is only one out put present at 2 kHz. In fact, most of the

spectrum-analyzer instruments specially oscilloscopes display energy with respect to the first Nyquist zone, which is limited to the  $f_s/2$ . In this case, the first alias of 6 kHz is 2 kHz and both sinusoid completely overlap as shown in Fig. 2.19.

Mathematically, we may conclude that for any sampling frequency,  $f_s$  we can decompose or write the carrier frequency  $f_c$  as

$$f_c = m(f_s/2) \pm \epsilon \quad (2.34)$$

where  $m$  is the highest odd integer such that  $f_s/2 \geq \epsilon$  then

$$f_a = f_s/2 - \epsilon \quad (2.35)$$

where  $f_a$  is aliasing frequency

#### Example 2.1

Let  $f_c = 300$  kHz and  $f_s = 96$  kHz, then we can write  $f_c$  as follow

$$f_c = 7(48) \text{ kHz} - 36 \text{ kHz}$$

therefore  $f_a = 48 - 36 \text{ kHz} = 12 \text{ kHz}$

#### Example 2.2

Let  $f_c = 300$  kHz and  $f_s = 172$  kHz, then we can write  $f_c$  as follow

$$f_c = 3(86) \text{ kHz} + 42 \text{ kHz}$$

therefore  $f_a = 86 \text{ kHz} - 42 \text{ kHz} = 44 \text{ kHz}$

In the literature, this phenomenon is also known as folding, since  $f_a$  is a mirror image of  $f_c$  about  $f_s/2$ . The sampling theory proposed by Shannon is also applicable for the case of an uneven sampling, that is, the case, when samples taken are not equally spaced in the time domain. In the literature, this is known as nonuniform sampling (NUS). According to Shannon theory for non-uniform sampling a band-limited signal whose  $X(f) = 0$  outside the SOI, can be perfectly reconstructed from its discrete sequence provided that, the average sampling rate satisfies the Nyquist condition [27]. This leads us to the conclusion that, it might be easier to develop reconstruction algorithms for uniformly spaced samples but it is not

a necessary or sufficient condition for perfect reconstruction. For an ideal NUS process,  $t_s(n) = t_n \neq nT_s$ . In the case of NUS, the frequency spectrum of  $x_s(t)$  is not necessarily periodic and the Fourier transform becomes

$$X_s(f) = \sum_{n=-\infty}^{\infty} x(t_n)e^{j2\pi f t_n}. \quad (2.36)$$

In the case of NUS the corresponding Energy Density Spectrum can be obtained by taking the square of the magnitude of the Fourier transform [28], i.e.,

$$\begin{aligned} E_s(f) &= |X_s(f)|^2 = [\dots + x(t_0) \cos 2\pi f t_0 + x(t_1) \cos 2\pi f t_1 \\ &+ x(t_2) \cos 2\pi f t_2 + \dots + x(t_n) \cos 2\pi f t_n + \dots]^2 \\ &+ [\dots + x(t_0) \sin 2\pi f t_0 + x(t_1) \sin 2\pi f t_1 \\ &+ x(t_2) \sin 2\pi f t_2 + \dots + x(t_n) \sin 2\pi f t_n + \dots]^2 \dots \end{aligned} \quad (2.37)$$

Non-uniform Sampling technique is well used in spectrograms for spectral analysis and also for obtaining oscillograms in oscilloscopes [29]. As described in [30], that when we sample a signal at the recommended Nyquist rate there will always be an aliasing error till the signal is ideally band-limited. So in order to avoid such odds for alias-free sampling, selected criterion must be based on unequally spaced instants of time referred as NUS. The aperiodic attribute of the frequency spectrum enables NUS to overpower the interfering signal spectrum caused by intentional or unintentional aliasing.

## 2.4 Receivers Architectures

a. **Superheterodyne receiver architecture.** This kind of receiver uses two stages to translates the signal to a low frequency band by down-conversion mixing. Generally, the second IF of a dual-IF superheterodyne receiver is equal to zero. In the such case, demodulation and detection are carried out at base-band level. Figure 2.20 illustrates the superheterodyne architecture as zero IF receiver.

In the zero IF architecture, second down-conversion is performed through quadrature mixers, which have a  $\pi/2$  radians phase shift between its LOs signals. Consequently, any offset of I and Q components from the nominal phase shift ( $\pi/2$ ) radians or amplitude mismatches shall produce the Bit Error Rate (BER). However, if the second IF is higher than zero (mostly by a frequency gap of more than the signal-bandwidth), the architecture may be considered as a digital-IF receiver. In the such case the IF bandpass signal is processed by an ADC, and the I/Q mismatches can be circumvented by signal processing in the digital domain.

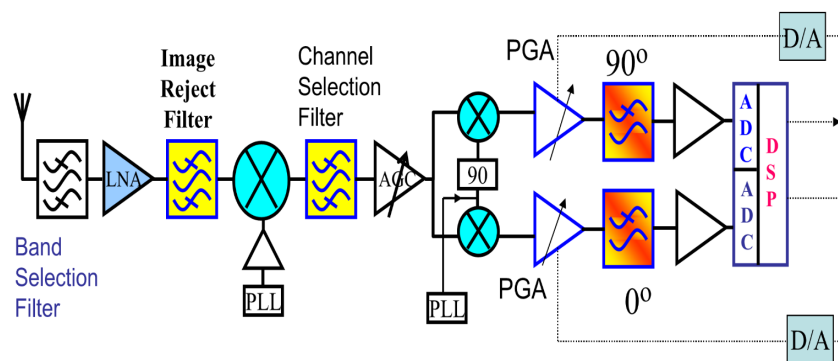


FIGURE 2.20: A conventional dual IF superheterodyne receiver with second IF as zero

b. **An homodyne receiver architecture.** An homodyne receiver may be the other choice, where there is no IF stage between passband and base-band. The input to the ADC is fed at base-band, as shown in the Fig. 2.21. This has a major advantage over the superheterodyne receiver, *i.e.*, image problem can be eliminated because of zero IF, consequently no IRF required. However, homodyne receiver gets effected from the problems of DC-offset and LO leakage. The leaked signal gets mixed with the output of the LO and generates a DC component. This undesired DC component and DC off set have adverse affect on the information signal.

c. **Low-IF receivers.** In the low-IF receiver, a low IF stage is cascaded between passband and base-band. The low IF signal is first filtered, amplified and then digitized by an ADC as shown in the Fig. 2.22. After this, frequency translation from the low-IF to base-band makes it more convenient to tackle problems in

digital domain, such as I/Q mismatches which are mostly found in the analogue domain. This design also offers some advantages in terms of simplicity and higher level integration with modern receivers. Moreover, low-IF receivers as compared to homo-dyne receivers, have no DC-offset issues since the signal after the first down-conversion is still considerably higher than DC. However, in low-IF receivers the IF is very low (it may be 1-2 times the information signal bandwidth), and this rises an issue of image-signal rejection in the RF bandpass filter. In this case, both the image and the wanted signal may be sampled and quantized in the ADC.

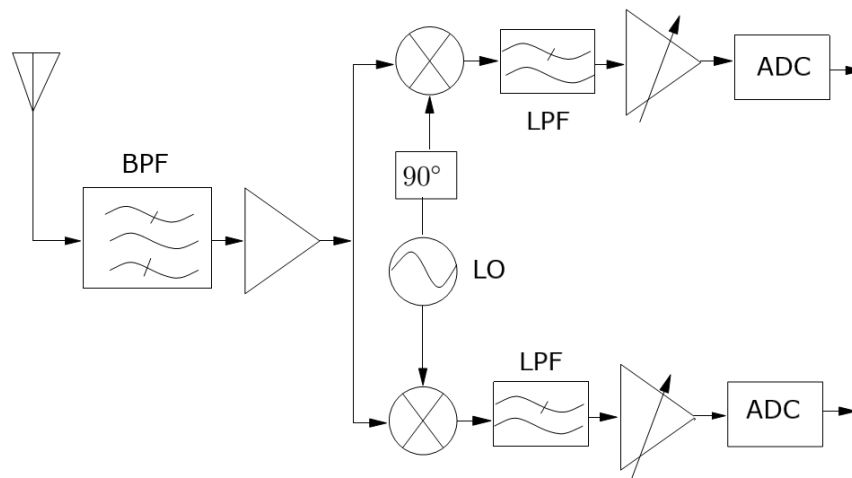


FIGURE 2.21: Homodyne receiver architecture with reduced discrete components

d. **Wideband IF receiver.** This architecture may be considered as an alternate to superhetrodyne receiver based on IF receiver architecture. In the wideband IF receiver, the entire RF-band containing the information signal is down-converted to IF. This is accomplished by multiplying the output of the first LO with a fixed frequency. The IF signal passes through a LPF such that the frequency components higher than the IF are filtered out. The desired channel out of the complete band is then further down-converted to DC using a tunable LO and fed into an LPF. The selected channel signal, which is frequency-translated is then processed by an ADC in the same fashion, as is carried out in the conventional superheterodyne or homo-dyne receivers.

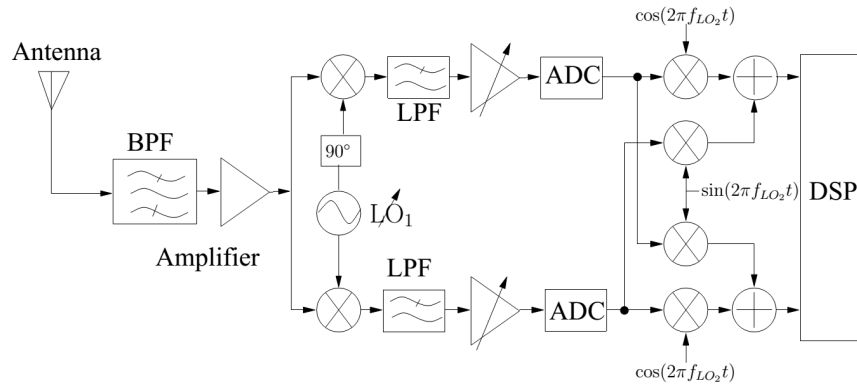


FIGURE 2.22: Low-IF receiver architecture

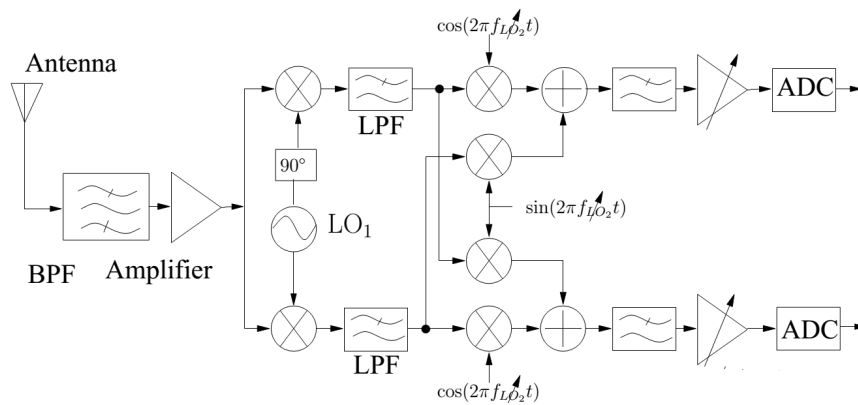


FIGURE 2.23: Wideband IF receiver architecture

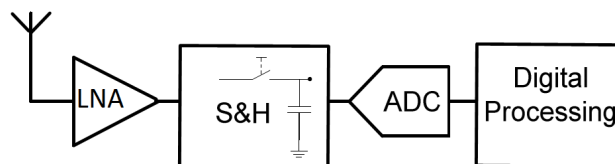


FIGURE 2.24: A sub-sampling SDR architecture

e. **Sub-sampling receiver architecture.** This architecture is mostly used in SDR. Two major concerns of SDR are position of the ADC with reference to antenna and DSP efficiency to deal with the higher sampling rate [31]. One of the solution is to place the ADC as close as possible to the antenna. Ideally both sampling and digitization are performed simultaneously on the RF signal. This however demands an ADC with a higher dynamic range because of the presence of strong interfering signals around desired SOI. Although this is possible to achieve with the present technology, however, it is not advisable in most of the cases. It is more reasonable to do an IF digitization as shown in Fig. 2.25. The sampling

function can be either classic lowpass sampling or bandpass sampling. In the case of LPS, the output of the BPF at IF stage is directly sampled and digitized by an ADC. The direct down-conversion and digitization is useful to overcome the problem of I/Q mismatches. However, in this case sampling rate on an IF bandpass signal is significantly high, based on Shannons sampling theorem, using interpolation formula. This leads to certain restrictions on the performance requirements of ADC, e.g., linearity and dynamic range etc. In the case of bandpass sampling the requirements on the digitizing ADC are relaxed due to a low sampling rate that is only slightly greater than twice the information bandwidth. It can be noticed

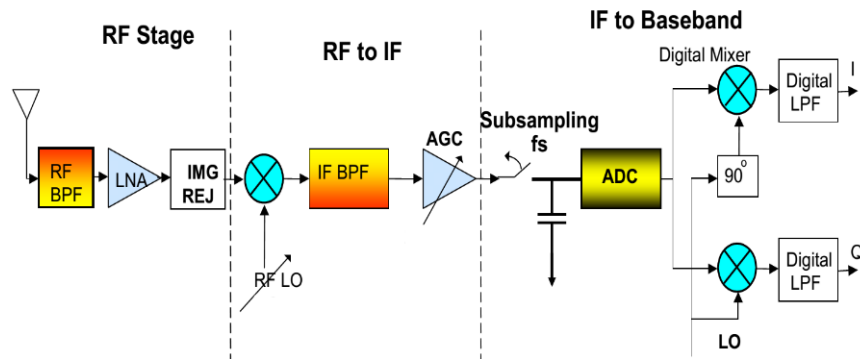


FIGURE 2.25: Subsampling receiver architecture

that out of the all of the above mentioned architecture only sub-sampling SDR architecture provides an opportunity to place the ADC as close to the antenna as possible. Moreover number of discrete components are considerably reduced in this type of architecture. However, still there are some constraints which needs to be settled. Mostly, these constraints are related to the sampling methodology; such that there would not be any frequency aliasing-overlap after down-conversion of complete SOI in the base-band.

## 2.5 Bandpass Sampling for Multiple RF Signals

Classical sampling techniques discussed till now are limited and applicable to a a spectrum composed of single band or signal. Consider an RF spectrum comprising  $N$  bandpass signals which are positioned in a nonlinear fashion and each signal



has a bandwidth  $W_1, W_2, \dots, W_N = B$ . These bandpass signals are spaced in such a fashion that their frequency separation  $\Delta f = f_{l_{i+1}} - f_{l_i} \gg W_k$ . Fig. 2.26 illustrates the spectral layout of the system, that is sparse in nature such that  $f_{l_1}$  is the lowest frequency of signal  $X_1^+$  and highest frequency in the spectrum under consideration is  $f_{h_N}$  belongs to the signal  $X_N^+$ .

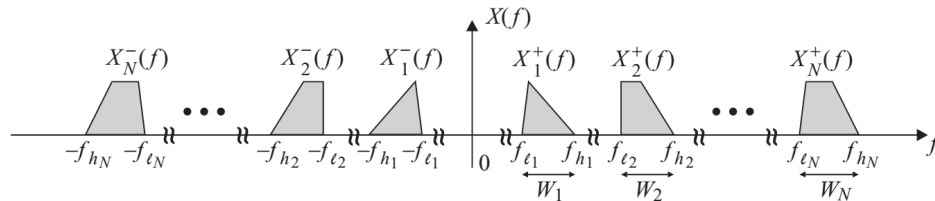


FIGURE 2.26: Passband spectrum of multiple RF bandpass signal

The basic rules for downconversion of such a spectrum using software-defined radio (SDR) are introduced in [32]. First, the ADC should be placed as near the antenna as feasible in the chain of radio frequency front-end circuitry. Second, the resulting samples should be processed on a programmable micro or signal processor. These two guidelines enables the realization of all the benefits associated with the SDR. If we desire to down-convert two contiguous bandpass signals  $X_{N-1}^+$  and  $X_N^+$  to the baseband, then there are two major factors which require our attention. One is the receiver architecture and other is the sampling technique. Using an efficient receiver architecture supplemented by appropriate sampling methodology enables us to utilize our maximum SOI; while committing minimum resources in terms of hardware and processing time etc. The common constraints, which are frequently referred in the literature, [32], [33] for direct downconversion of multiple RF signal generally known as ‘boundary constraint’ and ‘neighbourhood constraints’ can be described as follows:

### 2.5.1 Boundary constraint.

This constraint applies to the both single and multiple signals in the SOI. Boundary constraint implies that in the process of bandpass sampling none of the replicas of  $X_i^+(f)$  and  $X_i^-(f)$  should overlap at the edges of first-Nyquist zone i.e.  $[0, f_s/2)$

as illustrated in Fig. 2.27. Similarly in the case of multiple signals as shown in Fig. 2.28 it is mandatory that all replicas are completely positioned within  $[0, f_s/2)$ , else if 0 or  $f_s/2$  is contained inside the band of these replicas, there will be spectrum folding resulting in loss of information. Moreover, the center frequency of the replicas of  $X_k^+(f)$  or  $X_k^-(f)$  for  $k = 1, 2, 3, \dots, N$  should be positioned at a gap of  $B/2$  from either side of the first-Nyquist zone. Mathematically, this constraint is expressed by the following set of equations:

$$0 \leq f_{IF} - B/2 \tag{2.38}$$

$$f_s/2 \geq f_{IF} + B/2 \tag{2.39}$$

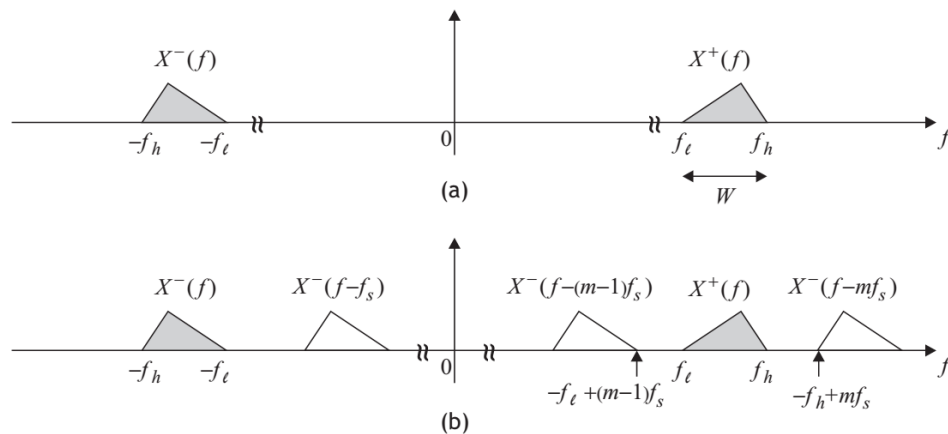


FIGURE 2.27: Spectrum of single bandpass signal (a) Prior to sampling (b) After sampling at  $f_s$

### 2.5.2 Neighborhood constraint.

This constraint is relevant only to the multiple RF signals in the SOI. Neighborhood constraint implies that any of the replicas of  $X_i(f)$  and  $X_j(f)$  should not overlap to its adjacent replica in the first-Nyquist zone i.e.  $[0, f_s/2)$ . For example as illustrated in the Fig. 2.28,  $X_i^-(f)$  should circumvent any overlap with  $X_{i+1}^-(f)$

for  $i = 1, 2, \dots, N - 1$ . Mathematically, it is defined as:

$$W_i/2 + W_{i+1}/2 \leq f_{IF_i} - f_{IF_{i+1}} \quad (2.40)$$

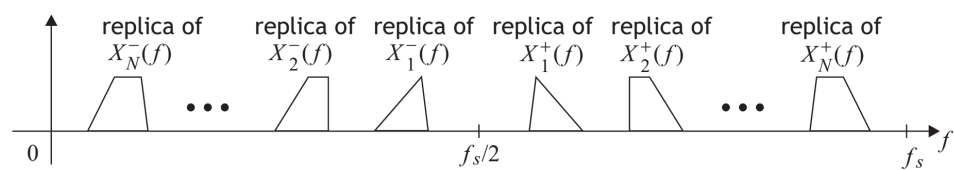


FIGURE 2.28: Downconverted spectrum of multiple RF signal using bandpass sampling

# Chapter 3

## Literature Review and Problem Formulation

### 3.1 Literature Survey.

In communication systems (voice, data, image, video), quality of communication i.e., whether the reconstructed signal distinctively characterizes the actual signal or not. This reconstruction with maximum matching to the actual signal is mainly dependent on the sampling features and their realizations in hardware. On the basis of this pretext, our literature survey may be broadly divided into three major parts; Part-I, Part-II, and Part-III. Part-I is generally limited to the contemporary sampling techniques and their evolution, Part-II presents down-conversion of multiple RF signals using subsampling techniques and Part-III refers to the applications of these techniques in various hardware architectures.

#### 3.1.1 Evolution of the Sampling Techniques

Keeping in view the sampling interval (or period), sampling can be ideally categorized into two classes, Non-Uniform Sampling (NUS) and Uniform Sampling (US).

According to the Shannons sampling theorem [34], any signal  $x(t)$ , which is band-limited to the bandwidth  $[-B, B]$  can be completely reconstructed from uniform sequence of values attained with the sampling rate that is at least two times of the maximum bandwidth. The reconstruction of  $x(t)$  is done by convolving the sampled sequence with a sinc function. This process is equivalent to an ideal low-pass filtering process in frequency domain. The reconstruction formula derived by Whittaker is given by

$$x(t) = \sum_{n=-\infty}^{\infty} x(nT_s) \text{sinc}(2B(t - nT_s)), \quad (3.1)$$

where  $\text{sinc}(x) = \sin(x)/x$  and the inter-sample time interval is given by  $T_s = 1/2B$ . Besides Shannons theorem on bandpass sampling, there exist several other methods to extract the data from the parent signal and yet are able to reconstruct the signal. These include, but are not limited to the nonuniform sampling or derivative sampling, where, the samples from the signal and its derivative at half the Nyquist rate at least for each can also uniquely determine the signal without corrupting the original signal. However, in the case of NUS, it is an uphill task to choose the non-uniformly distributed sampling technique in which, the input band-limited signal is exclusively identified from the sampled values without any destructive effects of aliasing. For instance, application of a sampling point process obtained by deliberate introduction of random fluctuations into a periodic point process do not lead to elimination of aliasing.

In the area of NUS, Shapiro and Silverman [35], were amongst the first researchers who claimed that it might be possible to perform the aliasing free sampling of random noise. In their work, they showed the reality of expanding the frequency range where, signal processing is not corrupted by aliasing. The general theory for non-baseband and nonuniform samples was developed in 1967 by Henry Landau. He proved that the average sampling rate (uniform or otherwise) must be twice the occupied bandwidth of the signal, assuming it is a priori known what portion of the spectrum was occupied[36]. Beutler [37]considered the general problem of alias-free sampling and presented criteria for alias-free sampling relative to various families of spectral distributions. Marsy [38], [39], further extended the work in

[37], for reconstruction of signals to a broad class of random sampling schemes, by keeping the sampling intervals dependent and showed that random sampling scheme is "alias free" relative to various families of spectra. It was further shown that the alias free property of this class (composed of independent sampling intervals) of sampling schemes is invariant under random deletion of samples. Shapiro [35] in his work also described that there are random sampling schemes, like Poisson sampling, which may eliminate aliasing and lead to a uniquely identifiable power spectral density.

Other approaches in use for the reconstruction of the analogue signal, taken from the NUS can be divided into three classes: interpolation (Spline Interpolating, Gridding Algorithm) [40], [41], [42], iterative (Iterative Algorithms)[43], and svd methods (Minimum-Energy Signals, Least Square Reconstruction Algorithm) [44], [45]. Besides these approaches significant efforts are made to reconstruct the signal from level crossing (LC) and zero crossing (ZC) using NUS [46]. Unfortunately, recovery of the signal from the level crossing information is not always robust to sampling noise and timing quantization. Logans theorem [47], provides no robustness guarantee for the reconstruction performance. In [48] attempt to make use of sparsity-based signal reconstruction from ZCs is made. However, the proposed algorithm being dependent on ZCs is not able to guarantee the reconstruction performance for the recovery of original signal. Such reconstruction algorithms need more number of samples so as to solve an overdetermined system of equations and have convergence dependent on choosing of algorithm parameters[46]. On the other hand, in the case of US, bandpass-sampling theory is well developed for a single RF signal that is to be down-converted with significantly-reduced sampling rate. Factually, it was Cauchy to had been the pioneer to theorise the bandpass sampling conditions [49], in the middle of last century. Besides, Nyquist [50], and Gabor [51], in their classic work, also mentioned the scenario of band pass sampling. Later, Kohlenberg [52], introduced second order sampling and provided the basic interpolation formula, which was then reported in the text by Goldman and Middleton [53]. Quadrature sampling was introduced by Grace and Pit [54] as a specific type of Kohlenberg's second-order sampling. The authors found a limit

to the minimum sampling rate  $f_s = 1/a$  for a given bandwidth  $B$  around carrier frequency  $f_c$ , such that  $f_s \leq B$ . The sampling of bandpass signal with reference to band position was first discussed by Vaughan *et al.* [55]. The authors, presented the acceptable and unacceptable using the first-order sampling. A specific emphasis was also given to practical sampling rates, which were nonminimum. In a number of text books, such as [56], state that for general cases, the minimum sampling frequency is

$$f_s = \frac{2f_u}{\left\lfloor \frac{f_u}{2f_B} \right\rfloor}, \quad (3.2)$$

where  $\lfloor func \rfloor$  stands for the largest integer not bigger than  $func$ . In reality, Eq. 3.2 only determines the lowest sampling frequency, and aliasing may occur for higher sampling frequencies [57]. Gaskill [58] modified Eq. 3.2 to yield the range of sampling frequencies for which aliasing can be circumvented. Authors in [55] describe additional restrictions and some stiff requirements on the front-end hardware due to bandpass sampling in terms of the bandpass filters and ADC. They insisted that bandpass filters with high Q factor should be centered at the carrier frequencies requiring narrow passbands, thereby requiring precise center frequencies and a high Q factor. The ADC input bandwidth needs to be very high, of the order of carrier frequencies of the bandpass signals. This increases complexity, hardware noise and power consumption.

### 3.1.2 Bandpass Sampling for Multiband Sparse Spectrum

In the past decade, several algorithms have been introduced for multiple signals to arrange each spectrum properly in a necessary order and find suitable sampling frequency for the direct down-conversion of spectrum of interest (SOI) [32, 59–61]. In [32], a basic method was proposed by Akos *et al.* that could check whether a sampling frequency could be available or not for the aliasing-free down-conversion of multiple RF signals using bandpass sampling. However, this method was not able to find valid frequency ranges. In the subsequent research work it was also observed that the complexity for finding the sampling frequency to simultaneously

down convert multiple bandpass signals using bandpass sampling also increases with number of input signals. In order to obtain the formula for the ranges of valid BPS frequency, Tseng *et. al* in [59], proposed an algorithm that was useful to thoroughly analyze the relations between the frequencies on the edges of each radio frequency signal. For  $N$  bandpass signals, a numerical solution for the sampling frequency was obtained by solving  $3 + (N/2)$  constraint equations. Often, these constraints could lead to considerable oversampling requirements i.e., the solution needed much higher sampling frequency than the sum of sampling rates required by all desired signals. Higher sampling rate not only increased the ADC complexity but also required higher DSP speeds, thereby also increasing the power consumption and processing time. In the technologies, introduced in the beginning of this century, maximum sampling frequencies were of the order of a few tens to a few hundreds of MHz. The passband frequencies used were also limited to a few thousands of MHz range, created suitable conditions to bandpass sub-sampling concepts [59, 60]. This, in turn, set relatively high demands for RF band-limitation filtering, prior to sampling, to control harmful aliasing effects. In addition to filtering requirements, the power consumption of the sampling circuitry itself could be somewhat higher, as compared to ordinary low-frequency or baseband sampling approaches. This is because the usable sub-sampling frequencies depend essentially on both the signal bandwidth and center-frequency, and are typically somewhat higher than the corresponding minimum sampling rates in ordinary low-frequency sampling.

In real bandpass sampling, not all the sampling frequencies between the minimum frequency ( $f_{s(min)} = f_H/n$ ) and Nyquist frequency ( $2f_H$ ) are allowed. This is because for some sampling frequencies, the aliasing occurs at the negative frequency part overlapping its positive frequency part. However, if sampling is applied to the single sideband signal, the complex bandpass sampled signal cannot generate aliasing if the sampling frequency is larger than bandwidth ( $f_H - f_L$ ). Hence, the constraints of real sampling could be easily relaxed. Consequently, the method presented in [59] can be much simplified. In [61], [62] the authors used graphical method to describe the useable sampling frequency ranges for each RF signal. By



overlapping the graphs of all desired signals, the intersection points of the graphs are obtained. The frequency available within the ranges of the intersection is the valid sampling frequency and may be considered suitable for all RF signals. However, this method is of less practical use, especially in the scenarios where large number of RF signals are to be down-converted or when the bandwidth of RF signal is too less than the  $f_H$ . In fact in such cases, it is very difficult to find the ranges of intersection or there may be large number of intersections to be identified correctly. In [63] Mahajan *et al.* proposed a front-end technique to directly down-convert frequency division multiplexed (FDM) signals. A down-conversion function was proposed in to simplify the down-conversion of multiband signals when the member bandpass signals are separated by a frequency larger than the sampling frequency. This imposed an additional constraint of a certain minimum frequency separation. In addition, an exclusive function for simultaneous down-conversion was derived to acquire aliasing-free signals in the baseband. Their proposed technique was based on DSP in the baseband and required a simple bank of parallel BPF and an ADC, which had baseband input as compared to bandpass sampling. It is a fact that, the baseband processing has an edge over pass-band that imposes BPF requirement of higher 'Q' factor and an ADC which can deal with pass-band RF inputs. However, the proposed method could not guarantee or claim about the minimum sampling rate and had a strict requirement of minimum frequency separation between the desired signals in the pass-band.

In [33], Lin *et al.* proposed an iterative algorithm for finding the minimum sampling rates of an RF spectrum that consisted of multiple band-pass signals. It had important application in SDR, where it was suitable to down-convert multiple bandpass signals simultaneously. In their proposed work, the authors derived a set of conditions for alias-free sampling. The minimum sampling frequency could be found by iteratively increasing the sampling frequency to meet the alias-free conditions [64]. It is easy to see that such methods may become increasingly more complex and harder with increase in the number of channels. Since, most of the work in the field of bandpass sampling is limited to the spectrum which is non-linear in nature, therefore, no closed form formula could be ever developed

which may guarantee the ideal or lowest sampling rate. However, *muñoz et al.* in [65] provided minimum sub-Nyquist sampling rate in the context of evenly spaced equal-bandwidth multiband systems. The authors recommended necessary conditions to circumvent aliasing for channel allocation but those conditions are not sufficient to make use of complete SOI. In other words, their work is not universal in nature and is not applicable to a large sparse ratios between the information-bandwidth and lull-bandwidth. Later, in [66], the authors derived the analytical rules which guarantee that the minimum sub-Nyquist sampling frequency avoids aliasing. However, these equations were only valid for the restricted case of evenly-spaced equal-bandwidth multichannel systems. In their work, a general dual-band case was analyzed that computed the aliasing-free set of frequencies for given channel bandwidths and the spectrum parameters. Extending their work, the authors provided simple guidelines for more than two channels cases. In [67], a frequency selection method for multiband RF signals was presented. The method was based on a cylindrical surface spectrum and arc distance, introduced a 3D visual expression for cylindrical surface spectrum of digital signal, that reflects the circulatory nature of the spectrum of digital signals. A function of arc distance between two frequency bands was also introduced which was claimed to be useful in the determination of sampling frequency and design of digital filters. Lastly, an approach to find a minimum sampling frequency for multi-band signals was introduced in [68, 69]. Instead of using the conventional constraints, *i.e.*, neighbour and boundary conditions, a new set of constraints on the useable sampling frequency was derived. The authors used the geometric approach to the bandpass sampling theorem, while formulating the new constraints. This reformulation of the constraints on the useable sampling frequency represented the problem as an optimization problem which was structured by the geometric and mixed-integer nonlinear programming methods. The convex optimization problem was then solved by the proposed algorithm applying interior point approach in the line search framework. However, the geometric approach becomes complex with the increase in number of bands in the SOI.

### 3.1.3 Bandpass Sampling Application

As for as the applications of BPS are concerned, we conducted a literature survey that pertains to BPS dependent communication systems in general, and SDR receiver and GNSS receiver in particular. RF-transceiver front-end, which is mostly comprised of analogue circuitry does not get the full advantage from technological scaling. As a result, research progress in analogue blocks (front-end of transceivers) and base band blocks (Digital Base Band Processors), and the Application Processors (DSP block) has not been similar in the past years. The latter being utilized to deep-submicron technologies scaling enjoyed tremendous developments. At the same time, the improvements in the switching characteristics of metal oxide semiconductor transistors offer significant time accuracy, and photo-lithography offers precise control on the capacitance ratios. The key performance of many analogue circuits is directly dependent on precise capacitance ratios [70].

#### 3.1.3.1 General Purpose Communication Receiver

In general, the progression of multiband-multistandard receivers can be divided into two major areas. The first area, which is already covered above in section 3.1.1 focuses on the sampling techniques like lowpass sampling, bandpass sampling and quadrature-bandpass sampling [71, 72], used in digital receivers for down-conversion and digitization of analogue signal. The second area is about the improvements and modifications in the hardware-architecture of receivers. It encompasses heterodyne [73], intermediate frequency (IF) receivers [74], homodyne [75] and direct RF sampling receivers [76]. In direct RF sampling receivers, a very high flexibility and re-configurability are among the most desired attributes, this can be acquired when signals are sampled directly at RF stage. Moreover, due to the reduced quantity of FE analogue components, there is considerable reduction in the size of the radio as compared to many other contemporary radio designs, eventually giving an advantage in terms of lower power requirements, costs and reduced complexity. However, there are still, other issues that need attention in direct RF sampling receiver design and concept [77]. One is that, in the ultra high

frequency ranges of the signals to be sampled, there is a substantial increase in the timing inaccuracies or jitter produced in the sampling process that starts to limit the overall performance of the receiver and system to an noticeable extent. The random jitter, which accumulates during the generation and distribution of the clock signal limits the SNR performance at high frequencies. A locked histogram test revealed that for a 1.5 ps rms jitter in the system including the clock generator, the synthesizer, and the ADC chip, translates the system SNR from 55-dB (at 1 MHz input) to a 70-dB SNR at approximately 40 MHz [78].

A systematic approach to classify the receiver designs is also proposed in [79] facilitates useful insights into the interrelations between different architectural approaches, and the architectural trade-offs that affect system-level performance. The objective during all the development of any modern state of the art receiver has always been to acquire a design, which on one side has reduced noise, hardware complexity and power requirement, and on the other side can receive wide-band of electromagnetic spectrum. These two categories converge to configurable, multimode-wideband receivers, which are capable to simultaneously digitize and down-convert multiple signals [80–82]. Eventually this trend led to the development of a Software Defined Radio (SDR) architecture.

### 3.1.3.2 Software Defined Radio.

The process of RF sub-sampling is to sample a signal at the input stage in RF band and to translate it to a near baseband through intentional aliasing without involving any IF stage. This methodology can be reliably implemented on a bandpass RF signal with a sampling rate of only two times the information bandwidth, that is sufficiently less than the Nyquist rate [83]. In addition to providing an interface between the RF stage at the input and the ADC, the bandpass sub-sampling technique also provides more options of sampling rates for a multimode or multiband radio architecture, which is a fundamental feature in the design of cognitive radio. This concept has its major applications in Software Defined Radios (SDRs) development and design. An SDR is a re-configurable radio receiver or transmitter whose functions are mainly defined software driven, thus

supporting multistandard, multimode and multiband radio communications [84]. For an SDR, it is mandatory to have a wideband analogue frontend (FE) and an A/D converter to allow a variety of signals from various systems to be processed. Considering the above mentioned development pattern, it was who Mitola first envisioned the idea of an SDR in 1995. The SDR, which was initially conceived for military communication and applications [85], has the provision of changing its functionality through replacement of the waveforms and hence provides a relatively swift and economical way to adopt the rapidly emerging mobile communication standards. In military and commercial wireless communication systems, there is a requirement for a single radio to communicate simultaneously with nets of different radios using different RF bands and different modulation techniques [86–88]. To achieve this goal, methods for direct down conversion of multiband RF signals using a single ADC has attained a lot of significance. Later, the use of an SDR concept in cellular applications has been a topic of interest for the last two decades. In [88], authors studied the two key issues in the implementation of a software radio. The first issue is the development of optimal receiver design that demands the least possible number of bits in the wide-band A/D convertor and the second is efficient channelizer that is capable of extracting individual channels from the digitized wide-band signal. A large portion of the the RF front-end and base band block become digital, by placing an A/D converter right after to the antenna. The A/D converter requirement for a BPS receiver is also studied in [89]. It is clear that the desired performance out of an A/D convertor should meet the exceptional specifications, particularly in the present scenario this turns into a mismatched relation that is desired in the context of energy-efficient solution[90]. Digital communication standards, with the exception of ultra wide band wireless standards for RF spectrum are authorized the frequency ranges from 800 MHz to 6000 MHz, however, for a single the bandwidth is limited to a maximum of 20 MHz. Therefore, in order to have multistandard digital circuitry demodulation and base band processing can be managed to this lesser frequency range of a few MHz. Signal processing operations prior to the A/D convertor in the real sense can be limited to amplification, filtering and down-conversion. Therefore, we can

visualize the scope of maximizing the flexibility and re-configurability while minimizing the power requirements, size and hardware complexity are some of the major design attributes. In modern radio transceivers, the over all implementation of the software defined concept is mainly limited by the FE. In fact, designing a flexible FE in classic ways is challenging because of the narrow bandwidth of intermediate frequency (IF) filters and limited range of the frequency synthesizers [91], [92].

### 3.1.3.3 Bandpass Sampling and GNSS Receivers

GNSS is another area, where multiple signals are accommodated and processed and hence involves the sub-sampling. As an SDR supports multiband radio communication and defines radio functionality in software, therefore it allows the development of reconfigurable GNSS terminals [93]. In the mass market, there are few commercial products that support more than one GNSS signal, such as the MAX2769 [94] that supports GPS, GLONASS and Galileo radio signals. Literature [95–97] describe multiband GNSS receiver solutions. Fundamentally, the navigational signals transmitted by these systems uses the same trilateration positioning principles as that of the GPS but they differ in terms of signal parameters like frequency, bandwidth and modulation etc, resulting in receivers design specially RF front end not being fully compatible with the other systems. At the same time, the combination of the various GNSS signals in a single GNSS receiver can help to satisfy the user requirement to a great extent. That is the reason, a universal GNSS receiver design is essential that could receive and process multiple signals from various navigation systems. However, one major restriction in the design of a universal GNSS receiver is the RF front end, which may be either complex or have limitations for covering all GNSS bands and signals. In [95] Barrak et al, propose a GNSS sub-sampling receiver. A hard-wire sub-sampling frequency is selected through iterative algorithms and used to down convert the GNSS signals. The latest to join the race is the Compass system, designed by China, which is currently ahead of the Galileo program, with eleven spacecrafts launched as of 2012 April [98]. An SDR receiver system capable to simultaneously process Global

Positioning System and Galileo signals is detailed in [99]. [96] describes the design features of a fully integrated dual-channel multiband RF receiver. In [100] a configurable multiband GNSS RF receiver using an heterodyne radio architecture for Compass/GPS/Galileo applications is used to accomplish the goal. A low-IF receiver proposed in [101] used variable local oscillator to directly down convert RF signals to base-band, and to control an analogue mixer. However, this architecture has certain drawbacks in terms of large constraints on LO specifications, like the phase noise imposed by the DC offset and tunable range and also the high gain between quadrature component of LOs and signal paths.

## 3.2 Gap Analysis

In order to have a clear understanding of the problem statement it is more appropriate to have a gap analysis of the past work that was carried out in the field of sampling theory. In this connection it may be summarized as follows.

- Most of the work, [13, 18–20, 30], [50]– [55] is limited to down-conversion of single band or signal to the IF stage or baseband. In the case of multiband signal the problem of aliasing overlaps comes across. To address this problem sampling rates in some cases becomes closer to the Nyquist rate.
- Most of the work, [59]– [64] is restricted to the down-conversion of the existing spectrum already in use. This spectrum is non-linear in nature and no specific closed form algorithm exists to ensure the minimum sampling rate without any additional constraint. There exist no literature which describes a relation between the spectrum layout and sampling rates,
- Most of the algorithm, [1, 4, 33, 60, 102] proposed for finding the minimum sampling frequencies are iterative in nature. Their emphasis is just

to determine the minimum sampling rate so that the desired SOI may be down-converted in the first Nyquist zone without any aliasing. In such type of algorithms, first a set of already existing conditions is satisfied for alias-free sampling of the desired signals. Later on, these conditions are checked with few computations. When any of these conditions is not satisfied, the sampling rate can be gradually incremented in a fashion that the prescribed condition is satisfied. Hence, the sampling rate is increased through iterations, and algorithm for finding the minimum sampling frequency is also satisfied for all essential conditions. After satisfying the algorithm for two bandpass signals the algorithms are generalized for more than two bandpass signals.

- The useable sampling frequencies for a desired SOI are not limited to a specific set of frequencies. Instead these are extended to aliasing free frequency intervals. Consequently, one needs to verify the complete range before its implementation
- For a given SOI, two sampling frequencies are calculated or proposed, each of which is supposed to be minimum with its own set of conditions. One of these frequency is minimum with the ordering constraint after the spectrum folding in the process of sampling and the other is without ordering constraint. For a nonlinear spectrum, the minimum sampling rates have been derived are limited to single-band and dual-band input signals. No universal bandpass sampling method is established to define a least possible bandpass sampling rate, that is valid as well for either linear or nonlinear systems by making an allowance for a multiband input signal.

### 3.3 Research Motivation

As identified above, in order to avoid any alias-overlap, there are two major types of constraints, which are common to most of the work: the first, is referred as



‘boundary constraint’ and the other is referred as ‘neighbor constraint’. However, no constraints like position of bands in SOI and their inter-position gaps are ever discussed. Only Vaughan [55] in his work has mentioned the significance of location of band in the case of single band has to be sampled and down-converted to the base-band region. It is pertinent to high-light that as per best of our knowledge no work has ever been presented that described the necessary and sufficient conditions, which ensure ideally minimum sampling rate (exactly equal to the twice of the information bandwidth of all signals in the SOI) for the RF signals in the passband. It is only in [65], where Munoz *et al.*, mentioned minimum sub-Nyquist sampling rate in the context of evenly spaced equal-bandwidth multiband systems. In [65], the authors recommended necessary conditions to circumvent aliasing after down-conversion but the condition are not sufficient to make use of complete or maximum use of SOI, while using the proposed sampling rates. As per our research minimum sampling rate (ideally  $f_s = 2NB$ ) is possible to achieve in the case, when the desired signals are uniformly spaced in our SOI. However, even then there is a case when  $f_s = 2NB$  can not be applied directly and hence requires an increment proportional to the bandwidth  $B$ . Our proposed conditions mainly relate to the position of the signal with minimum carrier-frequency in the SOI and the sparseness. In our research work, the case, where minimum sampling rate i.e.,  $2NB$  is not applicable is also highlighted.

### 3.4 Problem Statement

Keeping in view the classical sampling techniques, the literature survey and the gap analysis, it is now possible for us to define our problem as follows:

***To establish necessary conditions to find minimum sampling rates for a uniformly- spaced sparse-spectrum with any sparse ratio. Conversely, it is to find layout of SOI (set of frequencies) of the band-limited signals in the passband that can be simultaneously digitized and down-converted in the first Nyquist zone without causing any aliasing***

*overlap, while fulfilling the above mentioned constraints for a given sampling rate.*

### 3.5 Thesis Contributions

In our research work, we made an endeavor to explore bandpass sampling theory and its applications. Following are the major contributions towards this end:-

- a. Development of a generic algorithm to find the lay out of spectrum that may be sampled with minimum possible sampling rate. Prior to this, to the best of our knowledge, most of the works pertains to find out the minimum sampling rate for given multi-band spectrum. In this context, our work is novel and is reasonably helpful to carry out frequency selection and planing while designing a multi-band wireless transceiver.

- b. Although our work pertains to uniformly spaced spectrum, but it is also applicable to non-uniformly spaced spectrum by carrying some spectrum management. A case study is included in chapter 6 for Global Navigational Satellite System (GNSS) using a composite receiver design, which integrates the advantages of heterodyne and direct RF sampling receiver.

# Chapter 4

## System Model and Proposed Sampling Theory

### 4.1 Overview

In the last chapter, reference literature [32, 59, 60] clearly describes sampling algorithms for the down-conversion of single and multi-band signals. Similarly, there are other algorithms proposed by authors in [33, 64] to find minimum sampling frequencies for multi-signal spectrum. However, permissible sampling rates lies in the range of 2.5 to 4 times of the maximum information bandwidth. Moreover, no algorithm guaranties the minimum possible sampling rate of  $2B$  (twice of the BW of occupied spectrum) as described by bandpass sampling theorem, especially when the spectrum of interest is sparse in nature. Our objective is to establish the conditions which are necessary to find minimum sampling rates for a uniformly-spaced sparse-spectrum with any sparse ratio. By minimum sampling rate we mean that either  $f_s = 2B$  or it should be as close to  $2B$  as possible. Our concept is based on two factors: First is the sparsity ratio and the lowest carrier-frequency in the spectrum of interest. Although sampling rate does not change with the change in sparsity. However, selection of  $f_{c1}$  or  $f_{L1}$  depends on the pattern of the sparseness also referred as sparsity. Second is the lowest carrier-frequency

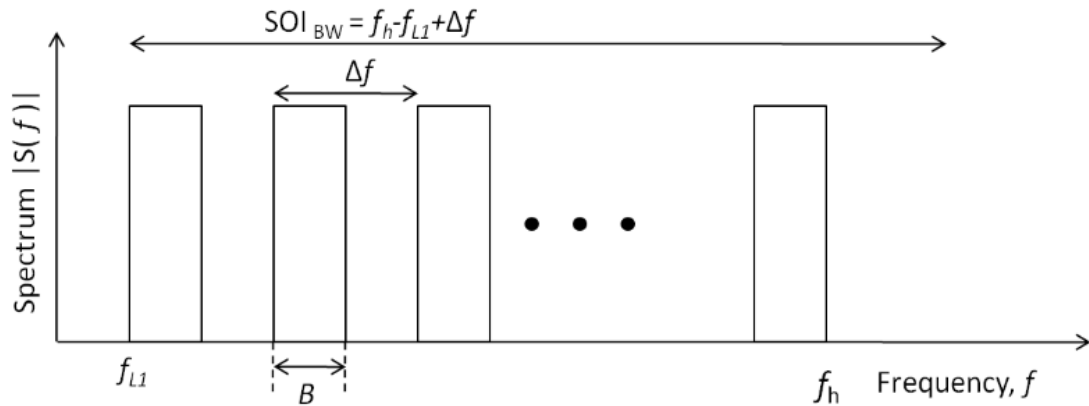


FIGURE 4.1: A spectrum comprising  $N$  number of RF signals

$f_{c1} = f_{L1} + B/1$  is the center frequency of the lowest-band in our spectrum of interest and is based on our algorithm presented in [8]. Any violation in selection of the lowest carrier-frequency other than the recommended will be at the cost of increased sampling rate and additional memory for storage of samples. Moreover, the sampling frequency,  $f_s = 2NB$ , should not be integer-multiple of the frequency separation,  $\Delta f$ , between information signals and vice versa.

## 4.2 System Model

In software defined radio (SDR) systems, it is desirable to down-convert multiple RF signals simultaneously by placing an analog-to-digital converter (ADC) as near the antenna as possible. However, this demands the ADC of very large bandwidth and also requires very high sampling rate in the case of low-pass sampling. Our system model reflects a multiband spectrum, that is comprised of  $N$  uniformly spaced RF bands each of bandwidth  $B$ . These bands are separated by space  $\Delta f = f_{i+1} - f_i$  as described in section 5 of chapter 2. Same model has been simplified and illustrated in Fig. 4.1. An RF front-end design of a radio receiver applicable to our model is as shown in Fig. 4.2.

A wide-band RF signal is received from the antenna and amplified with a low-noise amplifier (LNA). Then the signal is filtered with  $N$  parallel bandpass filters. The analogue-to-digital converter (ADC) is placed closed to the antenna so that

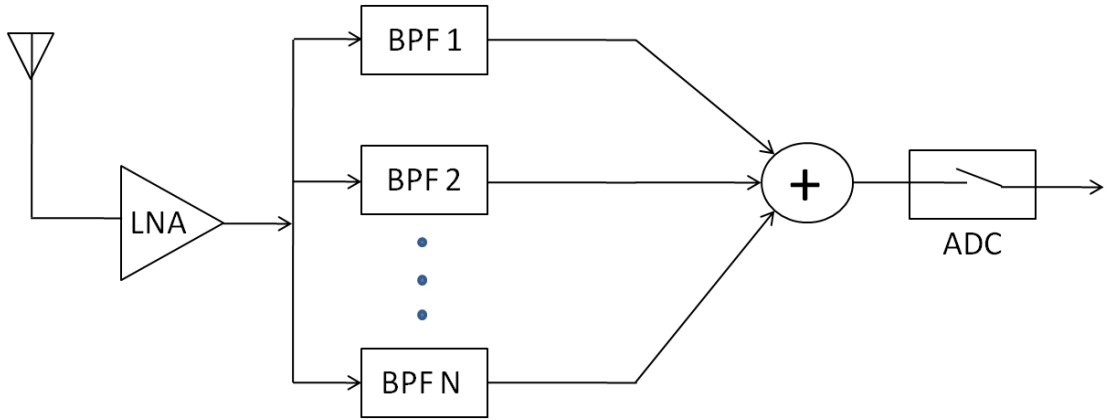


FIGURE 4.2: The front end of a receiver architecture with the functionality of digitizing multiband input signals

the analogue components can be reduced. Further signal processing of the input signal is carried out in digital domain. This is considered as direct RF sampling architecture, where minimum sampling rate is used to directly digitize the analogue signal without any spectrum folding or aliasing-overlap in the first-Nyquist zone.

### 4.3 Technical Details

Assume that spectrum is sparse such that the total bandwidth  $NB$ , contained by  $N$  information bands or signals is much less than the total bandwidth of spectrum of interest,  $SOI_{BW} = f_{L1} - f_h + \Delta f \gg NB$ . Consider  $f_{L1}$  is the lowest-frequency in the spectrum of interest, then the central frequency  $f_{cn}$  of each signal present in the spectrum is given by

$$f_{cn} = f_{L1} + (n - 1)\Delta f + B/2 \quad (4.1)$$

In the case, if there is a single band present in the signal or spectrum of interest, then the relation between the sampling frequency  $f_s$  and aliasing frequency  $f_a$  to avert the overlapping of aliased-band with zero (dc component) or the Nyquist

frequency  $f_s/2$  described in, [33], [62] is given as

$$0 < f_a - B/2 \tag{4.2}$$

$$f_a + B/2 < f_s/2 \tag{4.3}$$

However, for multiband spectrum, constraint formulated in Eq. 4.2 and Eq. 4.3 are not sufficient. Therefore, an additional constraint is introduced in [65] that is useful for down-conversion of  $N$ bands. The additional constraint prevents the aliases of the bands from overlapping to each other in first Nyquist zone. Considering  $B_x$  and  $B_y$  as information bandwidths of two neighbouring bands in base-band region with their intermediate frequencies as  $f_{ax}$  and  $f_{ay}$  the additional constraint may be described as follows:

$$|f_{ax} - f_{ay}| \geq (B_x + B_y)/2 \tag{4.4}$$

Here  $y = 2 \dots N$  and  $x = 1 \dots y$ . Eq. 4.4 implies that if  $B_y = B_x = B$  then  $(f_{ax} - f_{ay})/B$  should be non-fractional quantity greater than zero otherwise the optimal placing of aliases in the first-Nyquist zone will not be possible. In other words for any  $f_{ax} - f_{ay} = 0$ , implies 100 percent overlapping of respective aliases and any fractional quantity means partial overlap. The 100 percent overlap is due to the fact that, frequency separation between any of the two carriers being sampled, is multiple of  $f_s$ . For example, let  $f_{cx}$  and  $f_{cy}$  are centered at 50 kHz and 34 kHz respectively and have  $B = 2$  kHz. The minimum sampling rate required is 8 ksps. In this case, sampling at the rate of 8 ksps will produce aliases  $f_{ay} = f_{ax}$  at 2 kHz, means an 100 percent aliasing overlap.

**Theorem.** For  $N$  equidistant pass-band signals that are separated by frequency-gap of  $\Delta f$  Hz are digitized by an A/D converter at a sampling rate, which is integer multiple of  $\Delta f$ , then there will always be aliasing-overlap.

*Proof.*

If a, b and c are three integers such that

$$\text{rem}(a, c) = k_1, \dots \text{(i)}$$

and also

$$\text{rem}(b - a, c) = 0 \dots \text{(ii)}$$

$$\text{then } \text{rem}(b, c) = \text{rem}(a, c) = k_1$$

Let us proceed with the assumption that  $\text{rem}(b, c) = k_2$ , this implies that

$$b - l_1 c = k_2 \dots \text{(iii)}$$

where  $l_1$  is any positive integer. Similarly,

$$a - l_2 c = k_1 \dots \text{(iv)}$$

subtracting (iii) from (iv)

$$b - a - (l_2 - l_1)c = k_2 - k_1$$

$$b - a - lc = k_2 - k_1$$

$$\text{rem}(b - a, c) = k_2 - k_1 \dots \text{(v)}$$

from (ii) and (v) it can be concluded that  $k_1 = k_2$

Elimination of this overlap requires a gradual increment in the sampling frequency in steps of  $B$  Hertz. However, definitely sampling frequency used for such cases is not the one equal to twice of the information BW. In fact it becomes  $(2N + 1)B$ . Replacing  $f_{c1} = f_{L1} + B/2$  in Eq. 4.1, general expression for  $f_{cn}$  can be written as

$$f_{cn} = f_{c1} + (n - 1)\Delta f \quad (4.5)$$

Now if the complete spectrum is sampled with  $f_s$ , the replication  $f_{an}$  of non-zero energy contents can be obtained as

$$f_{an} = |f_{cn} \pm m f_s|, n = 1, 2, 3, \dots N \quad (4.6)$$

where  $m$  is an integer such that  $f_s/2 \geq f_{an} \geq 0$ . In the context of aliasing, it can be seen that left hand side of Eq. 4.5 is dependent on the central frequency of the first RF carrier and the inter-band space  $\Delta f$ . Here, the central frequency of the first carrier  $f_{c1}$  plays a vital role in defining the sampling frequency. By choosing  $f_{min}$  or  $f_{c1}$  analytically, we can avoid overlap between down converted aliases irrespective of the ratio between  $B$  and  $\Delta f$ , however, selection of  $f_{min}$  is not a trivial issue and requires deliberate calculations. Since there is no formula which

universally provides minimum sampling frequency for multiple input signals in the spectrum [65], therefore in such cases spectral intervals are derived which contains the permissible sampling frequencies. Later these frequencies are obtained through search algorithms [9], [33], [64]. Thereafter, by selecting an appropriate,  $f_{min}$  makes it possible to write a standard expression for minimum sampling frequency. For this purpose we are analyzing the minimum central frequency in the spectrum of interest and also the separation between each signal which are assumed to be evenly spaced. In the context of evenly spaced equal-bandwidth multiband spectrum, method proposed in [65] to determine the minimum sub-Nyquist sampling frequency does not imply any aliasing with constraint on lowest frequency in the band of interest. However, the proposed (minimum sampling frequency) and (smallest frequency of the lowest band in the spectrum of interest) in [65] does not hold true for all ratios of  $\Delta f$  and  $B$ . On the other hand, our proposed method is applicable to all ratios of  $\Delta f$  and  $B$ . Using proposed sample rate  $f_s$  with limitation on  $f_{min}$  aliases-overlap can be avoided for multiple signals present in the desired spectrum. Table 4.1 shows the values of  $\Delta f/B$  for  $N = 2$  to 10, where minimum sampling rate  $f_s = 2NB$  is applicable. However, it can also be noticed that the presented method in [65] is not applicable for all values of  $f/B$ . For example, in the case of  $N = 10$ , the values of  $\gamma = 3, 4, 5, 7, 8, 9, 10, 11, 12, 13, \dots$  are missing.

TABLE 4.1: A comparison of proposed methodology with [65]

N	Values of $\Delta f/B$	
	Muñoz-Ferreras et al	Proposed
2	1, 2, 5, 6, 9, 10, 13, 14, 17, 18, 21, 22, 25, ...	1, 2, 3, ...
3	1, 2, 4, 7, 8, 10, 13, 14, 16, 19, 20, 22, 25, ...	1, 2, 3, ...
4	1, 2, 6, 9, 10, 14, 17, 18, 22, 25, ...	1, 2, 3, ...
5	1, 2, 4, 6, 8, 11, 12, 14, 16, 18, 21, 22, 24, ...	1, 2, 3, ...
6	1, 2, 10, 13, 14, 22, 25, 26, ...	1, 2, 3, ...
7	1, 2, 4, 6, 8, 10, 12, 15, 16, 18, 20, 22, 24, ...	1, 2, 3, ...
8	1, 2, 6, 10, 14, 17, 18, 22, 26, 30, ...	1, 2, 3, ...
9	1, 2, 4, 8, 10, 14, 16, 19, 20, 22, ...	1, 2, 3, ...
10	1, 2, 6, 14, 18, 21, 22, 26, ...	1, 2, 3, ...



## 4.4 The Proposed BPS Methodology

The proposed architecture consists of the two major factors, i.e. the sparsity ratio and the lowest carrier- frequency .

### 4.4.1 Sparsity ratio

Let us represent the complete spectrum in form of a column matrix

$$\mathbf{F} = [f_{c1} \ f_{c2} \ f_{c3} \ \dots \ f_{cN}]^T \quad (4.7)$$

where  $\mathbf{F}$  represents carrier positions in compact form as a single column matrix. Eqs 4.8 and 4.9 show the carrier frequency of each band in the pass-band and in the base-band (first-Nyquist zone) respectively.

$$\begin{aligned} \mathbf{F} &= [f_{c1} \ f_{c2} \ f_{c3} \ \dots \ f_{cN}]^T \\ &= [B/2 \ (2\gamma + 1)B/2 \ (4\gamma + 1)B/2 \\ &\quad \dots \ (1 + 2\gamma(N - 1))B/2]^T \end{aligned} \quad (4.8)$$

$$\begin{aligned} \bar{\mathbf{F}} &= [f_{a1} \ f_{a2} \ \dots \ f_{aN}]^T \\ &= [(B/2 \pm 2mNB \ (2\gamma + 1)B/2 \pm 2mNB \\ &\quad \dots (1/2 - \gamma + N\gamma)B \pm 2mNB)]^T \end{aligned} \quad (4.9)$$

where  $\bar{\mathbf{F}}$  represents positions of the aliases in compact form as a single column matrix. For the ease of comprehension if we assume  $\gamma = 2$  and  $N = 3$ , the aliasing frequencies after down conversion can be determined using Eqs 2.34 and 2.35 given in chapter 2 as follows:

$$[f_{a1} \ f_{a2} \ f_{a3}] = [B/2 \pm 2mNB \ 5B/2 \pm 2mNB \ 9B/2 \pm 2mNB] \quad (4.10)$$

Now considering the constraints mentioned in Eqs 2.38 - 2.40 of chapter 2, value of  $m = 1$  satisfies the required aliasing conditions for  $f_{a1}$ ,  $f_{a2}$ , and  $f_{a3}$ . Finally, the down-converted replications are received at  $B/2, 5B/2, 3B/2$ , respectively. Similarly for  $\gamma = 4$  the down-converted signals do not overlap in the first-Nyquist zone and can be easily reconstructed without any loss of information, both the cases for  $\gamma = 2$  and  $\gamma = 4$  are shown in Fig. 4.3(a) and (b). However, when  $\gamma = 3$ , as shown in Fig. 4.3 (c), then after down-conversion  $f_{c3}$  completely overlaps with  $f_{c1}$ . As a result both bands are completely corrupted. To analyze the problem, it can be observed that the difference between central frequencies of  $f_{c1}$  and  $f_{c3}$  is equal to the sampling rate  $2NB$ . This is contrary to the theorem presented in section 4.3. Obviously whenever, two signals are spaced at a gap which is equal to or multiple of the sampling frequency; their replications will always overlap in first Nyquist zone. This can be avoided by changing the sampling frequency. Since any sampling rate less than  $2NB$  creates aliasing problem, therefore it is reasonable to increment the sampling rate by an integer multiple of bandwidth. This implies that besides  $N$  and  $B$ , the minimum sampling frequency depends on  $\gamma$  also. To elaborate it further a flow chart shown in Fig. 4.4 can be used to compute the minimum sampling rate based on the center frequency. The flow chart also suggests the suitable possible positions of the  $N$  carriers with reference to sparse ratio.

#### 4.4.2 Lowest Center-frequency

Intuitively lowest frequency of the carrier can never be less than  $B/2$ . Keeping in view the prescribed conditions, equation 4.5 defines the lowest possible passband positions of  $N$  bands depending on sparse ratio  $\gamma$ . Our next step is to find out the positions of the carriers in passband, which prevents aliases overlaps while sampled at the optimum sampling rates derived in the previous section.

**Theorem:** To downconvert a uniformly spaced multiband signal in the first-Nyquist zone using a sampling rate equal to  $2NB$ , all the bands should be centered

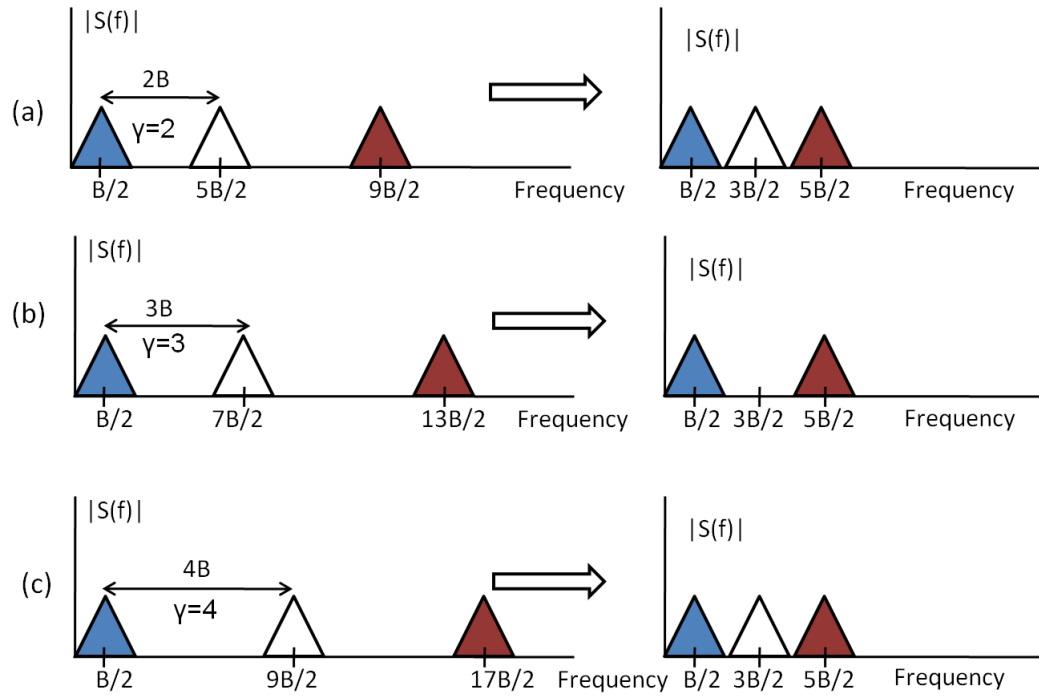


FIGURE 4.3: Direct down conversion of a tri-band RF spectrum

at  $kB/2$ , where  $k$  is an integer.

**Proof:** We know that total bandwidth required for  $N$  bands =  $NB$ , where position of each carriers can be defined as follow:

$$f_{c1} = B/2$$

$$f_{c2} = f_{c1} + \Delta f = B/2 + \gamma B = B/2 + 2\gamma B/2$$

$$f_{c3} = f_{c1} + 2\Delta f = B/2 + 2\gamma B = B/2 + 4\gamma B/2$$

.

.

$$f_{cn} = B/2 + 2(N-1)\gamma B/2$$

Using Eq. 4.6,

For  $N = 1$ ,

$$f_{IF} = \text{rem}(B/2, 2B) = B/2.$$

For  $N = 2$ ,

$$f_{IF} = \text{rem}(B/2 + 2\gamma B/2, 8B/2) = B/2 + B|B/2$$

For  $N = k$ ,

$$f_{IF} = \text{rem}(B/2 + 2(k-1)\gamma B/2, 4kB/2)$$

$$= B/2 + (k - 1)B,$$

where  $k = 1, 2, 3, \dots, N$

Since  $f_{c1}$  can never be less than  $B/2$ , therefore after a little manipulation Eq. 4.5 can be written as:

$$f_{cn} = (1 - 2\gamma + 2\gamma n)B/2 \quad (4.11)$$

This indicates that the center-frequency  $f_{cn}$  of any of the bands is limited to the set of frequencies as defined by Eq. 4.11, such that  $f_{cn} \leq f_h - B/2$ . To improve the illustration consider the case of a dual band spectrum, i.e.,  $N = 2$ . Obviously in this case,  $f_{c1}$  will be at  $B/2$  and position of second carrier will be at  $(1 + 2\gamma)B/2$ . This simple spectrum does not pose any problem when sampled at the rate equal to  $2NB$ . However, if both signals are shifted towards right (to higher frequencies), in small steps of the size  $\gamma < B/2$ , overlapping of aliases starts appearing. This phenomenon of aliasing-overlap remains present till the time  $f_{c1} = 5B/2$ , despite of the fact there is no change in the sampling rate. After shifting the lowest carrier at  $5B/2$ , there is no aliasing-overlap or spectral folding. By continuing the process, soon it can be observed that the positions of  $f_{c1}$  for which there is no aliasing-overlap on down conversion follow certain patterns. These patterns depend on the sparsity ratio  $\gamma$  and separation between any of the two carriers  $f_j - f_i$  and can be expressed by arithmetic sequences as follows:

#### 4.4.2.1 When $\text{mod}((f_j - f_i), 2NB) \neq 0$

When the separation between any two signals is not multiple of  $2NB$  then position of lowest carrier depends, whether the sparsity ratio  $\gamma$  is odd or even. For odd values of  $\gamma$ , to circumvent the overlap between aliases in the first Nyquist zone, the lowest carrier position should be member of the frequency set expressed as follows:

$$f_{ck} = (\gamma \pm 2(k - 1)N)B/2, \forall \text{mod}(\gamma, 2) \neq 0, k = 1, 2, 3... \quad (4.12)$$

Similarly for even values of  $\gamma$ , we have

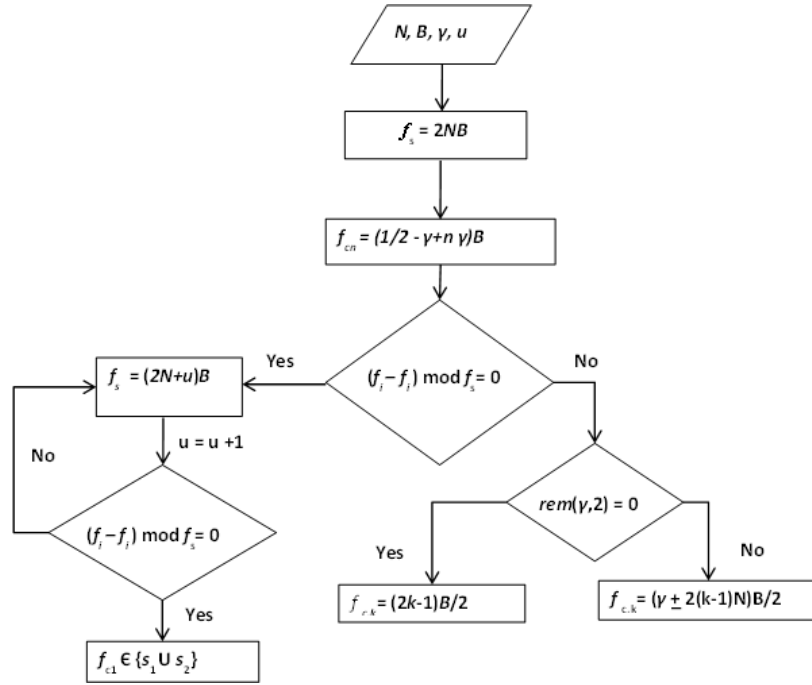


FIGURE 4.4: Flow chart to calculate sampling frequency and carrier positions in passband

$$f_{c1} = (2k - 1)B/2 \quad (4.13)$$

**Theorem:**

For even values of  $\gamma$ , the center frequency of lowest carrier should be  $f_{c1} = 2(k - 1)B/2$ .

**Proof:**

Let the lowest band in the SOI has its central frequency as follow:

$$f_{c1} = (2k - 1)B/2$$

$$f_{c2} = f_{c1} + \Delta f = f_{c1} + \gamma B = f_{c1} + 2\gamma B/2$$

$$f_{c3} = f_{c1} + 2\Delta f = f_{c1} + 2\gamma B = f_{c1} + 4\gamma B/2$$

.

.

$$f_{cn} = f_{c1} + 2(N - 1)\gamma B/2 = (2k - 1)B/2 + 2(N - 1)\gamma B/2$$

Using Eq. 4.6 we can calculate intermediate frequency of each band after down-conversion as follow:

For  $N = 1$

$$f_{IF} = \text{rem}((2k - 1)B/2, 2B) = B/2$$

For  $N = 2$ ,

$$f_{IF} = rem((2k - 1)B/2 + 2\gamma B/2, 8B/2) = B/2 + B|B/2$$

For  $N = k$

$$\begin{aligned} f_{IF} &= rem(B/2 + 2(k - 1)\gamma B/2, 4kB/2) \\ &= B/2 + (k - 1)B, \text{ where } k = 1, 2, 3 \dots N \end{aligned}$$

This clearly shows that for proposed value of  $f_{c1}$ , there would not be any aliasing for an equally spaced spectrum, while sampled at lowest possible sampling rate of  $2NB$ .

In order to ascertain validity of Eq. 4.13, consider the case of a single band  $X(f)$  of bandwidth  $B$ . It can be noticed that the minimum value of  $f_c$  is always  $B/2$ , which can be achieved by putting  $k = 1$  in Eq. 4.13. For an instance, consider Fig. 4.5(a) that shows position of  $X(f)$  in the passband region. This can always be achieved for an arbitrary value of  $k$  in Eq. 4.13.  $X(f)$  can be down-converted to frequency  $B/2$  if sampled at the sampling rate of  $2NB$  as shown in Fig. 4.5(b). As we know that any frequency in the passband may be expressed as:

$$f_c = mf_s/2 \pm \epsilon. \quad (4.14)$$

where  $0 \geq \epsilon \leq f_s/2$ . The signal  $X(f)$ , which is positioned at  $f_c$ , when digitized, is down-converted to an IF at  $(f_s/2 - \epsilon)$ . To accommodate the complete signal  $X(f)$  in the first-Nyquist zone,  $f_{IF}$  should be equal to  $f_s/4$ , which implies that the most suitable value of  $\epsilon$  is  $f_s/4$ . In such cases  $X(f)$  will always be down-converted to  $f_{IF} = f_s/4 = B/2$  and will fulfill the boundary constraint already described in chapter 2. Consider that there is small deviation,  $\pm\sigma$  in the position of  $X(f)$  as shown in Fig. 4.5(c). In this case, using the same sampling rate the signal is down-converted at an intermediate frequency:

$$f_{IF} = f_s/2 - (\epsilon \pm \sigma) \quad (4.15)$$

As we know that the optimized value of  $\epsilon$  is  $f_s/4$ , implies that  $f_{IF}$  shall al-

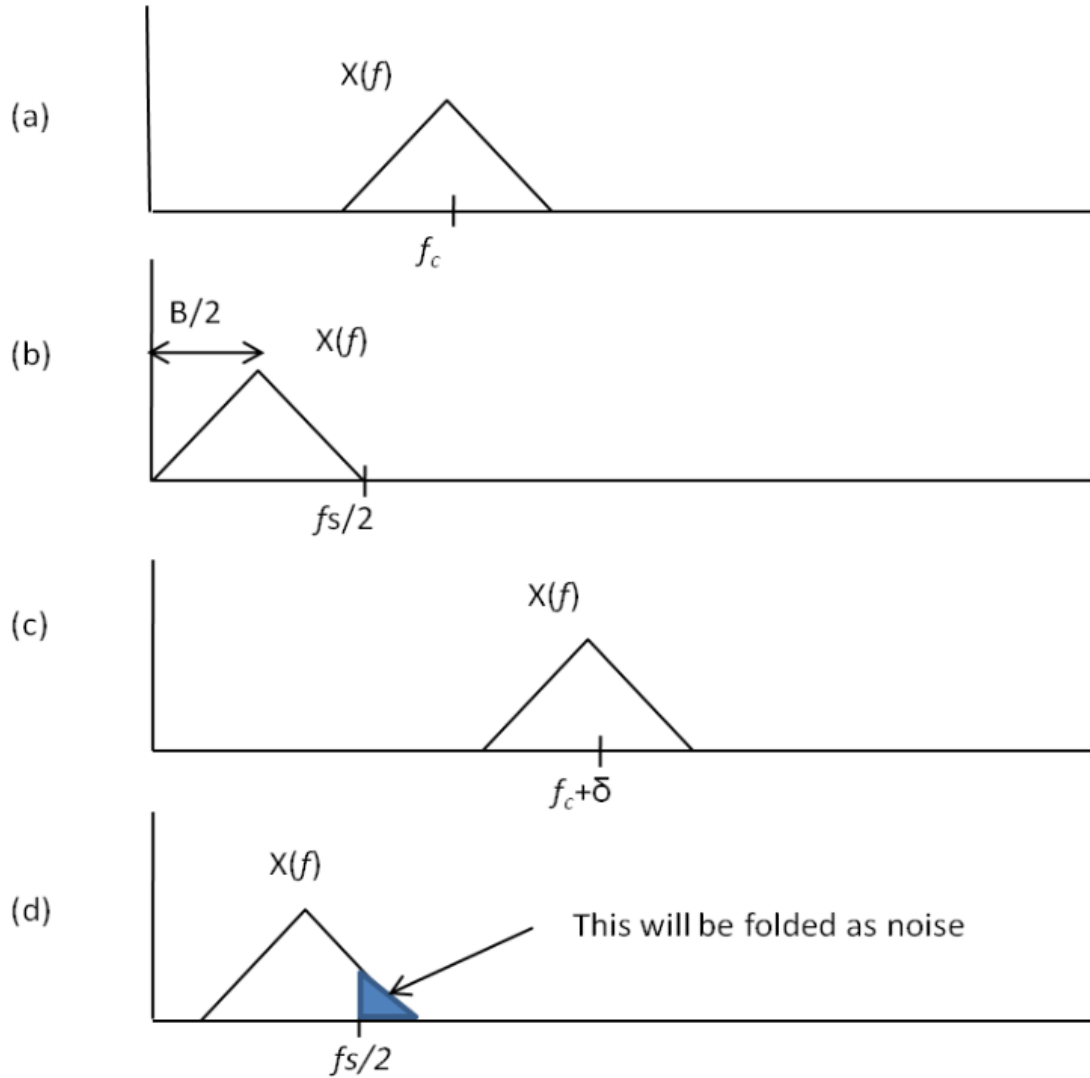


FIGURE 4.5: (a) Signal  $X(f)$  positioned at  $f_c$ . (b) Down-conversion of  $X(f)$  in the first-Nyquist zone. (c) Shift of  $\sigma$  Hz in the position of  $X(f)$ . (d) A boundary constraint overlap of  $X(f)$  after down-conversion

ways be shifted from the center positioned  $B/2$  as shown in Fig. 4.5(d). Since the space available in the first-Nyquist zone is equal to  $B$  and there is no additional space available to accommodate the signal such that  $0 \leq f_{IF} - B/2$  and  $f_s/2 \geq f_{IF} + B/2$ . As a result there will be a compromise to the boundary constraint. Any shift in the position of  $X(f)$  in the pass-band will lead to overlap with zero-frequency (dc-component) or  $f_s/2$ . Mathematically, this may be expressed as:

$$0 > f_{IF} - B/2 - \sigma \tag{4.16}$$

or

$$f_s/2 < f_{IF} + B/2 + \sigma \quad (4.17)$$

This is clearly against the basic rules defined in the literature, as described in Eq. 4.2 and 4.3. Similarly, in the case of multiple signals in the SOI there will be a violation of neighbouring constraint if the lowest carrier is not placed as recommended in Eq. 4.13

#### 4.4.2.2 When $\text{mod}((f_j - f_i), 2NB) = 0$

As described earlier that when two or more carriers have their frequency separation  $(f_j - f_i)$  multiple of  $2NB$ , there will always be loss of information due to violation of neighbouring constraint. In such the cases one of the bands has a 100% overlap in the frequency domain with its neighbouring band. This issue can be resolved by increasing the sampling frequency. For all such cases useable position of  $f_{c1}$  can be selected from a set of frequencies, composed of two sequences:  $s_1$  and  $s_2$ . Mathematically this may be expressed as follows:

$$f_{c1} \in s_1 \cup s_2 \quad (4.18)$$

The sequences  $s_1$  and  $s_2$  can be determined as follows:

$$s_1 = \gamma \pm k(2N + 1), \forall s_1 > 0 \quad (4.19)$$

where  $k \geq 0$  and

$$s_2 = 2\gamma \pm k(2N + 1), \forall s_2 > 0 \quad (4.20)$$

The results obtained are summarized with the help of flow chart as presented in Fig. 4.5. The given flow chart describes the complete process to compute the optimal sampling frequency, carrier separation and central frequency of the lowest signal  $f_{c1}$ . To illustrate it further consider the following example.



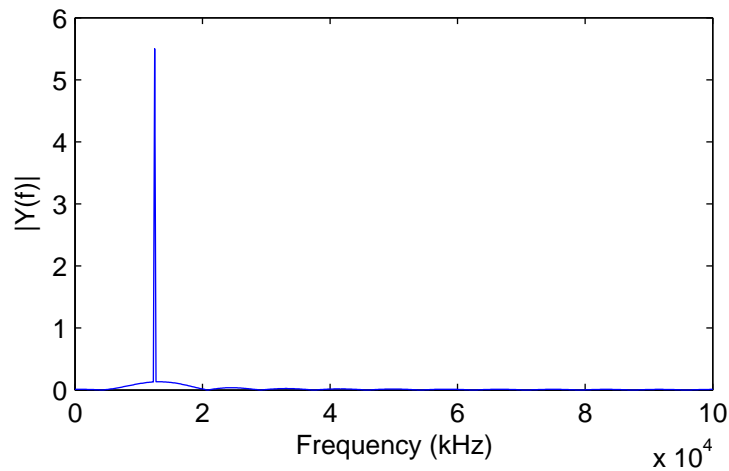


FIGURE 4.6: A down-conversion of quad-channel spectrum using a sample rate of 200 kps, resulted in complete aliasing-overlap at 12.5 kHz

*Example.*

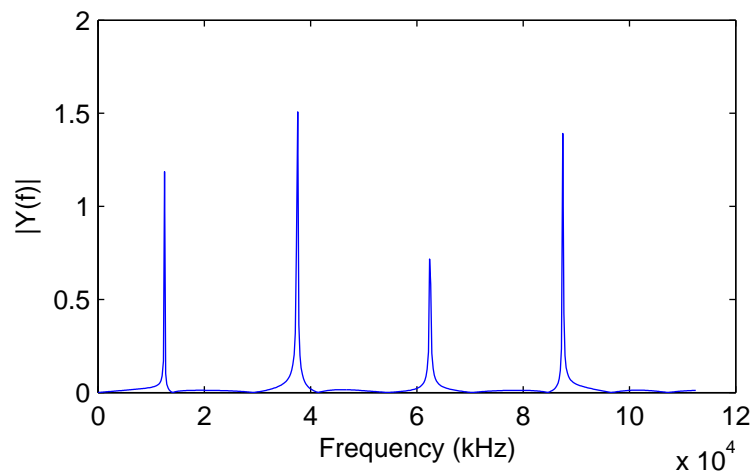


FIGURE 4.7: A down-conversion of quad-channel spectrum without any aliasing-overlap for a sample rate of 225 kps

Consider a quad-channel spectrum such that each channel has a bandwidth of 25 kHz. The channels are located on 136.1875 MHz, 136.5875 MHz, 136.9875 MHz and 137.3875 MHz as shown in table 4.2. In this case frequency separation between consecutive channels is 400 kHz. If we choose a sample rate of 200 kHz that is twice of the total bandwidth, i.e.,  $2NB$  certainly there is an aliasing-overlap after down-conversion. As it is evident from Fig. 4.6 that there is only one channel visible in the first-Nyquist zone. In fact all the channels are down-converted to 12.5 kHz. This can be explained in the light of above mentioned theorem. The

TABLE 4.2: Down-conversion of a quad-channel spectrum of 100 kHz bandwidth using a sample rate 200 kHz resulted in a complete aliasing-overlap in the first-Nyquist zone.

RF Spectrum (MHz)	IF Spectrum (kHz)
136.1875	12.5
136.5875	12.5
136.9875	12.5
137.3875	12.5

TABLE 4.3: Down-conversion of a quad-channel spectrum of 100 kHz bandwidth using a sample rate 225 kHz proved useful to circumvent aliasing-overlap.

RF Spectrum (MHz)	IF Spectrum (kHz)
136.1875	62.5
136.5875	12.5
136.9875	37.5
137.3875	87.5

reason is that frequency separation  $\Delta f$  of consecutive channels is 400 kHz, which is integral multiple of sample rate, i.e. 200 kHz. Under such circumstances the solution to the problem is an increment in the sample rate that is equal to bandwidth of a single channel. Now if we increase the sample rate upto 225 kHz our down-converted spectrum will shift to 12.5 kHz 37.5 kHz, 62.5 kHz and 87.5kHz, which resolves the problem of aliasing-overlaps. Down-converted frequencies using sample rates of 200 kHz and 225 kHz are shown in Table 4.2 and Table 4.3 respectively. Out come of both sample rates is also illustrated in Fig. 4.6 and 4.7

# Chapter 5

## Test Set up and Simulation

## Results

### 5.1 Overview

In order to validate our theoretical work presented in previous chapter, two strategies are adopted. Firstly, simulations are carried out using Matlab, where the number of signals or bands of interest vary from dual-band to multi-band spectrum. Theoretically, calculated sample rates are used to confirm the expected output. Also results are compared with those obtained by [65]. In the second part of our simulations we used Multisim which is a circuit teaching solution by National Instruments. Multisim simulation and circuit design software gives us the advanced analysis and design capabilities to optimize performance, reduce design errors, and shorten time to prototype. Again same bands are used as inputs to a general purpose ADC and sampling is carried out using the theoretically obtained sample rates. It is once again confirmed that the results achieved using Matlab simulations are similar to the results of Multisim simulations. In order to validate the results three scenarios are developed and discussed in section 5.5 for analysis purpose.

## 5.2 Analysis Parameters

### 5.2.1 Sparsity Ratio

As described in chapter 4 that sparseness  $\gamma$  is the sparsity ratio between total bandwidth of the spectrum of interest  $SOI_{BW}$  and the information-bandwidth  $NB$ , where total bandwidth includes the non-electromagnetic portion of spectrum and can be expressed as  $f_{L1} - f_h + \Delta f$ . This ratio may be further simplified as  $\Delta f/B$ . Our analysis shows that sparse-bandwidth (void of any electromagnetic spectrum) does not directly effect the sample rate and there are no constraints on sparse ratio in order to achieve the ideal sample rate  $2NB$  samples per second. The only factor which effects is the pattern of sparsity, i.e., whether the sparsity-ratio is even or odd. In our analysis we discuss the generic-aspect of the methodology and how widely it can be used for various ratios.

### 5.2.2 Number of Bands in the SOI

SOI is the number of signals or bands which are to be directly down-converted and digitized. SOI has direct impact on sample rate, greater the the number of signals or bands in SOI, greater is the sampling rate or sampling frequency,  $f_s$ . However, this aspect is common for almost all contemporary bandpass sampling techniques. We shall discuss this in terms of complexity in calculating the sample rate. In our case, there is hardly any adverse impact on complexity of algorithm with the increase in the number of bands or signals, because the  $f_s$  can be easily determined within couple of iterations. On the other hand for existing methods, increase in number of in bands has significant impact on complexity of algorithms. For example if we require to sample a spectrum consisting of  $N$  bandpass signals ( $2N$  bands), it needs to consider  $C_2^{2N}$  distinct cases, as every two of the pass-bands may cause mutual aliasing. However, due to symmetry these  $C_2^{2N}$  cases result in only  $N^2$  conditions [33]. Each of these  $N^2$  condition is examined and satisfied. If one condition is not satisfied, then sampling frequency is increased so

that the condition becomes satisfied. By iteratively examining the conditions and increasing the sampling frequency, the minimum frequency is found for alias-free sampling.

### 5.2.3 Minimum Frequency for SOI

The minimum frequency in the SOI has its own significance for a sampling technique that has overlap-free aliases so that minimum sample rate can be acquired. This implies that our sampling rate is also dependent on the minimum frequency component for a uniformly spaced spectrum.

### 5.2.4 Sampling Frequency

The ultimate objective of our research is to obtain a minimum sample rate or sampling frequency, which do not produce any error or aliasing-overlap after direct down-conversion. We see that for given set of signals in most of the cases our recommended sampling rate is  $2NB$ . However, there are cases when it is  $(2N+1)B$

## 5.3 General Assumptions

### 5.3.1 Guard-band Inclusion

The guard-band is required due to tolerance and non-ideal characteristics for analogue components used for filter design. In practical problems it is often desirable to have a spare bandwidth commonly referred as guard-band for aliasing-free sampling instead of just the theoretical-ideal sampling frequency. To fulfill this we have guard-bands between the adjacent bandpass signals after transformation to first Nyquist zone. Suppose the optimum guard-band is  $G_B$ . Then every 2 replicas from SOI should be spaced apart by a minimum interval of  $G_B$  after sampling operation. In our work, we are including the guard-band interval within the

information bandwidth. For example if  $B_i$  is the information bandwidth and  $B_G$  is guard-band then our operational bandwidth is  $B = B_i + B_G$ .

### 5.3.2 Post Folding Order of Signals

In DSP, sometimes it is desired that, the replicas of all bands in the SOI have a specific layout order, after the down-conversion process. However, this additional constraint, may be at the cost of an increase in the sampling rate and extra circuitry. Authors in [33] has drawn a comparison of various algorithms presented by [1, 60, 102] in terms of sampling rate, iterations and hardware (adders and multipliers). Table I and II of [33] show a comparison of  $f_{s,min}$ , with and without ordering constraint. It may be noticed that, when number of bands are more than two then sampling rate might increase ten times than that of without ordering constraint. However, it is worth mentioning that in our work ordering does not have an impact on  $f_{s,min}$ , that is, our sampling rate remains same with an additional constraint on  $f_{min}$ .

## 5.4 Simulation Tools

### 5.4.1 Multisim

Multisim is one of the top grade Circuit Design Suite by National Instruments. It is widely used for schematic capture and simulation applications. Specially the EDA (Electronics Design Automation) tools that assists student and engineers in carrying out the major and necessary steps for circuit design. Here in our simulation part we are using numerous virtual instruments and components provided as a part of package. The general procedures for attaching and configuring the instruments are self-explanatory, so less emphasis is given to them. The major purpose of using virtual instrument is to analyse the behaviour of our designed circuits using various measurements.

### 5.4.2 Matlab

Other simulation tool to validate our research work is Matlab. It has certain advantages over Multisim simulations. First, it can process large number of input signals (in tens and hundreds) with quick output, showing spectrum of all signals after sampling. The other advantage is that using Matlab we can generate a signal of desired parameters like bandwidth, frequency, modulation-type etc. On the other hand, in the case of Multisim, the desired signals are generated in the form of tones of desired frequencies using function generators.

## 5.5 Validation of Results

Before going into any detail discussion or analysis let us first describe Table 5.1. First two columns of the table are same as that of [65] presented by *Mũnoz et al.* These columns describes the number of signals or bands  $N$  in our SOI and values of  $\Delta f/B$ , which are suitable to avoid aliases-overlap. The third column is a new addition in the table and shows the values of  $\Delta f/B$ , which avoid aliasing as proposed in our work also presented in [8]. In the scenarios given below, we shall discuss the parameters discussed above and shall also draw a comparison that how our work has an edge over [65] in terms of the prescribed parameters.

### 5.5.1 Scenario-I

In this scenario, we emphasized that, how our methodology is applicable to the all sparsity ratios in a universal manner. In order to validate this, a number of analog signals (depicting various signal parameters like, carrier-frequency, null spectrum or sparsity *etc.*) are generated using function generator and applied as input to the ADC. The resulted output of ADC is again converted into the analogue form and is compared to that of [65]. Fig. 5.1 shows a simple arrangement of our test set up. This set up is used to generate three sinusoids with the help

three separate function generators. The platform used is that of Multisim by National Instrument. Outputs of these function generators are applied as an input to an 8-bit general purpose Analogue-to-Digital Converter [U4]. A separate clock [U6] is used to generate the desired sampling rate. Output of the ADC is fed to digital-to-Analogue Converter (DAC). This output is amplified through an operational amplifier and finally its spectrum is displayed on spectrum analyzer (XSA1) using FFT. Here it is also worth mentioning to highlight that keeping in view the characteristics of SOI like, the bandwidth of input signals and the total span covered by SOI *etc.* various operational amplifier are used for our requirement.

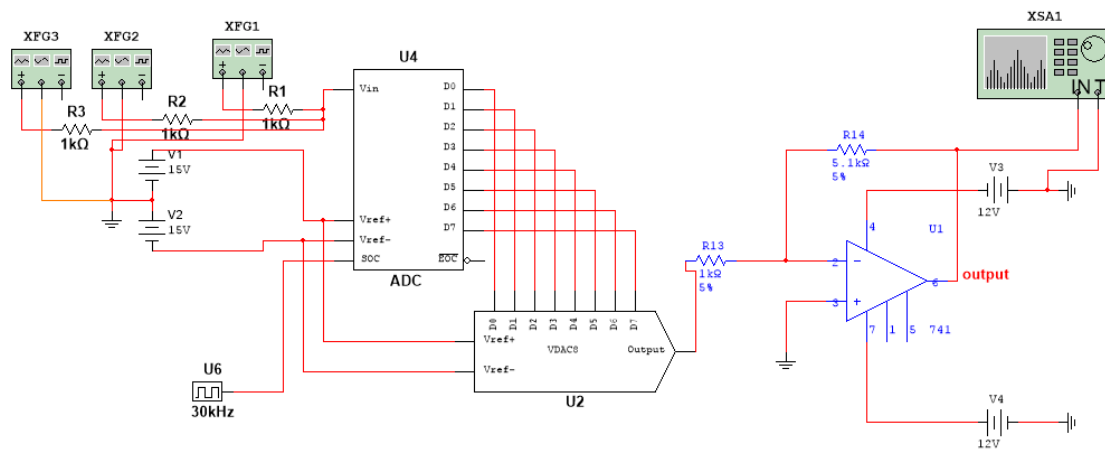


FIGURE 5.1: A Multisim based test set up for simultaneous downconversion and digitization of Multiband SOI

In the present scenario, three signals (represented by sinusoidal tones of three different frequencies) are generated with the help of signal generator. In order to depict a certain bandwidth of  $B$  Hz, it is ensured when down-converted by the ADC these sinusoids remain separated in the frequency domain with a difference of  $B$  Hz. This separation in the first-Nyquist zone depicts the bandwidth of the sinusoids that is manageable when sampled at the sampling rate of  $2NB$  samples per second. For each value of  $\Delta f/B$ , these sinusoids are uniformly spaced in the pass-band before the sub-sampling operation. Later, the  $\Delta f$  between the sinusoids is gradually increased, while the sample rate  $f_s = 2NB$  is kept fixed. Separate simulations are carried out for each value of the sparsity ratio using Multisim and



Matlab. Figs. 5.2, 5.3, 5.4 and 5.5 show the output for four different values of sparsity-ratio for a fixed sampling rate of  $2NB = 12$  ksps. In addition, results are validated both for the proposed method and the one presented in [65], and are compared with each other. According to [65], for odd number of sinusoids  $N$ , acceptable values of  $\Delta f$  should either be equal to  $(1 + 2nN)B$  or  $2(1 + 2m)B$ , where  $n$  is a positive integer and  $m$  is member of natural numbers. In addition to this some other constraints are also applied by [65] to define  $m$ . Table 5.1 shows the complete list of  $\gamma = \Delta f/B$  suitable for successful down-conversion of pass-band signals in the first-Nyquist zone. Clearly, [65] does not support all the ratios of  $\Delta f$  and  $B$ .

In order to make the scenario more illustrative and simple, in addition to the Multisim based simulations, we are using the same arbitrary values of the sparsity-ratio and are verifying the results based on the Matlab simulation. For our proposed method Table 5.2 shows the sparsity-ratio and position of the carrier frequency in pass-band and after down-conversion in first-Nyquist zone as well. It can be noticed that using proposed method for  $\gamma$  equal to 5, 13 and 40 there is no frequency overlap and all sinusoids are successfully down-converted from pass-band to first-Nyquist zone. Because both condition i.e.  $f_{min}$  and  $f_j - f_i$  are fulfilled. However, for  $\gamma$ , equal to 51, we see that  $f_j - f_i$  is multiple of  $2NB$ , which results in aliasing and complete SOI is down-converted to a single frequency i.e. 3 Hz. This is due to the fact that  $f_{c3} - f_{c1} = 204$  Hz, which is integral multiple of sampling rate. The issue can be resolved by calculating  $f_{c1}$  using Eq. 4.12, 4.13 and 4.18 - 4.20 given in chapter 4 and also by increasing  $f_s$  from  $2NB$  to  $(2N + 1)B$ . Fig. 5.6 shows the Matlab simulations of the same. It may be observed that all sinusoids have different magnitudes. This is done deliberately, so that, all of the sinusoids can be distinguished in the base-band region after down-conversion just by visual inspection, without going into complex mathematical calculations. On the other hand the methodology given in [65] is unable to directly down-convert the complete SOI without any frequency overlap. The methodology works well for the sparsity-ratio 13 and 40 only and does not hold for  $\gamma = 5$  and  $\gamma = 51$ . Fig. 5.7 shows the overlapping of sinusoids in the first-Nyquist zone for  $\gamma = 5$

and  $\gamma = 51$ , which also verifies the results of [65]. Table 5.2 clearly describes the frequencies of all sinusoids before and after down-conversion. Here, it is pertinent to highlight and also evident from the first and the third row of Table 5.2 that irrespective of the sparse ratio i.e, whether the sinusoid frequencies are 5 kHz, 15 kHz and 25 kHz or these are 1 kHz, 81 kHz and 161 kHz , in both cases these can be successfully down-converted to the first Nyquist-zone using same sampling rate. Finally, we shall finish this scenario by giving an example based on Matlab simulation, where we are generating the signal of desired bandwidth instead of a sinusoidal representation.

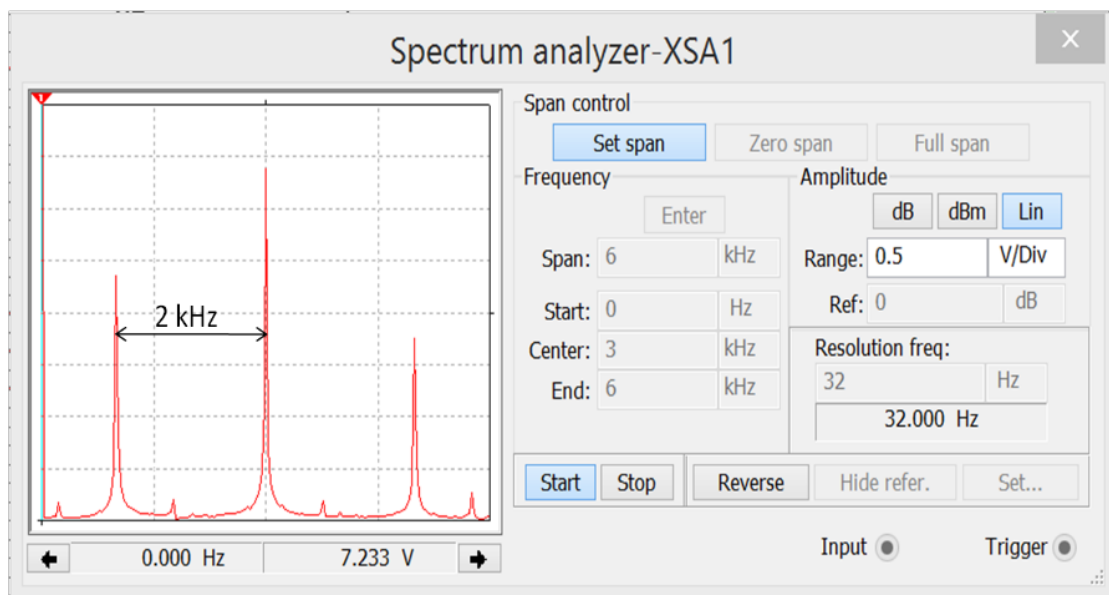


FIGURE 5.2: Down-conversion of a tri-band sparse-spectrum using  $f_s = 12$  kps. The input bands are sinusoidal-tones generated at 5, 15, 25 kHz and down-converted into the First-Nyquist zone, where these are positioned at a frequency gap of 2 kHz from the adjacent band. This separation of 2 kHz between their peaks shows that there is no aliasing-overlap for a bandwidth of 2 kHz.

*Example 5.1.* In the above discussion the complete bandwidth of a band or signal is represented by a sinusoid so that the gap between the adjacent bands can be clearly seen. In this example we are generating the exact bandwidth for each band separately. In the present scenario four RF signals of 6.25 kHz bandwidth each, are generated using QAM64 modulation. Carrier frequencies of RF signals are 2.428125 MHz, 2.440625 MHz, 2.453125 MHz and 2.465625 MHz. A frequency separation between adjacent signals is 12.5 kHz, which is twice of the bandwidth

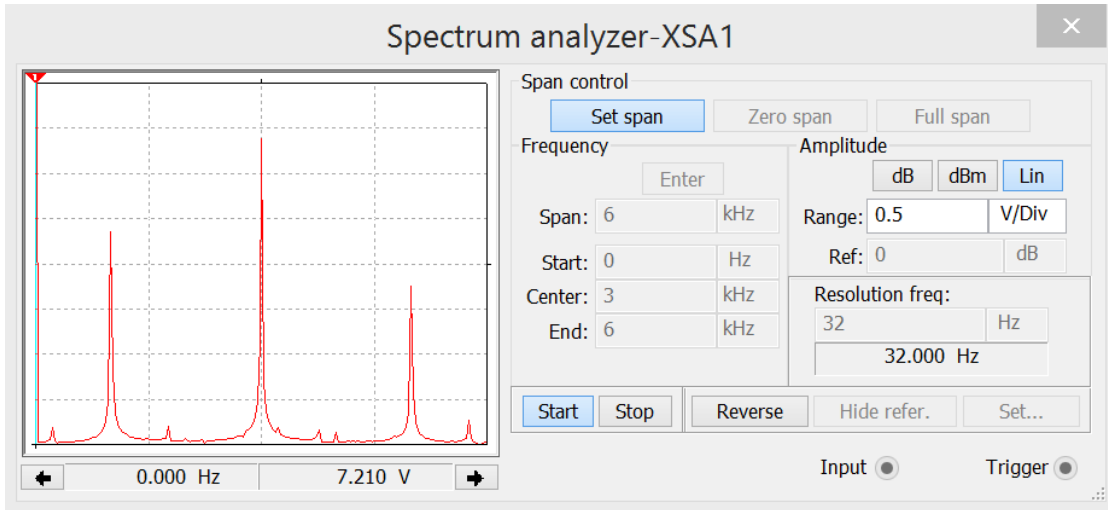


FIGURE 5.3: Downconversion of 13, 39, 65 kHz sinusoids using  $f_s = 12$  kbps and  $\Delta f/B = 13$

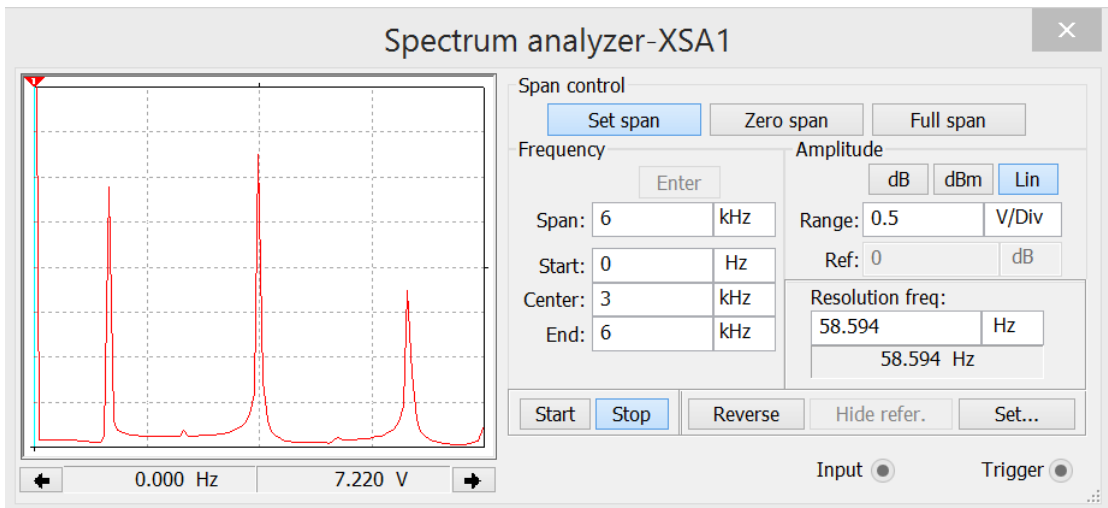


FIGURE 5.4: Downconversion of 1, 81, 161 kHz sinusoids using  $f_s = 12$  kbps and  $\Delta f/B = 40$

of each. Thus we have a even sparse ratio ( $\gamma$ ) equal to 2. In order to achieve a bandwidth of 6.25 kHz a symbol rate of 5.0 kHz is used with a sample rate of 10 samples/symbol. Thus we have a net sample rate of 50 kHz which is exactly equal to  $2NB$ . After carrying out modulation, we apply the pulse shaping using a square root raised cosine filter with a filter length of 8 symbols and a roll off factor of 0.2. A Welch spectrum estimator is created and used to verify that the frequency spectrum of the base-band signal is centered at zero Hz. In this connection Matlab commands 'design' and 'psd' are used for transmit filter and to estimate the spectrum of the pulse shaped signal. Fig. 5.8 shows the power

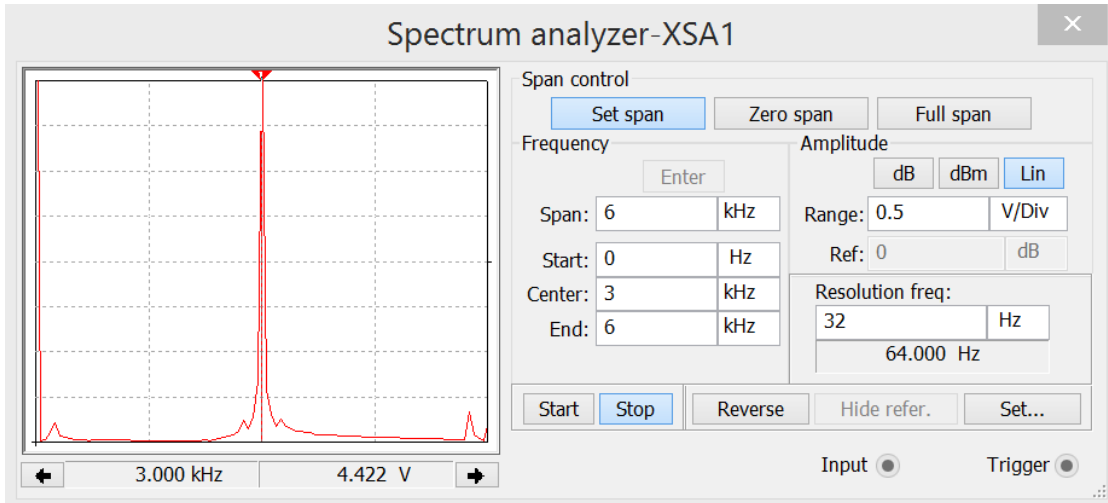


FIGURE 5.5: Downconversion of 51, 153, 255 kHz sinusoids using  $f_s = 12$  ksp/s and  $\Delta f/B = 51$

TABLE 5.1: Some possible values for  $\Delta f/B$ , which avoid aliasing when using the minimum sampling frequency ( $N = 2, 3, \dots, 12$ )

N	Values of $\Delta f/B$	
	Muoz-Ferreras et al [64]	Proposed
2	1, 2, 5, 6, 9, 10, 13, 14, 17, 18, 21, 22, 25, 26, 29, 30, . . .	1, 2, 3, . . .
3	1, 2, 4, 7, 8, 10, 13, 14, 16, 19, 20, 22, 25, . . .	1, 2, 3, . . .
4	1, 2, 6, 9, 10, 14, 17, 18, 22, 25, . . .	1, 2, 3, . . .
5	1, 2, 4, 6, 8, 11, 12, 14, 16, 18, 21, 22, 24, . . .	1, 2, 3, . . .
6	1, 2, 10, 13, 14, 22, 25, 26, . . .	1, 2, 3, . . .
7	1, 2, 4, 6, 8, 10, 12, 15, 16, 18, 20, 22, 24, . . .	1, 2, 3, . . .
8	1, 2, 6, 10, 14, 17, 18, 22, 26, 30, . . .	1, 2, 3, . . .
9	1, 2, 4, 8, 10, 14, 16, 19, 20, 22, . . .	1, 2, 3, . . .
10	1, 2, 6, 14, 18, 21, 22, 26, . . .	1, 2, 3, . . .
11	1, 2, 4, 6, 8, 10, 12, 14, 16, 18, 20, 23, . . .	1, 2, 3, . . .
12	1, 2, 10, 14, 22, 25, 26, . . .	1, 2, 3, . . .

spectral density using Welch psd estimate.

### 5.5.2 Scenario-II.

This scenario pertains to selection and validation of  $f_{c1}$  in order to use lowest possible sampling rates, i.e.  $2NB$ . Although in practical cases sampling rate is generally between 3.5 - 4 times of the information bandwidth, however, for reference and comparison we are discussing the ideal case i.e. to achieve a sample

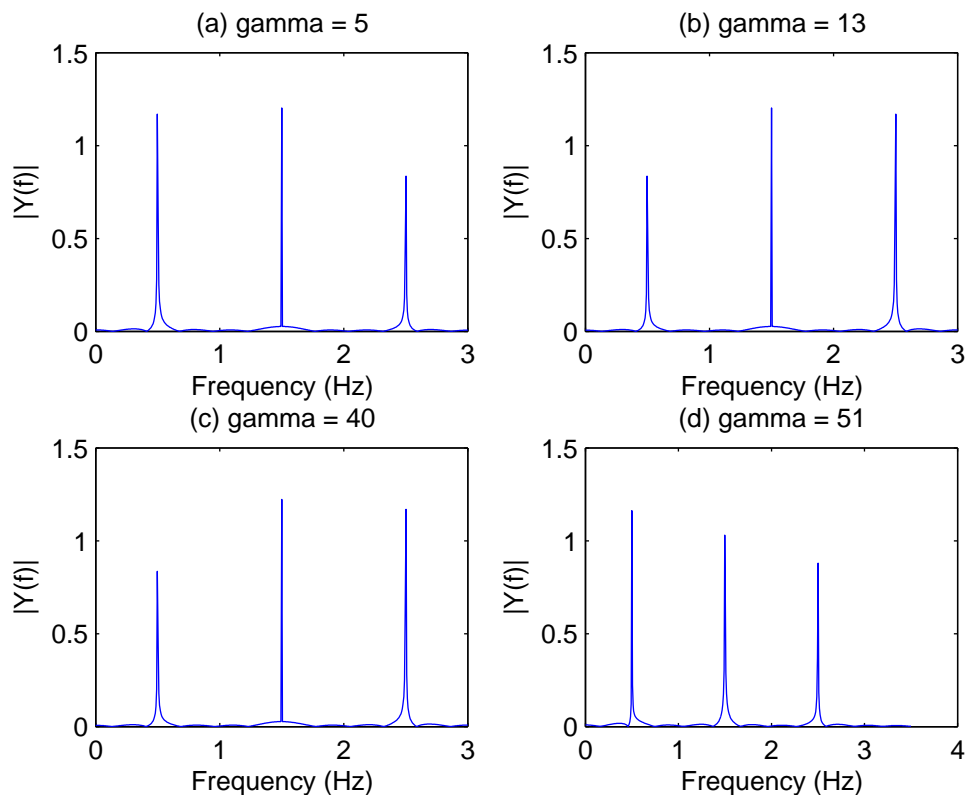


FIGURE 5.6: Direct down-conversion of three sinusoids for  $\gamma$  equal to 5, 14, 40 and 51 using proposed methodology

TABLE 5.2: A spectrum comprising three sinusoids with sparsity ratio 5, 13, 40 and 51.

Sparse Ratio	Pass-band			Baseband			Remarks
	$\gamma$	$f_{c1}$	$f_{c2}$	$f_{c3}$	$f_{a1}$	$f_{a2}$	
5	5	15	25	5	3	1	-
13	13	39	65	1	3	5	-
40	1	81	161	1	3	5	-
51	51	153	255	3	3	3	All channels overlap at 3 Hz

rate equal to twice of the information bandwidth. As described earlier that the sampling rate  $f_s = 2NB$  also caters the guard-bandwidth, which is desirable for successful filtering of base-band signal. For the ease of comprehension, let us start with an example of six-band system. This will help us to understand the significance of the lowest frequency  $f_{L1} = f_{c1} - B/2$  in the SOI, where  $f_{c1}$  is the lowest center-frequency of the first band.

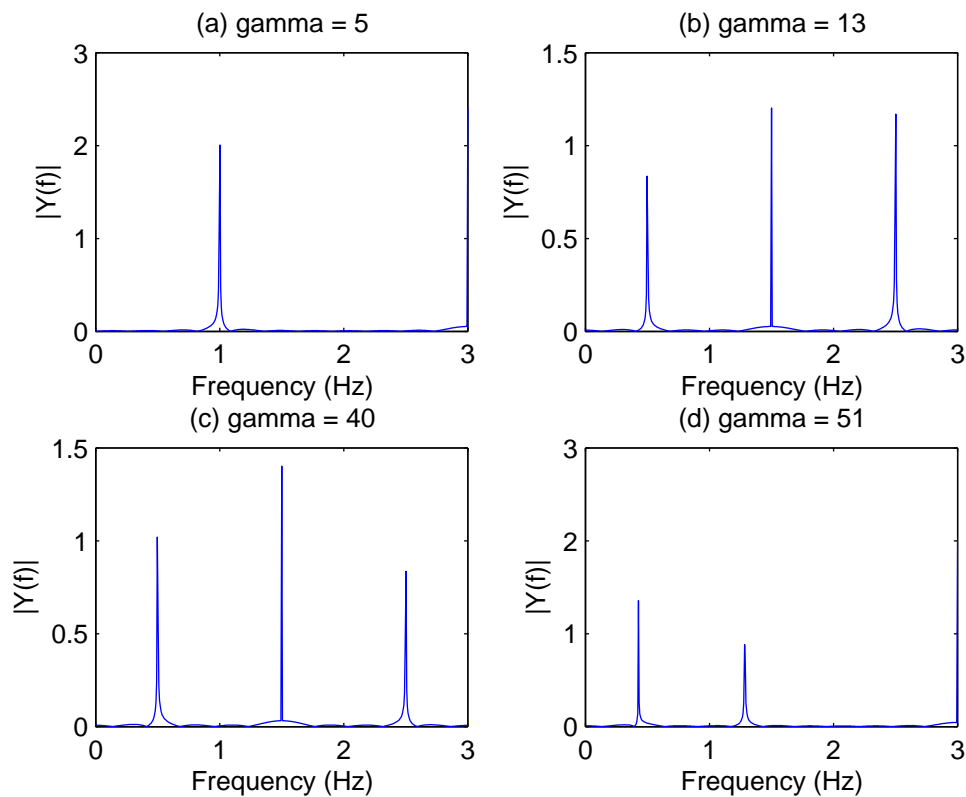


FIGURE 5.7: Direct down-conversion of three sinusoids using Munoz et al. shows a frequency overlap for  $\gamma$  equal to 5 and 51

*Example 5.2.* Consider a six-band system in a sparse-spectrum environment with a sparsity ratio of 83. Each band has a bandwidth of 4 kHz. The lowest center-frequency frequency selection is based on the arbitrary value of gamma, *e.g.* 83. The lowest center-frequencies are calculated for  $k = 1$  to  $k = 10$  using the expression  $(\gamma \pm 2(k - 1)N)B/2$  already described in chapter 4. The positions of other bands can be determined using the expression  $f_{cn} = f_{c1} + (n - 1)\Delta f$  and are presented in Table 5.3. It can be noticed that for each increment in the value of  $k$  there is a linear increase of  $NB$  Hz in the minimum center-frequency. The simulations are carried out using Multisim. Fig. 5.11 shows the down-conversion of the complete SOI using a sampling rate of 48 ksps. The point to be emphasized is that any change in the recommended minimum frequency shifts the entire spectrum towards left or right, which in return causes aliasing-overlap. Fundamentally our emphasis is on the selection of lowest useable frequency  $f_{L1}$  in SOI. This aspect is described in [65] by Mũnoz *et al.*, however their algorithm reduces the choice to select specific

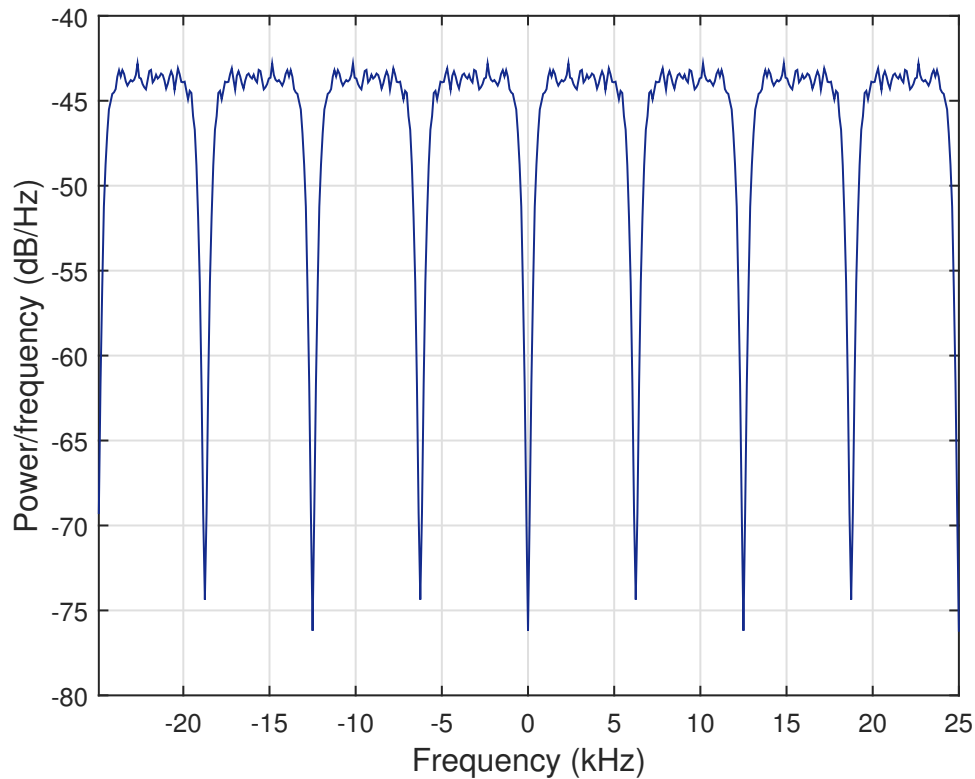


FIGURE 5.8: Baseband spectrum of a uniformly spaced quad-signal environment.

TABLE 5.3: Passband positions of six-band system

$k$	$f_{c1}$	$f_{c2}$	$f_{c3}$	$f_{c4}$	$f_{c5}$	$f_{c6}$
1	166	498	830	1162	1494	1826
2	190	522	854	1186	1518	1850
3	214	546	878	1210	1542	1874
4	238	570	902	1234	1566	1898
5	262	594	926	1258	1590	1922
6	286	618	950	1282	1614	1946
7	310	642	974	1306	1638	1970
8	334	666	998	1330	1662	1994
9	358	690	1022	1354	1686	2018
10	382	714	1046	1378	1710	2042

frequency for any radio design. Table 5.4 shows the suitable values of  $f_{L1}$  for a quad-band system presented in [65]. Each band has a bandwidth of 2 kHz. The first column represents the sparsity ratio in the SOI, which varies from 2 to 9. We can notice that a careful selection of minimum frequency helps us in two ways, first, it makes possible to achieve minimum sample rate and second we can make

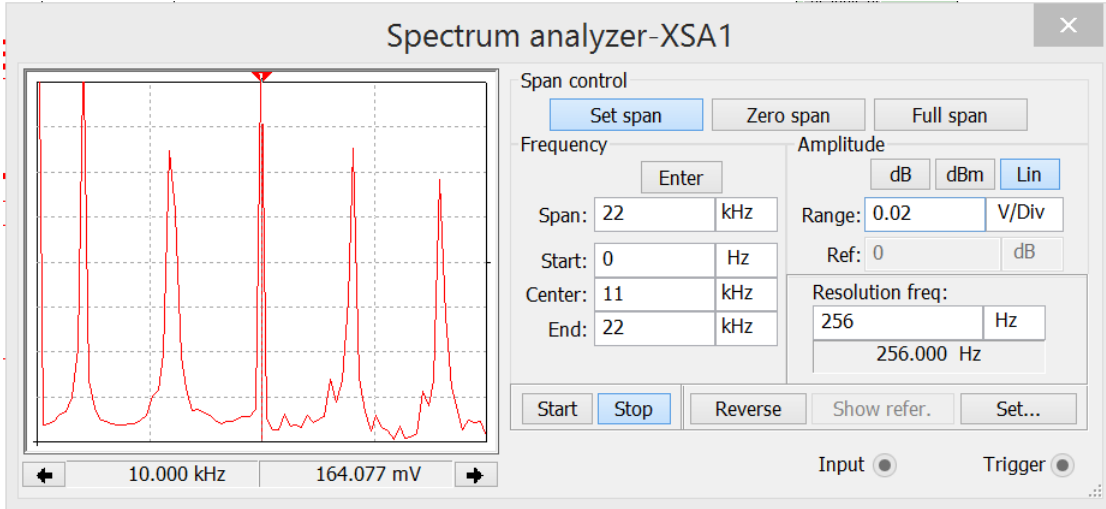


FIGURE 5.9:  $\gamma = 10$ .  $N=5$ ,  $B=4000$

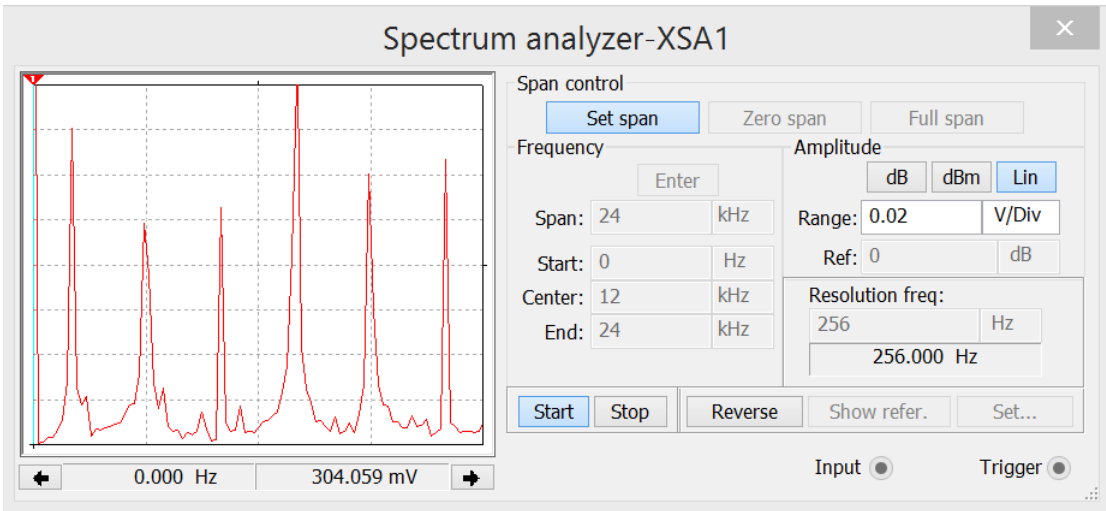


FIGURE 5.10:  $\gamma = 12$ .  $N=6$ ,  $B=4000$

the maximum use of any assigned bandwidth. The minimum frequency designated as  $f_{L1}$  in [65] is  $kf_{s,min}/2 = kNB$ , where  $k \in N \cup 0$ . This implies that their  $f_{min}$  is dependent on product of  $N$  and  $B$  and hence only one value of  $f_{min}$  is usable out of a bandwidth of  $NB$ . It is also evident from Table 5.4 that for  $N = 4$  and  $B = 2$  besides 0 other possible values of  $f_{L1}$  are multiple of 8 ( $NB$ ), which reduces the choice by a factor of eight. The other drawback of [65] is that it is not applicable to all values of  $\gamma$ . As we can see that for  $\gamma$  equal to 3, 4, 5, 7 and 8 their proposed technique is not workable. On the other hand our proposed methodology is much more flexible in terms of both aspects. First it does not depend upon the multiplication product  $NB$  and hence offers more flexibility to



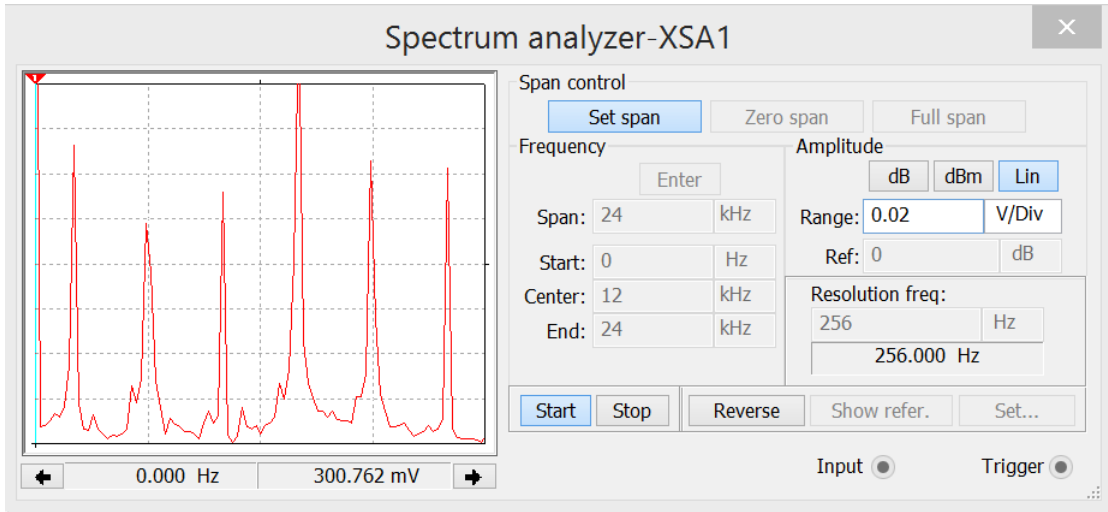


FIGURE 5.11: Down-conversion of a six-band sparse-spectrum with sparsity of 1:83

TABLE 5.4: Suitable values of lowest frequency  $f_{L1}$  to avoid aliases overlap.

$\Delta f/B$	Minimum Frequency	
	Munoz <i>et al.</i> [65] $f_{L1} = kNB$	Proposed
2	0, 8, 16, 24. . .	0, 1, 2, 3, 4, . . .
3	None	2, 10, 18, 26, 34. . .
4	None	3, 7, 12, 16, 21. . .
5	None	4, 12, 20, 28, 36. . .
6	0, 8, 16, 24. . .	0, 1, 2, 3, 4. . .
7	None	6, 14, 22, 30, 38. . .
8	None	7, 8, 16, 17, 25, 26. . .
9	0, 8, 16, 24. . .	0, 1, 2, 3, 4. . .

choose value of  $F_{L1}$ . Secondly, it is applicable to all values of  $\gamma$ .

### 5.5.3 Scenario-III.

Interoperability amongst various radio networks is one of the core objectives of software defined radios. To address this core concept for public safety, future radio networks would benefit, only if those would be dynamically adaptable and reconfigurable in order to ensure interoperability. These radios are supposed to be multi-band, multi-standard across wide radio frequency spectrum and also be

compatible with legacy transceivers systems. In this scenario we propose a land-mobileradio design as a simple and low cost solution for this key issue of interoperability in a public safety scenario. Our proposed radio design is capable to receive and simultaneously downconvert and digitize desired channels from the bands allocated by Federal Communications Commission, USA, for public safety radio. Based on direct RF bandpass sampling, our design requires a low speed ADC upto 10 Msps, having wide input bandwidth of 500 MHz and hence gives assurance in reduction of system cost, complexity without any compromise on fast detection and processing of radio channels.

Given that we have to design a 36-channel, 3-band LMR (land mobile radio) in the frequency range of 3 MHz to 512 MHz, such that each band has twelve channels of equal bandwidth. The bands are based on the HF (3-30 MHz), VHF (30-300 MHz) and UHF (300-512 MHz) wave propagation characteristics. The frequencies to be allocated are sparsely positioned in the given frequency range, forming three bands each of 48 kHz (12 Channels of 4 kHz each). Using the prescribed methodology we have to select the lowest possible sampling rate and the band-positions for four arbitrary sparsity-ratios, e.g., 206, 347, 620 and 805.

**Solution.** A careful analysis of the situation shows that there are three main constraints:-

- a. Selection of frequency from each band.
- b. Sparse ratio.
- c. Minimum possible sampling rate of our own choice.

After identifying our constraints we shall solve the problem in three steps as follows:

**Step. I.** To proceed further, we shall first calculate the complete set of available frequencies for  $N = 3$  and given sparse ratios, using equation 4.13 given in the previous chapter. All of the available frequencies in the given range are listed below. It can be noted that all frequencies are evenly spaced for the respective sparse ratio.

- **List of frequencies for  $\gamma = 206$ .**

– *HF Band*

\* 24000 9912000 19800000

– *VHF Band*

\* 029688000 039576000 049464000 059352000 069240000 079128000  
089016000 098904000 108792000 118680000 128568000 138456000  
148344000 158232000 168120000 178008000 187896000 197784000  
207672000 217560000 227448000 237336000 247224000 257112000  
267000000 276888000 286776000 296664000

– *UHF Band*

\* 306552000 316440000 326328000 336216000 346104000 355992000  
365880000  
375768000 385656000 395544000 405432000 415320000 425208000  
435096000  
444984000 454872000 464760000 474648000 484536000 494424000  
504312000

• **List of frequencies for  $\gamma = 347$ .**

– *HF Band*

\* 8328000 24984000

– *VHF Band*

\* 041640000 058296000 074952000 091608000 108264000 124920000  
141576000 158232000 174888000 191544000 208200000 224856000  
241512000 258168000 274824000 291480000

– *UHF Band*

\* 308136000 324792000 341448000 358104000 374760000 391416000  
408072000 424728000 441384000 458040000 474696000 491352000  
508008000

- **List of frequencies for  $\gamma = 620$ .**

- *HF Band*

- \* 24000 29784000

- *VHF Band*

- \* 014904000 059544000 074424000 089304000 104184000 119064000  
133944000 148824000 163704000 178584000 193464000 208344000  
223224000 238104000 252984000 267864000 282744000 297624000

- *UHF Band*

- \* 327384000 357144000 386904000 416664000 446424000 476184000  
505944000

- **List of frequencies for  $\gamma = 805$ .**

- *HF Band*

- \* 19320000

- *VHF Band*

- \* 57960000 96600000 135240000 173880000 212520000 251160000  
289800000

- *UHF Band*

- \* 328440000 367080000 405720000 444360000 483000000

**Step. II.** In the second step we shall select the set of frequencies meeting our requirement. This means that we have to select at least one band of 12-channels from each section. It is also important to high-light that calculated set of frequencies meets the first two conditions to avoid spectrum folding around dc-component or  $f_s/2$ . Also there is no partial overlap of any of the bands. However, a complete aliases-overlap with neighbouring band in the base-band may occur if  $f_s$  is integer multiple of  $f_{c1} - f_{c2}$  or  $f_{c1} - f_{c3}$  or  $f_{c1} - f_{c3}$ . After selection of suitable frequencies,

simulations are carried out using Matlab. A set of useable frequencies from each band is given in Table 5.5 for each value of sparsity-ratio. This means that we have sufficient flexibility to choose a frequency-set of our own choice for frequency planning. By implementing any of the given sets we can fulfill our design objective of a simple multi-band radio using a low-speed ADC. Initially, only carrier frequency is used to represent the pass-band signal or band. Fig. 5.12 shows that all bands are separated by 48 kHz from each other and are 24 kHz apart from dc and  $f_s/2$ . This shows that all necessary conditions are successfully met.

**Step. III.** In the last step we shall compose a 48 kHz wide signal using QAM and  $F_c = [8328000 \ 158232000 \ 424728000]$  as a set of their carrier frequencies. The selected frequencies are HF, VHF and UHF bands. First we shall initialize variables that define simulation parameters, such as carrier frequency, number of samples representing a symbol, and noise level. Following are the values of selected parameters

$F_c = [8328000 \ 158232000 \ 424728000];$  Carrier frequencies (Hz)

$R_{sym} = 32000;$  % Symbol rate (symbols/second)

$nSamps = 9;$  % Number of samples per symbol

$frameLength = 2048;$  % Number of symbols in a frame

$M = 16;$  % Modulation order (16-QAM)

$E_bN_o = 10;$  % Ratio of base-band bit energy to noise power spectral density (dB)

For simulation purpose, in order to calculate the sampling frequency besides Nyquist criterion we also need to ensure that  $f_s = R_{sym} * nSamps$ . After, initialization of basic parameters, we calculated passband SNR in dB. The noise variance of the base-band signal is double that of the corresponding bandpass signal [103]. To account for this difference we increased the SNR value by  $10 * \log_{10}(2)$  dB and have equivalent base-band and passband performance as expressed in equation 5.1.

$$SNR = E_bN_o + 10 * \log_{10}(\log_2(M)/nSamps) + 10 * \log_{10}(2) \quad (5.1)$$

Finally, in order to simulate a passband communication system we shall modulate the random data in the base-band. For this purpose we are generating random

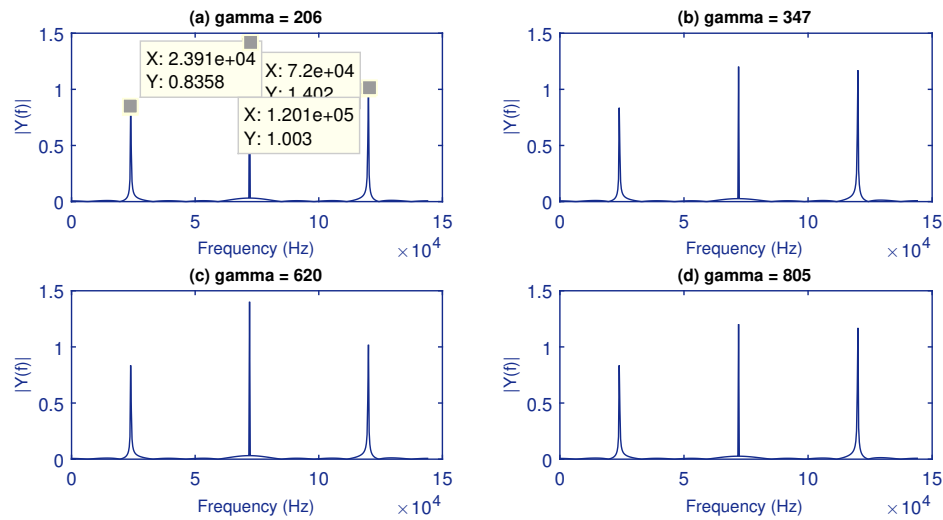


FIGURE 5.12: Triband downconversion using four different values of gamma

symbols. These symbols will be modulated with a 16-QAM modulator and applied for pulse shaping using a square root raised cosine filter. We shall use the spectrum estimator to verify that the frequency spectrum of the base-band signal is centered at zero Hz, and that it has been filtered properly. In this relation following measurement tools are being utilized.

*Scatter plot.* A scatter plot is used to analyze signals at different points in the transmitter-receiver chain. We are using the Welch Spectrum Estimator to estimate the spectrum of signals based on hamming window. Fig. 5.13 shows a Welch power density estimate with an attenuation of 50 dBs.

*Raised Cosine Filter.* In any data communication system, it is important to understand that pulses are sent by the transmitter and in the end detected by the receiver. At the receiver end, the objective is to maximize the probability of an accurate binary decision. This is achieved by carrying out appropriate sampling of the received signal at an optimal point in the pulse interval. In other words, the fundamental shapes of the pulses are designed in a manner that they do not meddle with their neighboring pulses. This is done by fulfilling two conditions. Condition one is that the pulse shape displays a zero crossing at the sampling point of all pulse intervals except its own. Otherwise, the residual effect of other pulses might produce errors due to faulty decision making. Condition two relates to the shape of the pulses, it is done such that their amplitude has a sharp roll off

TABLE 5.5: Set of useable frequencies for a multi-band radio design in a sparse electromagnetic environment

Sparsity-Ratio	HF-Band	VHF-Band	UHF-Band
206	09912000,	148344000,	494424000
347	08328000,	141576000,	491352000
620	29784000,	148824000,	476184000
805	19320000,	135240000,	444360000

outside of the pulse interval. This too, is a source of error in the decision making process, because the sharper a pulse decays outside of its pulse interval, the less is the probability to allow timing jitter to introduce errors when sampling adjacent pulses. The raised cosine pulse, is one of the suitable choice which meets the above mentioned conditions and is used in a wide variety of data communication systems. After modulation, we applied pulse shaping using a square root raised cosine filter. We also utilized the spectrum estimator to verify that the frequency spectrum of the base-band signal is centered at zero Hz, and that it has been filtered properly. In our case we used a filter length of 16 symbols and a roll off factor of 0.35.

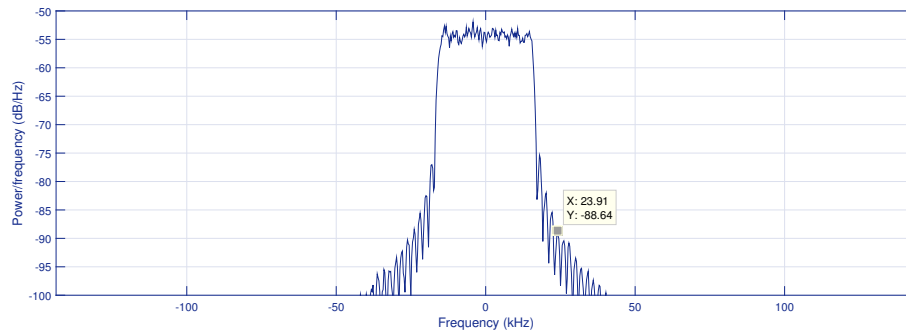


FIGURE 5.13: Welch power density estimate for 24 kHz bandwidth

Fig. 5.14 shows the Welch power density spectrum of the tri-band radio. It can be noticed that all bands are successfully down-converted in the base-band. There is no aliasing overlap of bands or spectrum folding at dc or  $f_s/2$ .

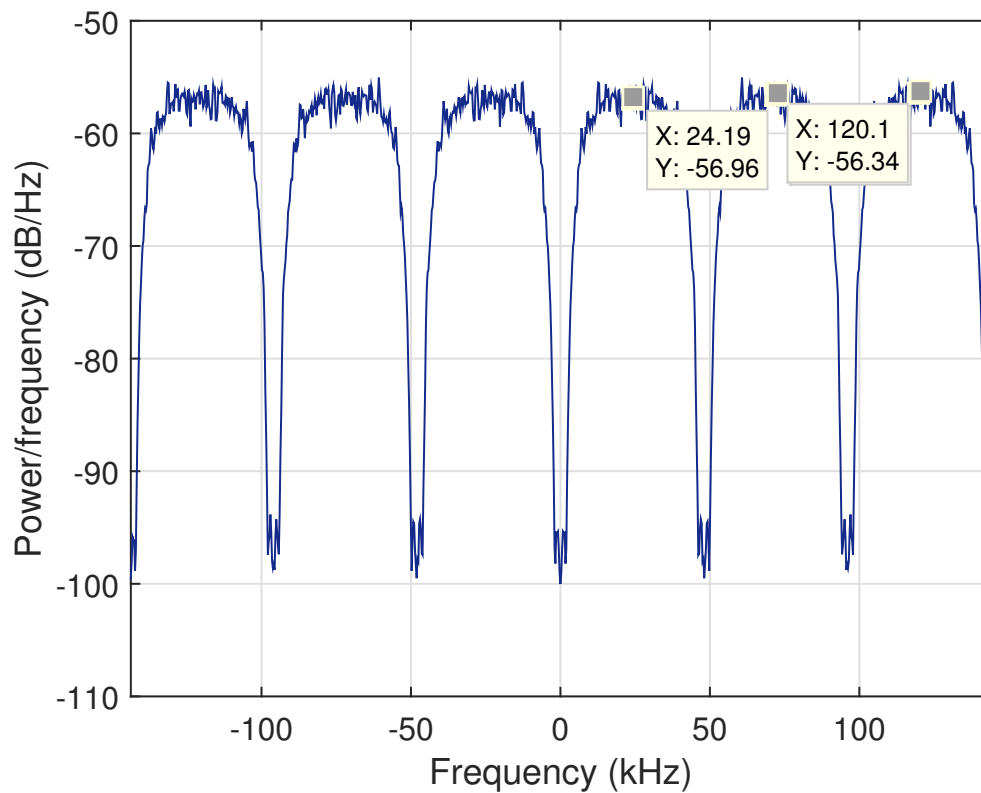


FIGURE 5.14: Welch power density of tri-band radio spectrum

#### 5.5.4 Scenario-IV.

In CR communication systems, fast and reliable detection of white spaces i.e. the channels which are not occupied by the primary user (PU) is one of the most fundamental requirements. In this scenario, we are simulating our proposed sampling methodology for the same. The fast detection technique is based on RF filters bank of equal bandwidths placed closed to the antenna as shown in the Fig. 5.15. In conventional heterodyne receiver, a low rate analog to digital convertor (ADC) is used, however that contains an analog bandpass filter. This results in a barrier in lowering detection time as significant time is used in scanning operation. While the homodyne receiver has the capability of fast detection due to the use of high rate ADC, which is an unfeasible or very costly approach. Compressive sensing based receiver architectures are proposed in recent years, however those receivers do not work efficiently under the condition when the spectrum is congested and the number of channels is increased. In this work, we propose a filter banks based



TABLE 5.6: A spectrum of nonzero energy contents with sparsity ratio 1 to 6. The last column lists values of normalized sparsity to avoid aliasing for given minimum sampling frequencies.

N	Usable values of $\Delta f/B$		% of usable $\Delta f/B$	
	Muñoz-Ferreras et al [65]	Proposed	[65]	Proposed
2	1, 2, 5, 6, 9, 10, 13, 14, 17, 18, 21, 22, 25, 26, 29, 30, . . .	1, 2, 3, . . .	53.33	100
3	1, 2, 4, 7, 8, 10, 13, 14, 16, 19, 20, 22, 25, . . .	1, 2, 3, . . .	52.00	100
4	1, 2, 6, 9, 10, 14, 17, 18, 22, 25, . . .	1, 2, 3, . . .	40.00	100
5	1, 2, 4, 6, 8, 11, 12, 14, 16, 18, 21, 22, 24, . . .	1, 2, 3, . . .	54.16	100
6	1, 2, 10, 13, 14, 22, 25, 26, . . .	1, 2, 3, . . .	30.77	100
7	1, 2, 4, 6, 8, 10, 12, 15, 16, 18, 20, 22, 24, . . .	1, 2, 3, . . .	54.16	100
8	1, 2, 6, 10, 14, 17, 18, 22, 26, 30, . . .	1, 2, 3, . . .	33.33	100
9	1, 2, 4, 8, 10, 14, 16, 19, 20, 22, . . .	1, 2, 3, . . .	45.45	100
10	1, 2, 6, 14, 18, 21, 22, 26, . . .	1, 2, 3, . . .	30.77	100
11	1, 2, 4, 6, 8, 10, 12, 14, 16, 18, 20, 23, . . .	1, 2, 3, . . .	52.17	100
12	1, 2, 10, 14, 22, 25, 26, . . .	1, 2, 3, . . .	26.92	100

receiver with bandpass sampling architecture capable of fast detection and using a low rate ADC as well. In addition, comparative analysis of classical designs with proposed architecture is done by considering performance parameters of detection time of the receivers. Figure 5.16 shows a comparison of detection time of our proposed design methodology with the contemporary receivers. The proposed filter banks based receiver with bandpass sampling architecture is shown in Fig. 5.15. The received signal is equally divided into  $L$  bandpass filters. Further it is sampled by an ADC with under-sampling rate using direct down-conversion method in [8] followed by digital signal processing to determine the status of the channel. The power spectrum is calculated by taking the squared magnitude of  $N$ -point FFT of the sub-bands. The estimated power, which is the power in each bin in the power spectrum is then compared with the threshold to determine the status of the channel. This process is continued until all the  $L$  number of channels corresponding to the  $L$  bandpass filters are processed. The switching time  $T_{sw}$ , which is the time taken in the switching between the  $L$  number of filters, is much less than the DSP time  $T_{fb-DSP}$ . It is worth mentioning that, the sampling rate of ADC will be decreased by  $L$  times with the use of filter banks. Detection time of the proposed receiver depends on three components, (1) Acquisition time, i.e.,  $T_{aq} = ((N.N_i/N.W_c)) = N_i/W_c$ , (2) Number of filters  $L$  and (3) Digital signal

processing time. Digital signal processing time decreases with number of filter banks  $L$ . This is because there are only  $N/L$  channels to be processed for FFT operations, where  $N$  is the total number of channels. The digital signal processing time can be written as:

$$T_{fb-DSP} = N_i(L.T_{FFT}^{N/L}) \quad (5.2)$$

where  $T_{FFT}^{N/L} = (N/L)/N_{ref} \cdot \log_2 \cdot N_{ref} \cdot T_{FFT}^{N_{ref}}$  and  $T_{FFT}^{N_{ref}}$  is 26 microseconds for 1024 point FFT operations on vertex -4 LX25 FPGA from Xilinx [104].

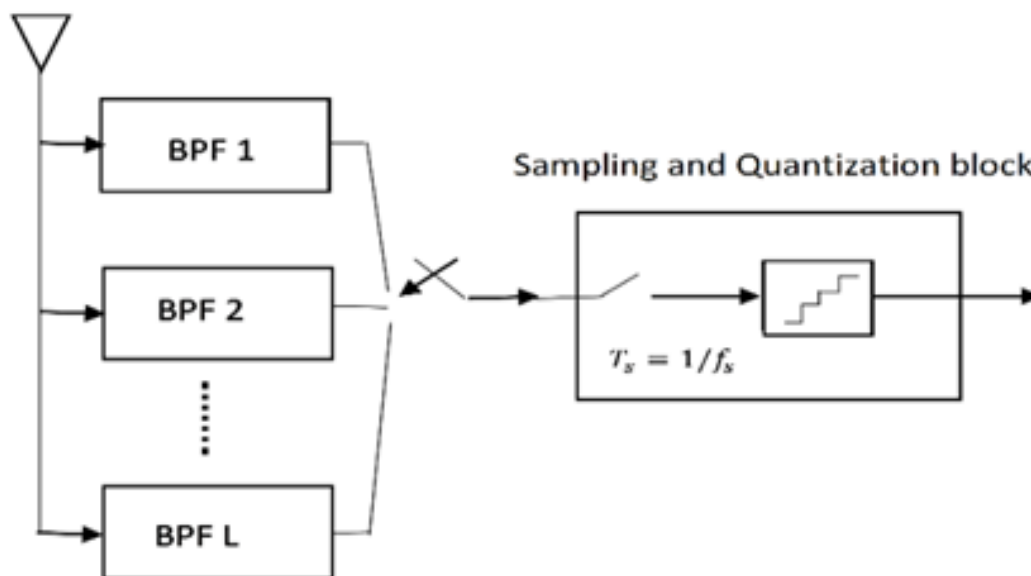


FIGURE 5.15: An RF output of a filters bank, comprised of  $L$  filters of equal bandwidth being sampled in a sequential order.

### 5.5.5 Conclusion.

In this chapter we made an effort to support our argument that the minimum frequency in the spectrum of interest has paramount importance in the selection of the minimum sampling rate. For a given number of input signals of a known bandwidth in the desired spectrum, it is not permissible to plan  $f_{min}$  as any arbitrary frequency. This is the reason that the suggested  $f_{min}$  (shown as  $f_{L1}$  by Muñoz-Ferreras et al. in [65]) is restricted to a set of frequencies  $\in 2kNB$ .

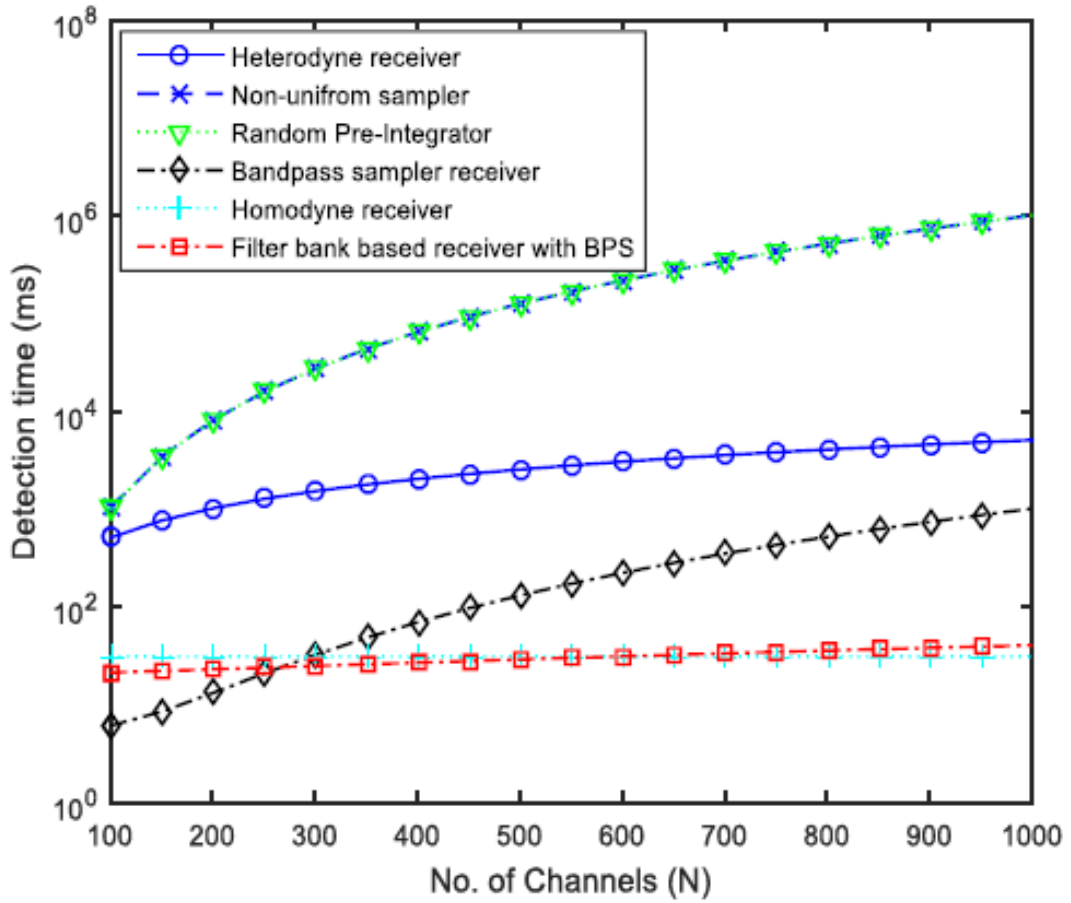


FIGURE 5.16: Detection time comparison for the heterodyne receiver, non-uniform sampler, random pre-integrator, bandpass sampling receiver, homodyne receiver and the proposed filters bank based receiver with BPS architecture.

Consider the example given in [65] for  $N = 4$  and  $\Delta f = 2B$ . It can be seen from Table 5.4 that selection of  $f_{min}$  is restricted to the set of frequencies. Using  $f_{min}$  other than the prescribed frequencies resulted in aliasing noise. In other words the lowest frequency in the spectrum of interest should either be 0 or a multiple of  $2NB$ , i.e.  $mod(f_{min}, 2NB) = 0$ ; otherwise there will be overlapping. This enables us to draw a conclusion that, [65] has a frequency selection flexibility of 1 ratio  $2NB$ . On the other hand, in our proposed technique,  $f_{min}$  can be placed at any frequency that is an even multiple of bandwidth  $B$ . Hence, it has a frequency selection flexibility of 1 to  $2B$ , which is  $N$  times greater than that presented in [65].

The other important feature that made the proposed method more generic is its flexibility in terms of sparsity ratio,  $\gamma$ . Flexibility in terms of sparsity ratio,  $\gamma$

offered by [65], as shown in Table 5.6 is applicable to 27% -54% of the values of  $\gamma$ . On the other hand, the proposal is applicable to 100% of the values of the sparsity-ratio. This clearly indicates that the proposed method is more universal in terms of sparseness in the spectrum of interest, and is also applicable to a greater number of signal locations. Finally, to make the advantages more evident, some statistics for different numbers of input bands ranging from  $N = 2$  to  $N = 12$  are shown in Table 5.6, which clearly shows that the work presented in [65] is limited to in the terms of useable average-value of the sparsity-ratio, *i.e.*, 0.404. This implies that their achievement of the ideal sampling rate of  $2NB$  is limited to 40.4% of the patterns of an uniformly spaced spectrum. On the other hand, our proposed technique is applicable for all (100%) integer values of  $\gamma$ .

# Chapter 6

## A Composite GNSS Receiver Design

### 6.1 Overview

In this chapter, we present a composite design for multiband-multistandard Global Navigation Satellite System (GNSS) receiver. The design efficacy is based on a novel bandpass sampling methodology for a sparse-spectrum electromagnetic environment, which is transformed into a quasi-uniformly spaced spectrum. We consider this more appropriate and useful for simultaneous digitization and down-conversion of analog signals. Besides, the composite architecture is also helpful to circumvent the higher-order intermodulation components. In fact, this arrangement of a spectrum of interest (SOI) is appropriate for our proposed composite receiver design, where only a part of SOI is transformed to an intermediate frequency. In this way, the desired frequency bands of information, which are widely spread, are grouped to form a contiguous-spectrum which is quasi-uniformly spaced. There on, a sub-sampling is carried out for simultaneous digitization and translation of input signals to the first-Nyquist zone. The proposed design is validated for conventional Global Positioning System L1 and L2 bands and also for new L5 band used in GNSS (GLONASS, Galileo and Beidou) receivers. Our results show a

considerable reduction in sampling rates, and improvement in signal-to-noise and distortion ratio, which can be easily managed by a low sampling analogue to digital conversion.

In this chapter, we propose a composite design which is more appropriate for a low-speed A/D convertor. In fact, we are highlighting a new dimension that pertains to management of RF spectrum of interest. Our contributions can be categorized in two areas. First is the arrangement of RF signals to minimize sampling rates, consequently leading to the requirement of a low cost, low bandwidth analogue to digital converter. Second, is the architectural modification in the design of general SDR receiver that helps to reduce the higher-order intermodulation components, when compared with the contemporary sub-sampling receiver.

The architecture has the capacity to incorporate the advantages of bandpass sampling technique and minimize the weaknesses conventional and contemporary receiver designs. It shows flexibility to up or down-convert the desired band at an appropriate  $IF$ , such that the TOI-components are completely eliminated from the base-band after digitization. Besides this, frequency translation of partial RF spectrum to form an equally spaced spectrum is found useful to minimize the sampling rate. The reduction in sampling rates varies from case to case. For example, in the case of L1, L2 bands there is a significant reduction in sampling rate from 99.23 Msps to 9.18 Msps. However, in the case of L1/E1/B1, L5/E5a the reduction in sampling rate is from 101.881 Msps to 90.20 Msps. Reduced frequency sampling rates for various desired input signals completely circumvent any spectrum folding and aliasing overlap. Moreover, achieved sampling rates also reduce the processing time in DSP block. In order to validate the proposed architecture, multiple scenarios are developed and results achieved commensurate with the theoretical results anticipated in the sections containing the research methodology and the proposed design.

## 6.2 GNSS Receiver Evolution

Importance of Global Navigational Satellite System (GNSS) devices and their usage such as Global Positioning System (GPS) is increasing with the passage of time. This started from portable electronic systems such as handheld cell phones, and notebooks to widely spread applications, which include but are not limited to tracking systems, intelligent transportation systems, automatic vehicle location, emergency calls and precise-positioning. Due to the exponential increase in the demands for low cost and high precision GPS for civil and military applications, efforts in terms of increased performance, and reductions in the size, cost and power requirements have been made, as a result of which, a number of fully integrated GPS RF receivers have been reported [105]-[106].

The architecture of a conventional analogue Global Positioning System (GPS) receiver is given in Fig. 6.1. This receiver includes a radio frequency (RF) and an intermediate frequency (IF) stage that down-converts the GPS analogue signals to a frequency close to baseband. A similar design is used in the Phase-III GPS receivers, manufactured by Collins [107]. A satellite tracking channel consists of code generation logic (Precise and Coarse/Acquisition code), analogue code correlators and mixers to generate In-phase (I) and Quadrature (Q) signals. The I and Q signals are sampled with a separate analogue to digital (A/D) converter in the receiver channel block, which in return increases the complexity of the receiver circuit, in terms of hardware to add extra satellite tracking channels. Moreover, the parametric differences in the analog components used, introduced varying delays in each receiver channel. This inter-channel bias produces inaccuracies in the pseudo-range observations that have to be calibrated by the receiver. In addition, the conventional GNSS receivers process the received signal using same complex circuitry for relatively low (less than or equal to 20 dB-Hz) and high (greater than or equal to 30 dB-Hz) carrier-to-noise ratio. This is configured to mitigate interference associated with a received signal, which in return may result in an unnecessary waste of power [108].

Other designs, which are more popular for GNSS are zero-IF or Low-IF and direct

RF subsampling receivers. Since the demands for high-level integration and low-power consumption in consumer mobile devices is on increase, zero-IF or low-IF architecture is favorable in GNSS receivers. The down-converted signal around DC with zero-IF architecture will be greatly affected by flicker noise and DC offset. Low-IF architecture is preferred despite that zero-IF receivers are more flexible for integration [109], [106], [110], [111]. This drawback of zero-IF gives low-IF architecture an edge for receiver design to balance flicker noise, and DC offset. However, in low-IF architecture, the IF is one or two times the information bandwidth, that makes it more vulnerable to image-signals. Presence of image-signals at IF stage is troublesome, and becomes a challenge when completely removing the image-signal in the IF bandpass filter. The image-signal and the desired-signal, both get sampled and quantized in the A/D converter. In addition, frequency down-conversion from the low-IF to baseband is materialized in the digital domain to get out of the problems such as inphase and quadrature component mismatches in the analogue domain. Using direct RF sampling architecture, placing A/D converter close to the antenna is significantly helpful to avoid the above mentioned problems.

In general, an RF front-end is mainly composed of pre-amplifiers, filters, and mixers. Each component has three basic parameters, which determine the overall performance of the receiver: gain (G), noise figure (NF), and third-order intermodulation product (IMD3) [112]. These three parameters together with the order of layout of the components establish the sensitivity, gain, and dynamic range of the receiver. The set of equations that is used to determine the overall gain, noise figure, and the resulting third-order intermodulation point are given in [112]. This arrangement is manageable up until the time the number of desired signals is limited to two or three. However, the complexity increases when spectrum of interest is sparse and contains multiple RF signals or bands. In such environment, direct RF sampling receiver demands a very high sampling rate A/D convertor, which as a result requires high power and large number of computations. In actual fact, there is no universal formula which, can calculate the minimum sampling rate due to non-linear nature of spectrum [65]. Composite receiver architecture is one of the suitable choices that can handle the problems like DC off set, image rejection,



IMD3 and high sampling rates by keeping IF in the RF band and managing the Spectrum of Interest (SOI) in a quasi-uniformly laid pattern.

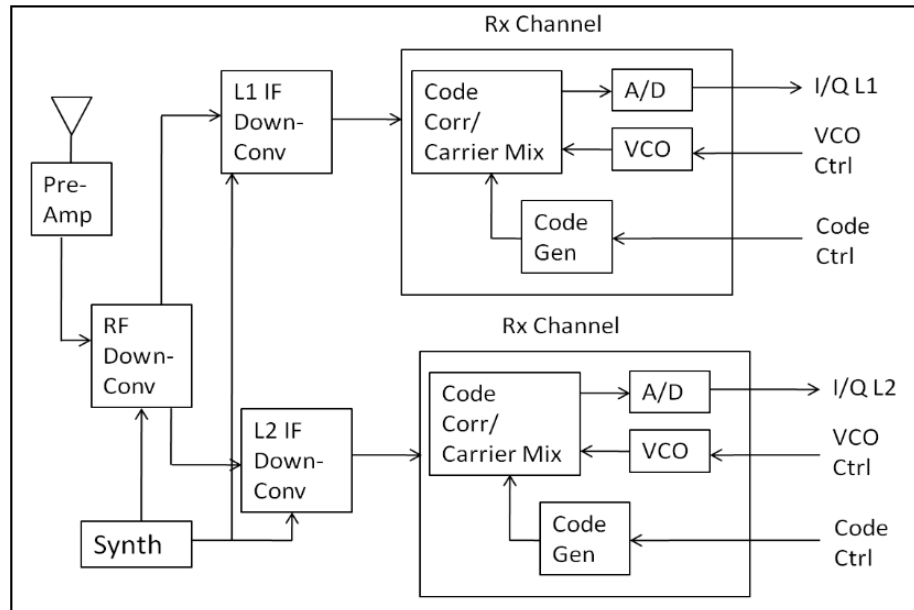


FIGURE 6.1: The architecture of a conventional analogue GPS receiver.

The proposed design is composite in nature when considered with conventional super hetero-dyne receivers and modern zero-IF receivers. As a case study, we intend to implement and simulate our proposed composite design for the development of GNSS receivers. In our proposed design a special emphasis is given on the selection of such RF band that is translated to the IF stage to form a contiguous spectrum containing all signals of interest. The GNSS receiver design is first simulated using Multisim 14.0.1 of National Instruments. The required software is installed on an ACPIx64-based PC having core i5-5200U CPU @2.2 GHz. However, it is noticed that for a simulated signal in the range of 1200-1500 MHz, the system takes considerably large time to down-convert and display the signals in first Nyquist zone. Therefore, further simulations are carried and verified using Matlab<sup>®</sup>, and results are discussed in terms of low complexity and reduced sampling rates. Simulation results are compared with those obtained in [9] - [12]. It is observed that using the proposed method minimized sampling rates can be achieved, which would reduce computational complexity for further signal processing.

The only major assumption, which we made, pertains to the characteristics of bandpass filters being used in our design. This means that our filters are practically realizable for our SOI and has same roll off, insertion loss and noise figure as those of [12]. The reason behind this is to keep the scope of study limited and simple.

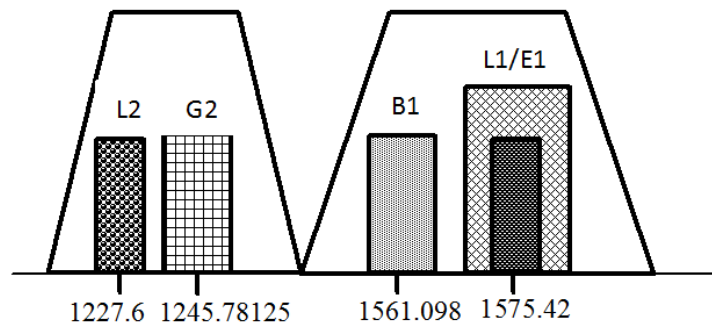


FIGURE 6.2: A scenario comprising a combination of GNSS signals of GPS, GLONASS, Galileo and Compass.

## 6.3 Receiver Architectures

### 6.3.1 GNSS Receiver

The ideal SDR receiver, where there is no Low Noise Amplifier (LNA) or RF filter is placed in the chain between antenna and A/D convertor as first envisioned by Mitola [31] has not (yet) been materialized [79]. Theoretically, the SDR design could hold all standards, including 5G, as long as the A/D convertor has enough sensitivity, dynamic range, sampling rate, etc. However, it poses very strict conditions on the A/D convertor which, even if they are achieved, would dissipate an unacceptably large amount of power [113] for wireless and portable applications. A conventional GNSS receiver normally corresponds a low IF architecture with an RF bandwidth of less than a few MHz and a low resolution A/D convertor [55]. Designs of dual-channel radios for compass applications are available in [100, 101, 114]. On the other hand, new Galileo E1B, E1C, Composite Binary Offset Sub-carrier (CBOC) signals or the new GPS L1C Time-Multiplexed-BOC

signals which have a bandwidth in excess of 24 MHz and can not be handled by the proposed designs in [115, 116]. One of the reasons for this is that RF spectrum for GNSS receivers is spilled over 1.6 GHz and is spread sparsely from  $1176.45 \pm 10.23$  MHz (L5) to  $1602 + n \times 0.5625 \pm 0.5625$  MHz (GLONASS). SDR based multi-band subsampling receivers [81], and reconfigurable architecture for multi-standard, that allows the combination of two or more GNSS standards [12] are the modern architectures used for multi-band GNSS. However, SDR based architectures are vulnerable to higher number of harmonics and intermodulation products, in particular, third-order intermodulation. Again the existing receiver architectures and sampling techniques require some modifications to manage this ultra-high frequency band and large bandwidth.

### 6.3.2 Proposed Design

A multi-band composite receiver architecture is presented and its performance to reduce sampling rates and TOI-components is analysed. Composite means that it uses a combination of hetero-dyne and direct RF sub-sampling approach. Keeping in view the pattern of SOI, the desired GNSS signals are categorized into two sub-groups. The first sub-group (Gp-1) is generally a single signal, that is placed asymmetrically in the spectrum of interest and is translated to an appropriate IF. The second sub-group (Gp-2) is comprised of signals which are already almost equally spaced. Gp-1 is translated either in the gaps, available between the signals of Gp-2 or on their flanks. The purpose is to form an equally-spaced spectrum. This sort of frequency translation of partial SOI has two advantages. One is the formulation of a contiguous-spectrum, out of the sparse-spectrum, which can be directly digitized and translated using an ordinary A/D convertor. The equally spaced signals, require the lowest possible sampling rates, which is one of our objectives. The second advantage is achieved by transforming one of bands to an IF of our own choice. This helps to reduce undesired harmonic components in general, and TOI in particular. As shown in Fig. 6.3, both sub-groups are made parallel and are input to the A/D convertor through LNA for simultaneous digitization and

translation to first Nyquist zone. Gp-1 signals path is comprised of a wideband antenna capable to intercept all GNSS signals, and a Low Noise Amplifier (LNA) to minimize the noise and increment the gain. The desired GNSS signals are first passed through a bank of parallel bandpass anti-aliasing filters. Gp-2 signals route through a mixer stage also fed by frequency synthesizers. The combined band is further amplified by an LNA. The output of LNA is sampled by an ordinary low-speed A/D convertor. Finally, digital signal processing is accomplished to ensure digital down-conversion, channel selection and baseband processing. Another im-

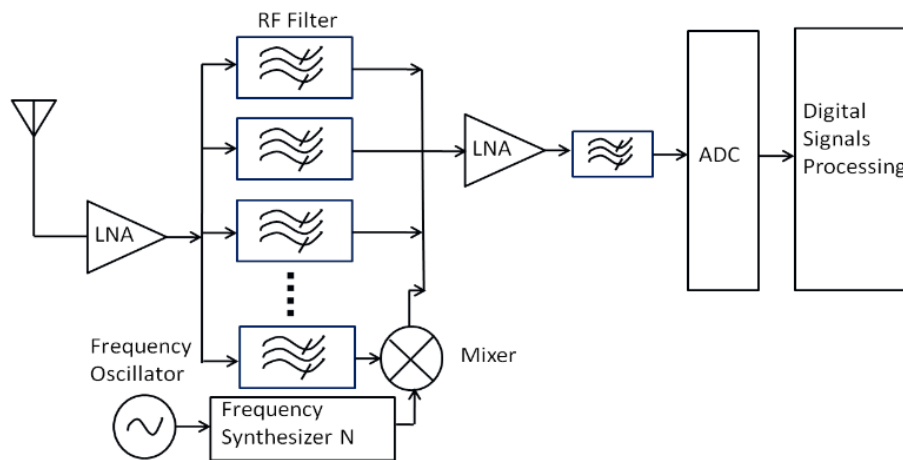


FIGURE 6.3: A composite receiver design for Global Navigational Satellite System signals.

portant aspect of the design is selection of signals to be down or up-converted to the IF stage. The IF is calculated in a way that all the signals become an almost equally-spaced band. The IF in the design is kept intentionally very high for maximum image rejection. Frequency sampling criterion of BPS is followed and the sampling is carried out approximately at the rate of  $2NB$ , including filter bandwidth. Selection of IF and sampling frequency is made in such a way that no spectrum folding or overlap of aliases is possible on sampling. This consequently leads to an added advantage for reconstruction of base-band signals.

## 6.4 Design Methodology.

Our design methodology is based on two important factors. The first is management of SOI so that, we can digitize and down-convert the entire spectrum simultaneously, while using the minimum sampling rate. Direct RF sub-sampling receiver design is one of the suitable options in this regard. However, besides noise folding in the the base-band region it has certain issues due to non-linearity of the LNA and A/D convertor at the front-end. The most common of these are the higher-order harmonics and third-order intermodulation (TOI). The second factor, which we are considering in our receiver design pertains to elimination of TOI-components. In this section we shall briefly analyze these two factors.

### 6.4.1 Sampling rate viz-a-viz spectrum layout

In a multiband-multistandard electromagnetic environment, signals are non-uniformly spaced and are long-drawn-out. Thereby any manipulation involving complete electromagnetic spectrum requires extraordinary resources. If such a type of spectrum is arranged tactfully, we can accomplish the same job with fewer resources. In a conventional receiver for analogue to digital conversion, sampling frequency  $f_s$  is always kept much greater than twice of the highest frequency  $f_h$  component present in the signal. The reason behind this is to separate spectral aliases at the folding frequencies of  $\pm f_s/2$ . This very important relationship of  $f_s \geq 2f_h$  is known as the Nyquist criterion. Although satisfying the majority of sampling requirements, the sampling of RF-signals is not limited to the Nyquist criterion. Besides low-pass sampling there is another technique known as bandpass sampling (BPS) that is used to sample an analogue bandpass signal that is centered about some non-zero frequency. BPS is not limited to reduction of the speed of A/D converters below that is essential with traditional low-pass sampling; it also contributes in reduction of digital memory necessary to capture a given time interval of an analogue signal. However, BPS faces issues when it down-converts and digitizes multiple input signals simultaneously. In fact there exists no formula

for a non-uniformly spaced sparse spectrum which may perform a simultaneous transformation and digitization without aliasing problem. In order to avoid overlap of the aliased bands, the resulting intermediate band frequency,  $f_{IF}$ , in the first Nyquist zone for a given  $f_s$ , can be calculated by satisfying the famous constraints in BPS theory [12, 32, 55, 60]. Considering  $f_l$  and  $f_u$  as lower and upper frequencies of a single input signal, sampling frequency given by [32] is given by

$$2f_u/m \leq f_s \leq 2f_l/(m-1) \quad (6.1)$$

where  $1 \leq m \leq \lfloor f_u/B \rfloor$  and the resulting IF as a function of sampling frequency can be written as

$$f_{IF} = \text{mod}(f_s/2, f_c) \quad (6.2)$$

However, this  $f_{IF}$  is subject to the constraints given in (3) and (4)

$$0 \leq f_{IF} - B/2 \quad (6.3)$$

$$f_{IF} + B/2 \leq f_s/2 \quad (6.4)$$

This also applies to  $N$  multiple input bands or signals having bandwidth  $B$

$$|f_{IF_j} - f_{IF_i}| \geq (B_i + B_j)/2 \quad (6.5)$$

for  $j = 2 \dots N$  and  $i = 1 \dots j$ . However, the constraints mentioned above help us to calculate acceptable sampling rates and do not guarantee the minimum sampling frequency for the given information bandwidth [23, 25, 117]. Indeed we can achieve the lowest sampling rate if all the signals of interest are equally spaced.

In order to explain, how equally spaced bands require minimum sampling rates for down-conversion, consider a spectrum of a system, consisting of  $m$  bands, and

has a total bandwidth of  $mB$  Hz. It means that the spectrum under consideration can accommodate  $m$  band each of bandwidth  $B$ . Moreover, each of the bands will have its centre frequency multiple of  $B/2$ , otherwise its intermediate-frequency will not be centred at frequency multiple of  $B/2$ , after down-conversion. Fig. 6.4a depicts a typical spectrum of such a system and shows the amplitudes of positive frequencies only. Fig. 6.4b shows the sparse-spectrum of  $N \ll m$  bands of the same system with a sparseness ( $\gamma = \Delta f/B$ ) of 10:1. This means  $\Delta f$  is ten times of bandwidth  $B$ . However, all bands are still located at frequencies multiple of  $B/2$ . Mathematically, centre frequency,  $f_{c,k}$  of the bands can be expressed as:

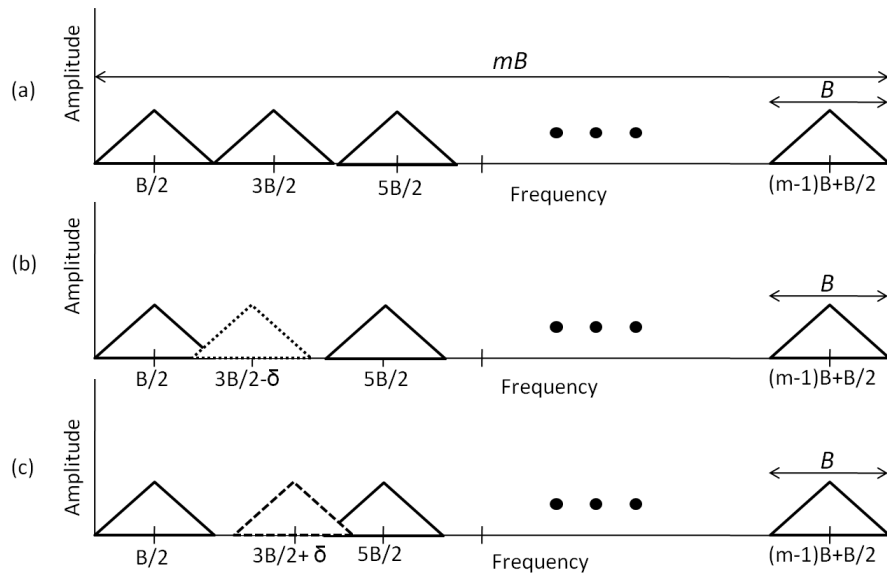


FIGURE 6.4: A  $m$ -bands spectrum with a total bandwidth of  $mB$  Hz.(a) All bands are equally spaced. (b) An equally spaced sparse-spectrum. (c) Band-II is shifted right at  $21B/2 + \delta$

$$f_{c,k} = (k - 1)B + B/2 \tag{6.6}$$

where  $k$  ranges from 1 to  $m$ .

If we sample the sparse-spectrum, shown in Fig. 6.4b at the sampling rate,  $f_s = 2NB$  samples per second, it is possible to down-conversion the selected bands to the first-Nyquist zone without any aliasing-overlaps. However, if there is any frequency shift,  $\delta$  Hz such that  $\delta \leq B/2$  as shown in Fig. 6.4c, there will always

be an aliasing-overlap after down-conversion, provided the sampling rate is kept  $2NB$ . This implies that, in order to down-convert the sparse-spectrum without any aliasing-overlaps we will have to increase the sampling rate. The other constraints to avoid the aliasing-overlaps are described in [8]. To illustrate it further, consider a system comprised of Band-I (B-I), Band-II (B-II) and Band-III (B-III) having their centre frequencies at 19 MHz, 35 MHz and 51 MHz, respectively, and each band is 2 MHz wide. This system has a sparseness of 8:1. The minimum sampling rate required to down-convert the complete sparse-spectrum to the first Nyquist zone is  $f_s = 2NB = 12$  Msps. Any changes in the positions of bands will require an increase in the sampling rate for down-conversion. Table 6.1 shows the impact of this frequency shift, where the B-I is fixed at 19 MHz, and the other two bands are shifted linearly from their original positions (to deform the uniformity). First-three columns in the table show the positions of bandpass signals in passband and the next-three columns show their aliases-frequencies, ( $f_{a1}$ ,  $f_{a2}$  and  $f_{a3}$ ) after down-conversion at the sampling rates  $f_s$ , given in the last column. It can be noticed that, all the three bands require the lowest sampling rate (12 Msps), when they are uniformly positioned. Fig. 6.5, exhibits the increase in the sampling rate as a function of frequency shift  $|\delta|$ .

In a real-world scenario for sparse spectrum signals of interest are not uniformly spaced. Therefore, in order to minimize the sampling rate a little improvisation is required. This implies that if we manage to achieve a uniform spectrum, we can achieve the lowest possible sampling rate with only one additional constraint. Authors in [65] explain the direct sampling theory for equally spaced multiband signals with an additional constraint on minimum frequency but that is not applicable to all values of the ratio  $\Delta f/B$ , where  $\Delta f$  is the spacing between adjacent signals. On the other hand, the model described in [8] is more generic and can be used as a reference to achieve the objective in sparse-spectrum environment. In this regard the most substantial factor which contributes to determine the valid optimum sampling rate is the carrier frequency of the signal centred at minimum frequency,  $f_{cl}$ . Defining sparseness,  $\gamma$  as the ratio between  $\Delta f$  and  $B$  permissible values of  $f_{cl}$  can be calculated using equation (6.7) and (6.8) for odd and even



TABLE 6.1: B-II and B-III positions are shifted from 35 MHz and 51 MHz to 42 MHz and 44 MHz respectively, in steps of 500 kHz. Last column shows that minimum sampling rate is required if the bands are equi-distant.

$f_{c1}$ (MHz)	$f_{c2}$ (MHz)	$f_{c3}$ (MHz)	$f_{a1}$ (MHz)	$f_{a2}$ (MHz)	$f_{a3}$ (MHz)	$f_s$ (MSPS)
19	35	51	5	1	3	12
19	35.5	50.5	2	6.5	8.5	21
19	36	50	2	6	8	21
19	36.5	49.5	1.5	3.5	8.5	20.5
19	37	49	1	3	9	20
19	37.5	48.5	1.5	3.5	7.5	20.5
19	38	48	4	8	2	23
19	38.5	47.5	4	7.5	1.5	23
19	39	47	3	7	1	16
19	39.5	46.5	1	3.5	7.5	18
19	40	46	1	4	8	18
19	40.5	45.5	3.5	6	1	15.5
19	41	45	5	1	3	14
19	41.5	44.5	14	8.5	11.5	33
19	42	44	5.5	1.5	3.5	13.5

values of  $\gamma$ , respectively.

$$f_d[k] = (\gamma \pm 2(k-1)N)B/2 \quad (6.7)$$

$$f_d[k] = (\gamma \pm 2k-1)B/2 \quad (6.8)$$

and in the case if  $\text{mod}(f_j - f_i, f_s) = 0$  then

$$f_d[k] = \{(\gamma \pm k(2N+1)B/2)\} \cup \{(2\gamma \pm k(2N+1)B/2)\} \quad (6.9)$$

However, in practical scenarios spectrum is not uniformly spaced. Due to this a manipulation is required to make the SOI as uniformly-spaced as possible such that  $f_d$  selected is always from the set obtained via (6)-(8). For example, GNSS signals (L1, L2C, E1, B1 and G2) are unevenly stretched in a BW of approximately 350 MHz but have an information bandwidth of 18.8385 MHz only. Thus it has the approximate sparse ratio of 18:1. Taking the advantage of sparseness we can readjust the position of desired signals by down conversion or up conversion. This has two advantages. Firstly, it offers more flexibility to choose the frequency of the

lowest carrier at a position permitted by (6)-(8). Secondly, we can transform the non-uniformly spaced signals in a quasi-uniformly spaced pattern. Nevertheless,

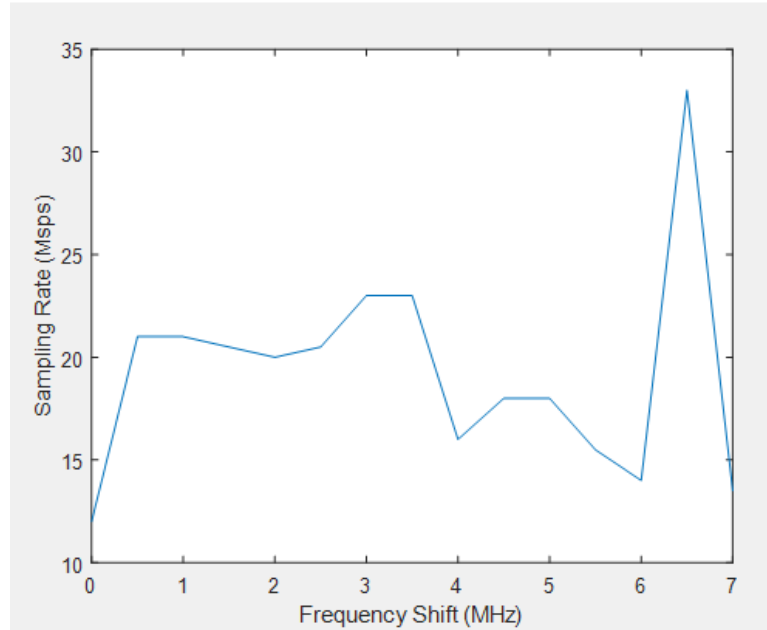


FIGURE 6.5: Sampling rate increases in a non-linear fashion for a non-uniform spectrum, when there is any frequency shift,  $|\delta|$  in the positions of B-II and B-III.

ideally it should be uniformly spaced up to perfection. It should also be considered the more the SOI is uniformly spaced the lesser is the sampling frequency required to digitize the analogue signals and consequently demands less signal processing and complexity. Consider the example of GNSS signals L1/E1, B1, G2 and L2C shown in Fig. 6.2. These signals are located at 1575.42 MHz, 1561.098 MHz, 1245.78125 MHz and 1227.6 MHz respectively. Let us form two groups of these signals; L1/E1/B1 and L2/G2 with central frequencies at 1567.275 and 1236.690625 MHz respectively. Now if we up-convert the latter group to 1547.80925 MHz, a contiguous spectrum is formed. This gives us an opportunity to sample at a sampling rate of 90.2 MHz which is 11.681 MHz less than the lowest sampling rate achieved in [12] and 23.88 MHz less than that acquired by using iterative algorithm proposed by [118].

### 6.4.2 Intermodulation Distortion (IMD) Components.

Non-linearities at any stage in the receiver chain may cause intermodulation interference [119]. When signals with different frequencies are applied to the input of the nonlinear component, the non-linearity gives rise to spurious distortion signals on other frequencies [120]. The magnitude of intermodulation products cannot be predicted easily but it is well-known that their amplitude gradually decreases with the increase in order. Second order components have an amplitude proportional to the square of the input signal, whereas TOI-components have an amplitude proportional to the cube of the input signal [121]. Thus, if two input signals, equal in magnitude, each rise by 1 dB then the second-order components rise by 2 dB, the TOI-components rise by 3 dB, and so on. However, the design of most high-speed A/D convertors is such that differential non-linearity is spread across the entire A/D convertor range. Therefore, for signals which are within a few dB of full scale, the overall integral non-linearity of the transfer function determines the distortion products. For lower level signals, however, the harmonic content becomes dominated by the differential non-linearities and does not generally decrease proportionally with decreases in signal amplitude [122].

The greatest performance problem with the RF sub-sampling architecture is distortion due to harmonics aliasing and higher-order intermodulation. In general, an RF sub-sampling architecture displays worse performance compared to other architectures due to folding of wide-band noise into the desired IF-zone. Theoretical studies show that the performance degradation, due to noise folding, is based on the sample frequency. The higher the sample frequency the lesser the noise folds into desired band (the first-Nyquist zone in the case of direct sub-sampling receiver). However, the theoretical studies have also shown that the noise folding is not a problem in the typical RF sub-sampling receiver. If enough gain is provided by the front-end, the total performance degradation due to noise folding is very limited. A high T/H sample frequency does not only decrease noise folding, but, it also improves SNR degradation caused by clock noise and aperture jitter. Since, the degradation in SNR caused by noise folding can be effectively managed, the threatening performance problem with the RF sub-sampling design

is harmonics aliasing and intermodulation distortion. Harmonics aliasing increase the total harmonic distortion of the A/D convertor output due to aliasing of the T/H output harmonics, spurious signals and other signals. In this sense, the T/H sub-sampling suffers from similar problems as the mixer circuit does. Again, the higher-order harmonics can be filtered out easily, but intermodulation, especially TOI is much more challenging. In multiband direct RF sub-sampling receivers, an A/D convertor is placed as close to the antenna as feasible; in most of the cases just after a series of BPF and LNAs. In such cases, the A/D convertor is vulnerable to spurious signals which are bi-products of signals in the spectrum of interest. These intermodulation products are of two types. The first, are the spurious noise components due to third-order intermodulation, which are results of in-band or out of band frequencies. It is worth mentioning that these components are not because of non-linearity of LNA or A/D convertor. From this intermodulation interference problem communications systems can suffer. An example of this can come from maritime communication. The problem is aggravated by having evenly spaced channels, such as the VHF maritime communications example, where 50 kHz channel spacing is used. In this example if a user attempts to use channel-3 at 156.15 MHz, communication systems could falter to a great degree. There are nearby users operating on channel-4 at 156.20 MHz and channel-5 = 156.25 MHz. The second harmonic of channel-4 is 312.4 MHz. A third order intermodulation product falls squarely on channel-3, which causes performance degradation. When such channel is down-converted to an IF and are digitized, the TOI component gets mounted above it, resulting in severe distortion.

In the second case, the third-order intermodulation products directly interfere with the basic signal in the first- Nyquist zone. Such type of noise components are a result of non-linearity of components. Given the case that a single CW tone is applied to a non-linear element, additional signals, the so-called harmonics, will be generated at n times of the original frequency, with n being the order of the harmonic. Any non-linear element can be described by a Taylor-series :-

$$P_s = a_0 + a_1s + a_2s^2 + a_3s^3 + \dots \quad (6.10)$$

with  $P(s)$  being its transfer function and  $s$  being the input signal. We will not look in detail on the factors, but focus on the powers of  $s$ . Assuming a CW input signal, the general formula for a signal,  $s(t)$  as a function of time  $t$  is

$$s(t) = B \cos(2\pi ft + \phi) \quad (6.11)$$

Clearly, harmonics of a single tone are outside the usable band of an application, since they are at multiples of the original frequency. Once a second tone joins the input signal at a small frequency offset, i.e., the resulting output signal looks different. In contrast to the single tone scenario above, the signal  $s(t)$  is now

$$s(t) = B_1 \cos(2\pi f_1 t + \phi_1) + B_2 \cos(2\pi f_2 t + \phi_2) \quad (6.12)$$

Since the dominating intermodulation products are the third order products, the following equations focus on them only. Calculating the third power terms (responsible for the third order intermodulation and third order harmonics) of the Taylor series with the two-tone input signal from Eq. 6.12 yields the following result:

$$\begin{aligned} S^3(t) &= B_1^3 \cos^3(2\pi f_1 t + \phi_1) \\ &+ B_2^3 \cos^3(2\pi f_2 t + \phi_2) \\ &+ 3B_1^2 B_2 \cos(2\pi f_1 t + \phi_1) \cdot \cos(2\pi f_2 t + \phi_2) \\ &+ 3B_1 B_2^2 \cos(2\pi f_1 t + \phi_1) \cdot \cos(2\pi f_2 t + \phi_2) \end{aligned} \quad (6.13)$$

The first two lines describe the third order harmonics for each of the input tones ( $\cos^3$ -terms), whereas lines 3 and 4 represent the third order intermodulation terms (mixed terms). From the above equations, the third order intermodulation (TOI) frequencies can be derived using the addition theorem (for trigonometric functions) as

$$f_{TOI1} = 2f_1 - f_2, f_{TOI2} = 2f_2 - f_1 \quad (6.14)$$

While the 3rd order harmonics ( $3f_1$  and  $3f_2$ ) of the individual input tones can easily be suppressed by a low-pass filter. The third order intermodulation terms

are often more critical for the application. The resulting frequencies are often in-band for a given application and therefore interfere with the wanted signal. Additionally, under the assumption  $B_1 = B_2$ , i.e. both tones have the same level, the intermodulation terms exceed the harmonic terms by a factor of 3 in amplitude. A factor of 3 in amplitude converts to a 9.54 dB difference between the third-order harmonics of the individual tones and the third order intermodulation products. This is illustrated in the following example.

Example: Consider a two-bands (C1 and C2) land mobile radio (LMR) used for national security and defence purpose, where C1 has a bandwidth ( $B_{c1}$ ) of 5 MHz (161.5-166.5 MHz) and C2 has bandwidth ( $B_{c2}$ ) of 5 MHz (316.5-321.5MHz). A 16 bit A/D convertor with 82 dB SNR is used for sampling the input signal. A sampling frequency of 50 MHz (5 times of total bandwidth) is sufficient to down-sample both bands without loss of any information. The transformed intermediate frequencies centred at  $f_{IF1} = 14$  MHz and  $f_{IF2} = 19$  MHz of C1 and C2 respectively can be calculated using equation

$$f_{IF} = f_{RF} - mf_s \quad (6.15)$$

In this case, the third-order intermodulation products can be found centred at  $f_{IM3} = 9$  MHz and 24 MHz. It is pertinent to note that these TOI products have their footprints from 1.5 MHz to 16.5 MHz ( $TOI_1$ ), extended over 15 MHz wide ( $2.B_{c1} + B_{c2}$ ), and 16.5 MHz to 25 MHz ( $TOI_2$ ), which is further folded around dc component upto 6.5 MHz. These spurious products directly interfere with down-converted bands C1 and C2 in the first-Nyquist zone, while having almost a complete overlap with the both bands, as shown in the Fig. 6.6. The same can be verified through Matlab<sup>®</sup> simulations on simulink as shown in the Fig. 6.7. However, to keep the simulation simple, we are using the central frequencies (sinusoidal tones of 1 Hz each) of both the bands. It can be seen that their TOIs are centred at 9 and 24 MHz. Both of the TOI-products have an amplitude attenuation of -65 dBc in relation to the basic sinusoids located at 14 and 19 MHz having amplitude

of 27 dBm each. Despite of the attenuation by 65 dBs, TOI products are a major cause of distortion, degrading, SINAD ratio. Here, it is worth mentioning that, the SINAD is the ratio of the root-mean-square value of the signal amplitude to the mean value of the root-sum-squares (RSS) of all other spectral components, including basic harmonics, and their intermodulation products less the DC component. However, for ease of calculations we are restricting ourselves to the TOIs only. Despite of this, the Noise Figure (NF (dB)), the decibel equivalent of noise factor (F) of the A/D convertor gets worse, resulting in the performance degradation.

Noise factor of a device is the power ratio of the SNR at the input ( $SNR_{in}$ )

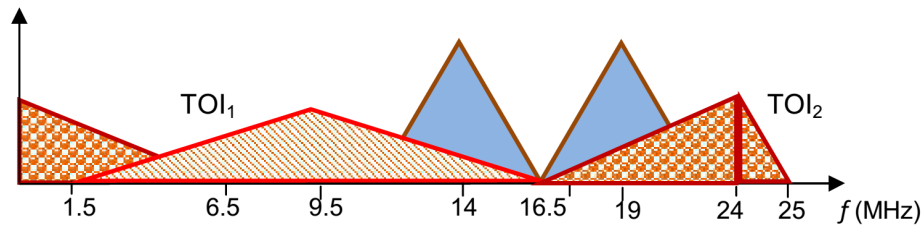


FIGURE 6.6: TOI product formation in the first-Nyquist zone of the dual-band LMR.

divided by the SNR at the output ( $SNR_{out}$ ) and can be expressed as :-

$$F = SNR_{in}/SNR_{out} \tag{6.16}$$

The output signal ( $S_{out}$ ) is equal to the input signal ( $S_{in}$ ) times the gain: ( $S_{out}$ ) = ( $S_{in}$ ) $G$ . The output noise is equal to the noise at the input ( $N_{in}$ ) from the source plus the noise contributed by the A/D convertor ( $N_{ADC}$ ) and noise due to harmonic distortion  $N_H$  times the gain:  $N_{out} = (N_{in} + N_{ADC} + N_H)G$ . Here, the only assumption we are making is that all noise contributing factors have correlation and can be added. Substituting into Eq. 6.16 and simplifying, we get

$$F = \frac{SNR_{in}}{SNR_{out}} = 1 + \frac{(N_{ADC} + N_H)}{N_{in}} \tag{6.17}$$

Now let us calculate each of the noise contributing factors.  $N_{in}$  can be calculated with the assumption that, the input is terminated in the same impedance as the

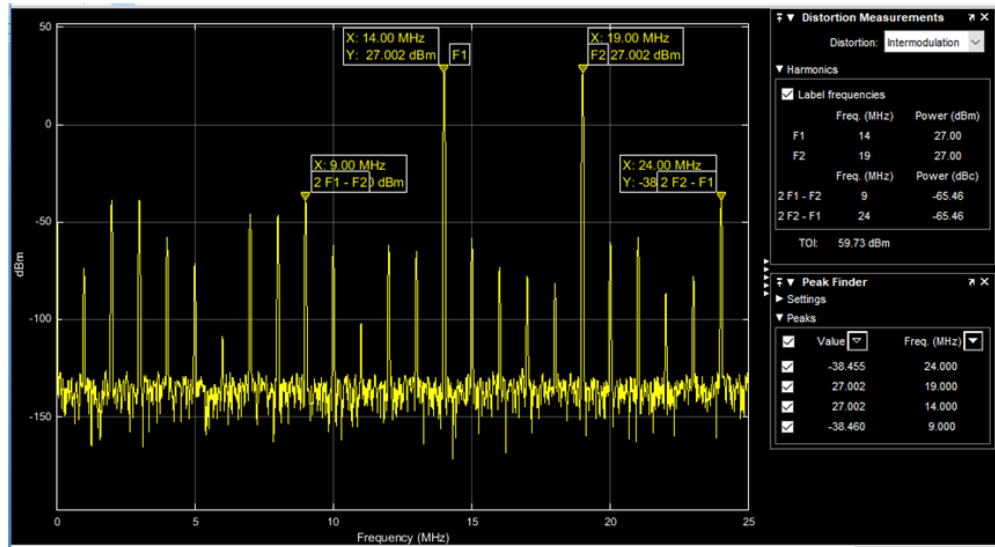


FIGURE 6.7: TOI and spurious-noise components for a dual-band LMR (using dual tones at centre-frequencies) in the case of direct RF sub-sampling.

source,  $N_{in} = kT = 174 \text{ dBm/Hz}$ , where  $k$  is Boltzmann's constant and  $T = 300$  Kelvin. To find the input noise spectral density, we divide the signal level by the SNR divided by half the sampling frequency (SNR is calculated by dividing the signal by the noise integrated over  $f_s/2$ ).

$N_{out}(\text{dBm/Hz}) = 1\text{dBFS}(\text{dBm}) + \text{SNR}(\text{dBc})f_s/2(\text{dBHz})$ . Since an A/D converter is a voltage-driven device, so we must choose an input resistance to find the signal power with the formula  $P = V_{rms}^2/R$ . Assuming that full scale (FS) voltage is 20V p-p and  $R = 50\Omega$ , the full-scale input is +30 dBm.

Given that  $f_s = 50 \text{ MSPS}$ ,  $\text{SNR} = 82$ , then  $N_{ADC}(\text{dBm/Hz}) = +27\text{dBm} - 82\text{dBc} - 73.98\text{dBHz} = -129.02\text{dBm/Hz}$ . Finally,  $N_H$  can be measured from through simulation, as shown in Fig 6.7. It should be noted that We are using only one spurious-noise component, i.e. third-order intermodulation product (TOI). This gives a value of -38 dBm/Hz, resulting an increase in the noise figure of A/D converter by 38 dBs. Placing these values in Eq. 6.17, we get the Noise Figure of 83 dBs. This clearly shows an enormous attenuation to the SNR at the input and even beyond the given SNR of the A/D converter. However, it should be noted that the distortion due to TOI is coloured noise and does not have any correlation with other noise-contributing factors. Hence, it will not rise the noise floor of the A/D converter. Nevertheless, the measured distortion power is much more



greater than the noise contributed by the device and will overcome the noise floor. On the other hand composite receiver design provides us the flexibility to up or down-convert any of the band to an IF of our own choice and then sample both the bands simultaneously. Here we are using an LO of 183 MHz and are upconverting the C1 to 347 MHz. This gives us an advantage to circumvent both the problems (the image frequency and the TOI interference). Fig. 6.8 shows that third-order intermodulation products are successfully eliminated from the first-Nyquist zone. Further still, a number of other harmonics of lesser amplitudes (which we are not considering) are also reduced to two-third of the direct RF sampling method. Another advantage of our proposed design is its flexibility for selection of desired

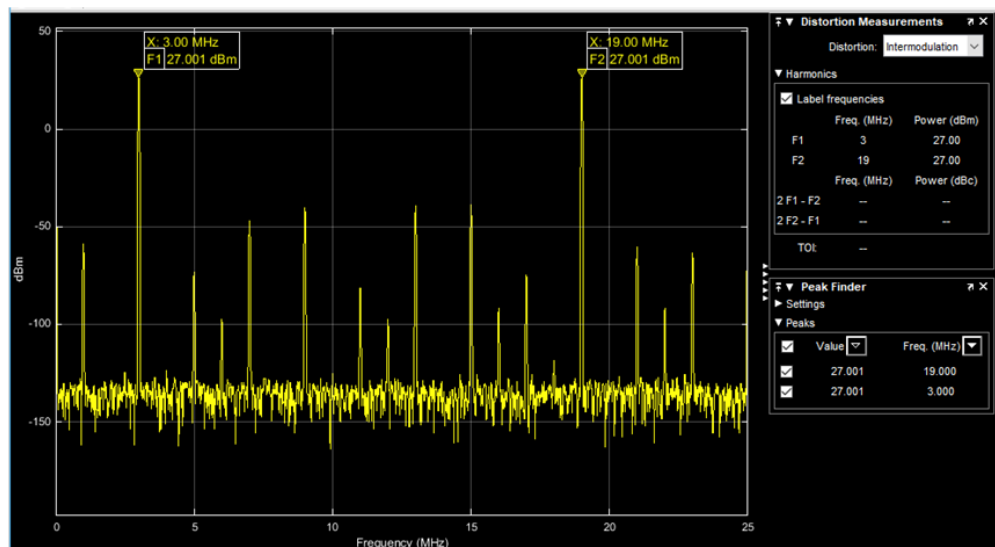


FIGURE 6.8: Reduction of spurious components using composite receiver methodology.

sampling frequency. In the case of direct RF sub-sampling receiver, the acceptable sampling frequency intervals, do not guarantee the distortion due to TOI. Table 6.2 shows sampling frequencies intervals, which are legitimate, and fulfil all the necessary conditions as stated in the literature [55, 118]. However, it can be noticed that despite this, there are intermodulation components which may interfere with basic signal after down-conversion. Figure 6.9 illustrates the presence of a TOI-component, despite of the fact that sampling rate is almost twenty-times than the combine bandwidth of Filter-1 and Filter-4 presented by [12]. These filters are

TABLE 6.2: Regions of acceptable bandpass sampling rates for down-conversion of L1/L5a and L1/E1/B1 signals and location of third-order intermodulation component

Sampling Frequency Interval (MHz)	TOI-Component (MHz)
103.32-103.92	-
139.62-141.72	5.39876, 5.92249, 5.26601, . . .
166.32-166.62	-
185.82-186.20	41.3559, 41.3412, 41.3419, . . .
215.82-222.72	17.6767, 17.6769, 17.6361, . . .
286.92-291.42	-
350.82-372.42	82.9940, 82.9961, 82.9966

tuned at centre-frequencies 1174.450 MHz and 1568.259 MHz, and are covering L5/E5a and L1/E1/B1 respectively.

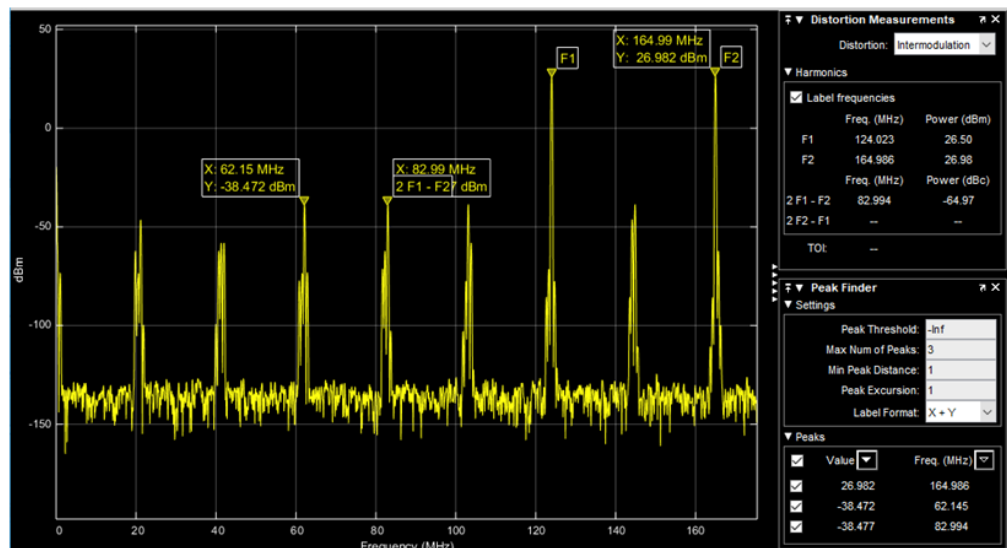


FIGURE 6.9: An illustration of TOI-component at 82.994 MHz alongwith other spurious-noise components causing distortion.

TABLE 6.3: Group-formation of GNSS signals and the minimum sampling rates for their down-conversion.

GNSS Received Signals	Bands	Contiguous Bands	Translated Spectrum	Spec-	Sampling Rate (MSPS)
L1, L2*	2	1575.42/1596.077*/-/-/-	3.54/1.243/-/-/-		9.18
L1/E1, B1*	2	1575.42/1585.0*/-/-/-	7.42/2.6/-/-/-		19.60
L1/E1/B1, L2/G2*	2	1567.275/1547.80925*/-/-/-	34.859/14.40925/-/-/-		90.20
L1/B1/E1*, E5b/B2/ G2/L2	2	1155.707*/1223/-/-/-	75.707/37.0/-/-/-		180.0
L1/E1/B1*, L5/E5a	2	1131.0*/1176.45/-/-/-	13.56/34.11/-/-/-		93.12
L1/E1/B1*, L5/E5a, E5b/B2, L2/G2	4	1155.707*/1176.45/ 1207.14/1237.81975/-	99.293/78.55/47.86/ 17.18/-		251.0
L1/B1/E1*, L5/E5a, E5b/B2, L2/G2, B1-2/G1*	5	1155.707*/1176.45/ 1207.14/1237.81975/1136*	124/103.55/72.86/ 42.18/144		320.0
L1/E1/B1/B1-2/G1*, L5/E5a*/E5b/B2/ L2/G2/E6	2	1131.0*/1232/-/-/-	89.0/190.0/-/-/-		521.0
L1/E1/B1/B1-2/G1*, L5/E5a/E5b/B2/ L2/G2/E6	2	1131.0*/1232/-/-/-	174.0/73/-/-/-		435.0

## 6.5 Results and Simulations

In order to validate the composite design GNSS signals are grouped as presented in Table 6.3. Major purpose of this group-formation is to arrange the spectrum in a uniformly-spaced fashion. However, since our signals of interest vary in bandwidths, it is not possible to form a perfect uniformly-spaced spectrum. In other words, we are arranging the SOI in a manner, which is quasi-uniformly spaced. This quasi-uniformly spaced SOI is based on (6)-(8) and is the key to acquire minimum sampling rate. The group-formation is also helpful in reducing out of band noise when compared with direct RF sub-sampling architecture. Besides noise folding, a receiver-design based on direct RF sub-sampling is more vulnerable to higher-order harmonics and intermodulation products. The spectrum management using composite design is also helpful in reducing noise due to harmonic distortion, especially third order intermodulation (TOI) distortion. This in return improves the noise figure (NF) of the receiver architecture. Consider a design example of RF front end of a GPS receiver, implemented in [9] in which we can realize both of

the above-mentioned advantages. In [9] Psiaki *et al.*, present a dual-frequency direct RF sampling front end, where information signals are almost 348 MHz apart. These signals are directly fed to LNA using a single BPF and digitized there after. In order to remove out of band noise, the signals are filtered by an active dual-frequency assembly. Minimum sampling rate achieved in [9] is 99.23 MHz. On the other hand, our proposed design reduces the sampling rate significantly to 9.18 MHz, which is 9.25% of [9]. In Table 6.4, we can see that in the case of dual-frequency (L1 C/A and L2C bands of GPS) sampling rate can be reduced down to 9.18 MHz. In Fig. 6.10 a simulation circuit is implemented using Multisim. For simplicity input sinusoidal signals at frequencies 1575.42 MHz and 1596.077 kHz are directly generated using function generators XFG1 and XFG2. These are fed to an A/D convertor with a sampling rate of 9.18 MHz. The output of the A/D convertor is further given to a wide-band operational amplifier AD8067ART. A spectrum analyzer XSA1 is used to monitor the output. Fig. 6.11 shows the output spectrum of our designed circuit. It can be noted that both signals are successfully down-converted in the first Nyquist zone without any compromise. In this case, sampling rate is less than one-tenth of that achieved in [9] through a rigorous iterative algorithm.

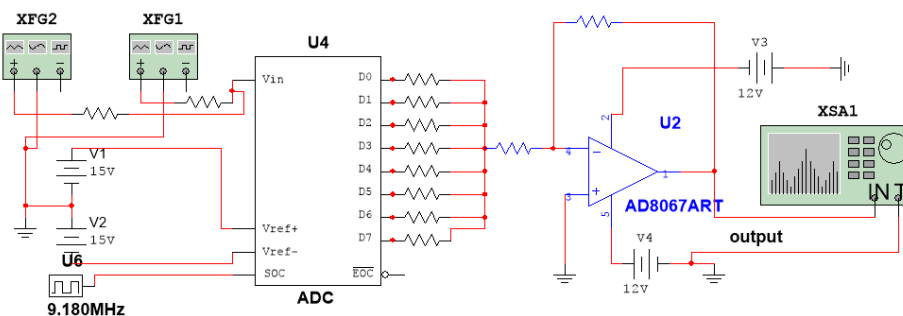


FIGURE 6.10: A simplified circuit of composite receiver using a sampling rate of 9.18 MHz.

As discussed earlier, in the case of GNSS, simultaneous down-conversion and digitization of the combination of GPS/GALILEO/GLONASS/COMPASS signals require a high speed A/D convertor having large input-bandwidth. In this context, theoretically permissible sampling rates for various combinations are shown

in the last column of Table 6.3. GNSS signals, which are grouped together are presented using symbol ‘/’, where as we used commas ‘,’ to separate groups. For example, in the third row of Table 6.3, L1, E1, B1, L2 and G2 forming two groups are shown as L1/E1/B1, L2/G2. The ‘\*’ mark shows that frequency translation operation is performed on that particular group to construct a contiguous spectrum.

Now let us consider an example of a combination of signals from GPS, GALILEO and COMPASS. The selected signals L1 C/A, E1 and B1, have modulation schemes BPSK, BOC (1,1) and QPSK. Taking the advantage of different modulations L1 and E1 are centred at the same frequency of 1575.42 MHz and B1 is centered at 1561.098 MHz. In [12] these signals are down-converted using BPF centred at a

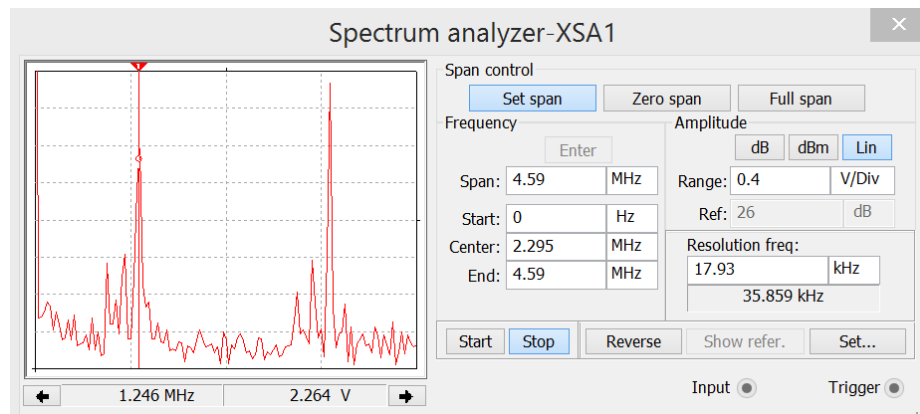


FIGURE 6.11: Down conversion of L1, L2 to 1.243 MHz and 3.54 MHz using a sampling rate of 9.18 MHz.

frequency of 1568.259 MHz, which has a total bandpass-bandwidth ( $B_T$ ) of 18.414 MHz. Minimum workable sampling rate proposed by [12] is 43.865 MHz which is more than seven times of the information bandwidth. It is noticeable that the total information bandwidth of these signals is 6.138 MHz because L1 and E1 are centred at the same frequency (1575.42 MHz). This means that an additional bandwidth of 12.276 MHz contributes towards adding out of band noise, which is undesired. On the other side, our proposed design makes it possible to down-convert all these signals simultaneously using a much less sampling rate of 19.60 MHz. Clearly, this is less than 50% of that proposed in [12]. Fig. 6.12, shows a successful down-conversion of L1/E1 and B1 in the first-Nyquist zone ( $0 \geq f_s/2$ ) using Matlab<sup>®</sup> simulation. Similarly, for other combinations of GNSS shown in

Table 6.3, we can form the contiguous bands, which can be down-converted using reduced sampling rates.

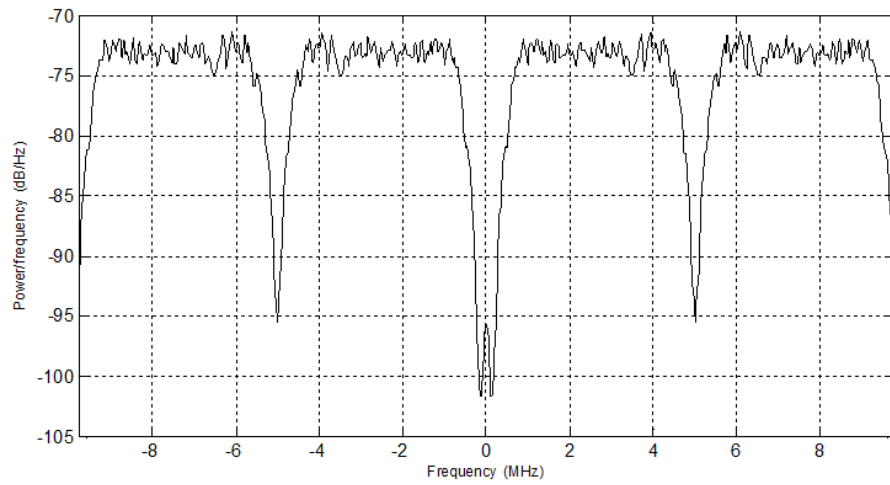


FIGURE 6.12: Down conversion of L1/E1, B1 to 2.6 MHz and 7.42 MHz using a sampling rate of 19.6 MHz.

Table 6.4, shows the comparison of sampling rates with work already done in [9]-[12]. It is very much evident that our proposed rates are significantly less than those proposed in [9]-[12].

TABLE 6.4: A comparison of sampling rate, useable for Global Navigational Satellite Signals receiver .

GNSS Signals	Psiaki et al. 2005	Yuan et al. 2000	Kouki et al. 2012	Barrak et al. 2014	Proposed Composite
L1, L2	99.23	-	-	-	9.18
L1/E1, B1	-	-	-	43.865	19.60
L1/E1/B1, L2/G2	-	-	-	101.881	90.200
L1/B1/E1, E5b/ B2/ G2/L2	-	-	-	192.48	180.0
L1/E1/B1, L5/E5a	-	-	-	103.694	93.120
L1/E1/B1, L5/E5a, E5b/B2, L2/G2	-	-	-	257.298	251.00
L1/B1/E1, L5/E5a, E5b/ B2, L2/G2, B1-2/G1	-	-	-	443.232	320.0
L1/E1/B1/B1-2/ G1, L5/E5a/E5b/ B2/L2/G2/E6	-	744	1080	-	435.0

# Chapter 7

## Conclusion and Future work

In this dissertation, various sampling techniques have been extensively studied with a view to find the minimum sampling rate. It has been investigated that solutions based on bandpass sampling are useful to directly down convert and digitize multiband RF signals. It has been observed that the contemporary sampling techniques being used to acquire minimum sampling rate were not able to explain the relation between sampling rate and the sparseness in the spectrum of interest. In order to overcome the gap, a novel direct RF sampling method has been presented to find out the minimum sampling frequency for an evenly spaced spectrum comprising multiband RF signals. The presented methodology describes the set of rules to achieve the lowest possible sampling frequency rates. In the presented methodology it has been proved that the minimum sampling rate has a unique relation with the layout of the SOI. It shows that for a given spectrum of interest comprised of evenly spaced energy contents of equal bandwidth, any number of information signals, it is possible to down-convert the complete SOI using the minimum possible sampling rate,  $2NB$  which was twice of the total information bandwidth.

The results have been validated through two different platforms. One was the Multisim, where input signals were generated through a signal generator in the form of sinusoidal tones. In order to depict different scenarios of specific sparse-ratio,  $\gamma$ ,



and bandwidth,  $B$ , the generated sinusoids were evenly spaced with a frequency-gap  $\Delta f = \gamma B$  Hz. The output signals, as envisaged in the theoretical part were successfully translated to the first-Nyquist zone with a frequency separation of  $B$  in all of the scenarios. The separation of  $B$  Hz between the adjacent bands in the first-Nyquist zone validated that the selected sampling rate as well as band position in pass-band were complementing each other to circumvent any aliasing-overlap. It has also been confirmed that position of minimum center-frequency depends on sparse-ratio. For even values of sparse-ratio, the minimum center-frequency,  $f_{c1}$  can be  $kB/2$ , where as for odd values of sparse-ratio, it should be at least equal to the half of the frequency-gap between adjacent bands, i.e.  $\Delta f/2$ . However, it can be any frequency determined through the expression,  $f_{ck} = (\gamma \pm 2(k - 1)N)B/2$ , for  $k = 1, 2, 3 \dots$ . The other platform used for validation of results was Matlab, which had an edge over Multisim, since it was more capable of processing more number of input signals of the desired bandwidth.

The proposed methodology has been found more generic and flexible to the number of input signals or bands as well as to their positions in the desired spectrum. It has been observed that for evenly spaced sparse-spectrum the relation between number of signals in SOI and sampling rate is linear, however, it is non-linear in the case of non-linear sparse-spectrum. In addition, the proposed methodology has been found more flexible in selection of suitable frequency for a radio design. As described in chapter 5, scenario-III for a land mobile radio design, there was a considerable frequency range, that was available to select the suitable frequencies of own choice in all of the RF-bands.

In the application part, a composite-receiver design of a global navigation satellite system receiver has been presented. The receiver has the capability to down-convert a spectrum, that might be spread over a frequency range in the GHz, using a low sampling analogue-to-digital converter. The design usefulness has been validated by applying the proposed bandpass sampling methodology to a quasi-uniformly spaced spectrum. The simulation showed that the usefulness of the composite-architecture for simultaneous digitization and down-conversion of analog signals. In the case of dual frequency (L1 C/A and L2C bands of GPS)

sampling rate was reduced down to 9.18 MHz, which was one-tenth of the sampling rate used in [9]. The composite design was found more useful for reducing the out-of-band noise as well. For example, in the case of multiple signals, several combinations of signals from GPS, GALILEO and COMPASS were used for simulations. In one of the cases, the selected signals L1 C/A (BPSK), E1 (BOC (1,1)) and B1 (QPSK), that had a total information bandwidth of 6.138 MHz, were grouped around a frequency of 1568.259 MHz and filtered by a BPF, which had a total bandpass-bandwidth of 18.414 MHz. Minimum workable sampling rate expressed in [12], for the same signals was 43.865 MHz which was more than seven times of the information bandwidth. It was noticed that the total information bandwidth of these signals was one-third of the filter bandwidth because L1 and E1 were centered at the same frequency (1575.42 MHz). This means that an additional bandwidth of 12.276 MHz contributed towards adding out of band noise, which was undesired. On the other side, our proposed design made it possible to down-convert all these signals simultaneously using a much less sampling rate of 19.60 MHz. Clearly, this was less than 50% of that proposed in [12]. Moreover, the group-formation has been found helpful in reducing out of band noise when compared with direct RF sub-sampling architecture. Besides noise folding, a receiver-design based on direct RF sub-sampling were more vulnerable to higher-order harmonics and intermodulation products. The spectrum management using composite design has been helpful in reducing noise due to harmonic distortion, especially third order intermodulation (TOI) distortion. This in return improved the noise figure (NF) of the receiver architecture. Finally, when compared with the iterative algorithms, in terms of iteration the presented methodology has been found significantly efficient as it could always find the minimum sampling rate within couple of iteration.

As a future work, the proposed method of finding the minimum sampling rate is useful in the design of a low-cost digital oscilloscope based on bandpass sampling. At present, the sampling oscilloscopes are used for analyzing very high frequency signals. These oscilloscopes are utilized for looking at repetitive signals which are higher than the sample rate of the scope. These scopes construct the

information signal by assembling samples from several successive waveforms, and by assembling them during the processing, they are able to build up a picture of the waveform. The oscilloscope specifications for these attributes may sometimes require a frequency or bandwidth as high as tens of GHz, which might be a very expensive solution. On the other hand the presented BPS methodology has the capability to present a low cost solution to analyze high frequency signals using low rate and high bit ADC.

The proposed work can also be extended in cognitive radio communication systems for detection of cognitive radio. In the conventional heterodyne receiver the detection time is high not only because of the use of analogue bandpass filter but also due to the use of a low rate analogue-to-digital convertor. In other receiver architectures that are used for fast CR detection, the homodyne receiver has the capability of fast detection due to the use of high rate ADC, which is unfeasible in a sparse-spectrum environment or may be a very costly approach. A filter-bank based receiver with bandpass sampling that may have a low rate ADC by using the proposed methodology can be a suitable approach in such environment.

# Bibliography

- [1] J. Bae and J. Park, “An efficient algorithm for bandpass sampling of multiple RF signals,” *IEEE signal processing letters*, vol. 13, no. 4, pp. 193–196, 2006.
- [2] H. Steyskal, “Digital beamforming antennas-An introduction,” *Microwave journal*, vol. 30, p. 107, 1987.
- [3] G. Hill, “The benefits of undersampling,” *Electronic Design*, vol. 42, no. 14, p. 69, 1994.
- [4] J. Bae and J. Park, “A searching algorithm for minimum bandpass sampling frequency in simultaneous down-conversion of multiple RF signals,” *Journal of Communications and Networks*, vol. 10, no. 1, pp. 55–62, 2006.
- [5] A. Kipnis, A. J. Goldsmith, Y. C. Eldar, and T. Weissman, “Distortion rate function of sub-nyquist sampled Gaussian sources,” *IEEE transactions on information theory*, vol. 62, no. 1, pp. 401–429, 2016.
- [6] H.-J. Kim, J.-u. Kim, J.-H. Kim, H. Wang, and I.-S. Lee, “The design method and performance analysis of RF subsampling frontend for SDR/CR receivers,” *Industrial Electronics, IEEE Transactions on*, vol. 57, no. 5, pp. 1518–1525, 2010.
- [7] I. Bilinskis, *Digital alias-free signal processing*. John Wiley & Sons, 2007.
- [8] T. Ahmed and N. M. Khan, “Direct radio frequency sampling methodology for multiple signals in an energy-sparse spectrum,” *Turkish Journal of Electrical Engineering & Computer Sciences*, vol. 24, no. 6, pp. 4637–4647, 2016.

- [9] M. L. Psiaki, S. P. Powell, H. Jung, and P. M. Kintner, "Design and practical implementation of multifrequency RF front ends using direct RF sampling," *IEEE Transactions on Microwave Theory and Techniques*, vol. 53, no. 10, pp. 3082–3089, 2005.
- [10] Y. Yu, Q. Chang, and Y. Chen, "Design and Simulation of a Fully Digitized GNSS Receiver Front-End," *Discrete Dynamics in Nature and Society*, vol. 2011, pp. 1–11, 2011.
- [11] G. Lamontagne, A. B. Kouki *et al.*, "Direct RF sampling GNSS receiver design and jitter analysis," 2012.
- [12] J. Thabet, R. Barrak, and A. Ghazel, "A new reconfigurable architecture for multistandard GNSS subsampling receiver," in *Fourth International Conference on Communications and Networking, ComNet-2014*. IEEE, 2014, pp. 1–5.
- [13] L. R. Carley and T. Mukherjee, "High-speed low-power integrating CMOS sample-and-hold amplifier architecture," in *Custom Integrated Circuits Conference, 1995., Proceedings of the IEEE 1995*. IEEE, 1995, pp. 543–546.
- [14] G. Xu, "Charge Sampling Circuits and A/D Converters-Theory and Experiments," 2004.
- [15] G. Xu and J. Yuan, "Comparison of charge sampling and voltage sampling," in *Circuits and Systems, 2000. Proceedings of the 43rd IEEE Midwest Symposium on*, vol. 1. IEEE, 2000, pp. 440–443.
- [16] G. Zhou and X.-G. Xia, "Multiple frequency detection in undersampled complex-valued waveforms with close multiple frequencies," *Electronics letters*, vol. 33, no. 15, pp. 1294–1294, 1997.
- [17] S. Haykin, "Cognitive radio: brain-empowered wireless communications," *Selected Areas in Communications, IEEE Journal on*, vol. 23, no. 2, pp. 201–220, 2005.

- [18] A. Rosie, "Principles of communications, systems, modulation and noise. re ziemer and wh tranter, houghton mimin, usa, 1985, 0-395-35724-1," *International Journal of Adaptive Control and Signal Processing*, vol. 1, no. 1, pp. 92–92, 1987.
- [19] E. Re, "Bandpass signal filtering and reconstruction through minimum-sampling-rate digital processing," *Alta Frequenza*, vol. 47, no. 9, pp. 675–678, 1978.
- [20] R. G. Lyons, *Understanding digital signal processing*. Pearson Education, 2010.
- [21] K. S. Shanmugam, "Digital and analogue communication," *John Wily Sons Inc, Canada*, 1979.
- [22] P. F. Panter, *Modulation, noise, and spectral analysis: applied to information tranmission*. McGraw-Hill Companies, 1965.
- [23] R. C. Webb, "IF signal sampling improves receiver detection accuracy," *Microwave and RF*, vol. 28, no. 3, p. 99, 1989.
- [24] C. B. Feldman and W. R. Bennett, "Band width and transmission performance," *Bell System Technical Journal, The*, vol. 28, no. 3, pp. 490–595, 1949.
- [25] F. G. Stremler, "Introduction to communication systems," *Introduction to Communication Systems, Ferrel G. Stremler, 3rd edition, Addison-Wesley*, 1990.
- [26] B. Xenakis and A. Evans, "Vehicle locator uses spread-spectrum technology," *RF Design*, vol. 15, pp. 58–58, 1992.
- [27] F. Marvasti, "Nonuniform Sampling: Theory and Practice. Information Technology," 2000.
- [28] J. G. Proakis and D. G. Manolakis, "Digital signal processing 3rd edition," 1996.

- [29] Y.-R. Sun and S. Signell, "Effects of noise and jitter in bandpass sampling," *Analog Integrated Circuits and Signal Processing*, vol. 42, no. 1, pp. 85–97, 2005.
- [30] A. J. Jerri, "The Shannon sampling theorem-Its various extensions and applications: A tutorial review," *Proceedings of the IEEE*, vol. 65, no. 11, pp. 1565–1596, 1977.
- [31] J. Mitola, "The software radio architecture," *Communications Magazine, IEEE*, vol. 33, no. 5, pp. 26–38, 1995.
- [32] D. M. Akos, M. Stockmaster, J. B. Tsui, and J. Caschera, "Direct bandpass sampling of multiple distinct RF signals," *Communications, IEEE Transactions on*, vol. 47, no. 7, pp. 983–988, 1999.
- [33] Y.-P. Lin, Y.-D. Liu, and S.-M. Phoong, "A new iterative algorithm for finding the minimum sampling frequency of multiband signals," *Signal Processing, IEEE Transactions on*, vol. 58, no. 10, pp. 5446–5450, 2010.
- [34] C. E. Shannon, "Communication in the presence of noise," *Proceedings of the IRE*, vol. 37, no. 1, pp. 10–21, 1949.
- [35] H. S. Shapiro and R. A. Silverman, "Alias-free sampling of random noise," *Journal of the Society for Industrial and Applied Mathematics*, vol. 8, no. 2, pp. 225–248, 1960.
- [36] H. Landau, "Necessary density conditions for sampling and interpolation of certain entire functions," *Acta Mathematica*, vol. 117, no. 1, pp. 37–52, 1967.
- [37] F. Beutler, "Alias-free randomly timed sampling of stochastic processes," *IEEE Transactions on Information Theory*, vol. 16, no. 2, pp. 147–152, 1970.
- [38] E. Masry, "Random sampling and reconstruction of spectra," *Information and Control*, vol. 19, no. 4, pp. 275–288, 1971.
- [39] E. Masrey, "Alias-free sampling: An alternative conceptualization and its applications," *IEEE Transactions on Information Theory*, vol. 24, no. 3, pp. 317–324, 1978.

- [40] E. Margolis and Y. C. Eldar, "Nonuniform sampling of periodic bandlimited signals," *IEEE Transactions on Signal Processing*, vol. 56, no. 7, pp. 2728–2745, 2008.
- [41] R. Kumaresan and N. Panchal, "Encoding bandpass signals using zero/level crossings: A model-based approach," *IEEE transactions on audio, speech, and language processing*, vol. 18, no. 1, pp. 17–33, 2010.
- [42] S. Chandrasekhar and T. V. Sreenivas, "Instantaneous frequency estimation using level-crossing information," in *Acoustics, Speech, and Signal Processing, 2003. Proceedings.(ICASSP'03). 2003 IEEE International Conference on*, vol. 6. IEEE, 2003, pp. VI–141.
- [43] M. Malmirchegini and F. Marvasti, "Performance improvement of level-crossing A/D converters," in *Telecommunications and Malaysia International Conference on Communications, 2007. ICT-MICC 2007. IEEE International Conference on*. IEEE, 2007, pp. 438–441.
- [44] H. Sedarat and D. G. Nishimura, "On the optimality of the gridding reconstruction algorithm," *IEEE Transactions on Medical Imaging*, vol. 19, no. 4, pp. 306–317, 2000.
- [45] H. Zhao, Q.-W. Ran, L.-Y. Tan, and J. Ma, "Reconstruction of bandlimited signals in linear canonical transform domain from finite nonuniformly spaced samples," *IEEE Signal Processing Letters*, vol. 16, no. 12, pp. 1047–1050, 2009.
- [46] N. Sharma and T. V. Sreenivas, "Sparse signal reconstruction based on signal dependent non-uniform samples," in *Acoustics, Speech and Signal Processing (ICASSP), 2012 IEEE International Conference on*. IEEE, 2012, pp. 3453–3456.
- [47] D. Mart, "A computational investigation into the human representation and processing of visual information," *Free-man, San Francisco, CA*, 1982.



- [48] P. T. Boufounos and R. G. Baraniuk, "Reconstructing sparse signals from their zero crossings," in *Acoustics, Speech and Signal Processing, 2008. ICASSP 2008. IEEE International Conference on*. IEEE, 2008, pp. 3361–3364.
- [49] H. S. Black, *Modulation theory*. van Nostrand, 1953.
- [50] H. Nyquist, "Certain topics in telegraph transmission theory," *Transactions of the American Institute of Electrical Engineers*, vol. 47, no. 2, pp. 617–644, 1928.
- [51] D. Gabor, "Theory of communication. Part 1: The analysis of information," *Journal of the Institution of Electrical Engineers-Part III: Radio and Communication Engineering*, vol. 93, no. 26, pp. 429–441, 1946.
- [52] A. Kohlenberg, "Exact interpolation of band-limited functions," *Journal of Applied Physics*, vol. 24, no. 12, pp. 1432–1436, 1953.
- [53] D. Middleton, I. of Electrical, and E. Engineers, *An introduction to statistical communication theory*. IEEE press Piscataway, NJ, 1996.
- [54] O. Grace and S. Piti, "Quadrature sampling of high-frequency waveforms," *The Journal of the Acoustical Society of America*, vol. 44, no. 5, pp. 1453–1454, 1968.
- [55] R. G. Vaughan, N. L. Scott, and D. White, "The theory of bandpass sampling," *Signal Processing, IEEE Transactions on*, vol. 39, no. 9, pp. 1973–1984, 1991.
- [56] P. Z. Peebles Jr, "Digital communication systems," *Englewood Cliffs, NJ, Prentice-Hall, Inc., 1987, 445 p.*, 1987.
- [57] J. Liu, X. Zhou, and Y. Peng, "Spectral arrangement and other topics in first-order bandpass sampling theory," *IEEE Transactions on Signal Processing*, vol. 49, no. 6, pp. 1260–1263, 2001.

- [58] J. D. Gaskill, “Linear systems, fourier transforms, and optics,” *Linear Systems, Fourier Transforms, and Optics by Jack D. Gaskill New York, NY: John Wiley and Sons, 1978*, 1978.
- [59] N. Wong and T.-S. Ng, “An efficient algorithm for downconverting multiple bandpass signals using bandpass sampling,” in *Communications, 2001. ICC 2001. IEEE International Conference on*, vol. 3. IEEE, 2001, pp. 910–914.
- [60] C.-H. Tseng and S.-C. Chou, “Direct downconversion of multiple RF signals using bandpass sampling,” in *Communications, 2003. ICC’03. IEEE International Conference on*, vol. 3. IEEE, 2003.
- [61] C. Miheung, “Bandpass sampling algorithm with normal and inverse placements for multiple RF signals,” *IEICE transactions on communications*, vol. 88, no. 2, pp. 754–757, 2005.
- [62] S. Yu and X. Wang, “Bandpass sampling of one RF signal over multiple RF signals with contiguous spectrums,” *Signal Processing Letters, IEEE*, vol. 16, no. 1, pp. 14–17, 2009.
- [63] A. Mahajan, M. Agarwal, and A. K. Chaturvedi, “A novel method for downconversion of multiple bandpass signals,” *IEEE transactions on wireless communications*, vol. 5, no. 2, pp. 427–434, 2006.
- [64] S. Sen and V. M. Gadre, “An algorithm for minimum bandpass sampling frequency for multiple RF signals in SDR systems,” in *Statistical Signal Processing, 2005 IEEE/SP 13th Workshop on*. IEEE, 2005, pp. 327–332.
- [65] J.-M. Muñoz-Ferreras, R. Gomez-Garcia, and F. Perez-Martinez, “RF front-end concept and implementation for direct sampling of multiband signals,” *IEEE Transactions on Circuits and Systems II: Express Briefs*, vol. 58, no. 3, pp. 129–133, 2011.
- [66] J.-M. Muñoz-Ferreras, R. Gómez-García, and F. Pérez-Martínez, “Acquisition of multiband signals with minimum sub-nyquist sampling,” in *Circuits*

- and Systems (ISCAS), 2012 IEEE International Symposium on.* IEEE, 2012, pp. 830–833.
- [67] Y. Haijiang Wang, B. Deng, L. Dong, Z. Yang, D. Yao, and Su, “A multiband RF signal sampling frequency selection method based on cylindrical surface spectrum analysis,” pp. 1–9, 2016.
- [68] E. Saatci and E. Saatci, “Determination of the minimum sampling frequency in bandpass sampling by geometric approach and geometric programming,” *Signal, Image and Video Processing*, pp. 1–9, 2018.
- [69] R. Boute, “The geometry of bandpass sampling: A simple and safe approach [lecture notes],” *IEEE Signal Processing Magazine*, vol. 29, no. 4, pp. 90–96, 2012.
- [70] R. B. Staszewski, K. Muhammad, D. Leipold, C.-M. Hung, Y.-C. Ho, J. L. Wallberg, C. Fernando, K. Maggio, R. Staszewski, T. Jung *et al.*, “All-digital TX frequency synthesizer and discrete-time receiver for Bluetooth radio in 130-nm CMOS,” *IEEE Journal of Solid-State Circuits*, vol. 39, no. 12, pp. 2278–2291, 2004.
- [71] A. G. Dempster, “Quadrature bandpass sampling rules for single-and multi-band communications and satellite navigation receivers,” *IEEE Transactions on Aerospace and Electronic Systems*, vol. 47, no. 4, pp. 2308–2316, 2011.
- [72] M. Mishali and Y. C. Eldar, “From theory to practice: Sub-Nyquist sampling of sparse wideband analog signals,” *IEEE Journal of selected topics in signal processing*, vol. 4, no. 2, pp. 375–391, 2010.
- [73] B. Razavi, *RF microelectronics*. Prentice Hall New Jersey, 1998, vol. 1.
- [74] H. Darabi and A. A. Abidi, “A 4.5-mw 900-mhz CMOS receiver for wireless paging,” *IEEE Journal of Solid-State Circuits*, vol. 35, no. 8, pp. 1085–1096, 2000.

- [75] B. Razavi, “Design considerations for direct-conversion receivers,” *IEEE Transactions on Circuits and Systems II: Analog and Digital Signal Processing*, vol. 44, no. 6, pp. 428–435, 1997.
- [76] M. L. Psiaki, D. M. Akos, and J. Thor, “A comparison of direct RF sampling and down-convert sampling GNSS receiver architectures,” in *Proceedings of the 16th International Technical Meeting of the Satellite Division of the Institute of Navigation*, 2001, pp. 1941–1952.
- [77] M. Frerking, *Digital signal processing in communications systems*. Springer Science & Business Media, 2013.
- [78] Y. Chiu, P. R. Gray, and B. Nikolic, “A 14-b 12-MS/s CMOS pipeline ADC with over 100-dB SFDR,” *IEEE Journal of Solid-State Circuits*, vol. 39, no. 12, pp. 2139–2151, 2004.
- [79] S. Bronckers, A. Roc’h, and B. Smolders, “Wireless Receiver Architectures Towards 5G: Where Are We?” *IEEE Circuits and Systems Magazine*, vol. 17, no. 3, pp. 6–16, 2017.
- [80] M. E. Domínguez-Jiménez, N. González-Prelcic, G. Vazquez-Vilar, and R. López-Valcarce, “Design of universal multicore sampling patterns for compressed sensing of multiband sparse signals,” in *2012 IEEE International Conference on Acoustics, Speech and Signal Processing (ICASSP)*. IEEE, 2012, pp. 3337–3340.
- [81] M. A. Messaoud, F. M. Ghannouchi, R. Barrak, and A. Ghazel, “SDR based multi-band subsampling receivers for GNSS applications,” in *Advanced Technologies for Signal and Image Processing (ATSIP), 2014 1st International Conference on*. IEEE, 2014, pp. 497–501.
- [82] A. M. Wyglinski, D. P. Orofino, M. N. Ettus, and T. W. Rondeau, “Revolutionizing software defined radio: Case studies in hardware, software, and education,” *IEEE Communications Magazine*, vol. 54, no. 1, pp. 68–75, 2016.

- [83] R. Barrak, A. Ghazel, and F. Ghannouchi, "Optimized multistandard RF subsampling receiver architecture," *Wireless Communications, IEEE Transactions on*, vol. 8, no. 6, pp. 2901–2909, 2009.
- [84] A. Willig, "Recent and emerging topics in wireless industrial communications: A selection," *Industrial Informatics, IEEE Transactions on*, vol. 4, no. 2, pp. 102–124, 2008.
- [85] R. J. Lackey and D. W. Upmal, "Speakeasy: the military software radio," *Communications Magazine, IEEE*, vol. 33, no. 5, pp. 56–61, 1995.
- [86] P. G. Cook and W. Bonser, "Architectural overview of the speakeasy system," *IEEE Journal on Selected areas in Communications*, vol. 17, no. 4, pp. 650–661, 1999.
- [87] T. Turetti, H. J. Bentzen, and D. Tennenhouse, "Toward the software realization of a GSM base station," *Selected Areas in Communications, IEEE Journal on*, vol. 17, no. 4, pp. 603–612, 1999.
- [88] K. C. Zangi and R. D. Koilpillai, "Software radio issues in cellular base stations," *Selected Areas in Communications, IEEE Journal on*, vol. 17, no. 4, pp. 561–573, 1999.
- [89] M. Patel and I. Darwazeh, "A software radio OFDM bandpass sampling receiver and the effects of aperture jitter on performance," 2003.
- [90] L. Lolis, "Agile bandpass sampling RF receivers for low power applications," Ph.D. dissertation, Université Sciences et Technologies-Bordeaux I, 2011.
- [91] N. Vun and A. Premkumar, "ADC systems for SDR digital front-end," in *Consumer Electronics, 2005.(ISCE 2005). Proceedings of the Ninth International Symposium on*. IEEE, 2005, pp. 359–363.
- [92] T. Fujii, Y. Kamiya, and Y. Suzuki, "Multi-band ad-hoc cognitive radio for reducing inter system interference," in *Personal, Indoor and Mobile Radio Communications, 2006 IEEE 17th International Symposium on*. IEEE, 2006, pp. 1–5.

- [93] I. F. Hernández, “Galileo Receiver Research in Europe,” in *GALILEO Positioning Technology*. Springer, 2015, pp. 249–271.
- [94] F. Palhinha, R. Pereira, D. Carona, A. Serrador, M. Véstias, J. Silva, T. Peres, and P. Silva, “RF Front End Receiver for GPS/Galileo L1/E1,” *Procedia Technology*, vol. 17, pp. 73–80, 2014.
- [95] R. Barrak, I. Labidi, A. Ghazel, M. Muller, and N. Samama, “RF subsampling GNSS receiver: Potential advantages and feasibility study,” in *Microelectronics (ICM), 2011 International Conference on*. IEEE, 2011, pp. 1–6.
- [96] D. Chen, W. Pan, P. Jiang, J. Jin, T. Mo, and J. Zhou, “Reconfigurable dual-channel multiband RF receiver for GPS/Galileo/BD-2 systems,” *Microwave Theory and Techniques, IEEE Transactions on*, vol. 60, no. 11, pp. 3491–3501, 2012.
- [97] X. Li, G. Dick, C. Lu, M. Ge, T. Nilsson, M. Fritsche, J. Wickert, and H. Schuh, “Multi-GNSS meteorology: Real-time retrieving of atmospheric parameters from GPS, GLONASS, BeiDou and Galileo observations,” 2015.
- [98] N. Bonnor, “A brief history of global navigation satellite systems,” *Journal of Navigation*, vol. 65, no. 01, pp. 1–14, 2012.
- [99] M. Rao, G. Falco, and E. Falletti, “SDR joint GPS/Galileo receiver from theory to practice,” *International Journal of Aerospace Sciences*, vol. 1, no. 1, pp. 1–7, 2012.
- [100] Z. Zhang, W. Li, W. Wen, W. Wu, and Y. Li, “A configurable multi-band gnss receiver for compass/gps/galileo applications,” in *Circuits and Systems (ISCAS), 2013 IEEE International Symposium on*. IEEE, 2013, pp. 161–164.
- [101] C. G. Tan, F. Song, T. Y. Choke, M. Kong, D.-C. Song, C.-H. Yong, W. Shu, Z. H. You, Y.-H. Lin, and O. Shanaa, “A universal GNSS (GPS/Galileo/-Glonass/Beidou) SoC with a 0.25 mm<sup>2</sup> radio in 40nm CMOS,” in *2013*

- IEEE International Solid-State Circuits Conference Digest of Technical Papers.* IEEE, 2013, pp. 334–335.
- [102] V. K. S. Bose and A. Chaturvedi, “A low-cost algorithm to find the minimum sampling frequency for multiple bandpass sampling,” *IEEE Signal Process. Lett.*, pp. 193–196, 2008.
- [103] W. Zhang and M. J. Miller, “Baseband equivalents in digital communication system simulation,” *IEEE Transactions on Education*, vol. 35, no. 4, pp. 376–382, 1992.
- [104] Z. H. Derafshi, J. Frounchi, and H. Taghipour, “A high speed fpga implementation of a 1024-point complex fft processor,” in *Second International Conference on Computer and Network Technology.* IEEE, 2010, pp. 312–315.
- [105] F. Behbahani, H. Firouzkouhi, R. Chokkalingam, S. Delshadpour, A. Kheirkhahi, M. Nariman, M. Conta, and S. Bhatia, “A fully integrated low-IF CMOS GPS radio with on-chip analog image rejection,” *IEEE journal of solid-state circuits*, vol. 37, no. 12, pp. 1721–1727, 2002.
- [106] G. Gramegna, P. G. Mattos, M. Losi, S. Das, M. Franciotta, N. G. Bellantone, M. Vaiana, V. Mandará, and M. Paparo, “A 56-mW 23-mm/sup 2/single-chip 180-nm CMOS GPS receiver with 27.2-mW 4.1-mm/sup 2/radio,” *IEEE Journal of Solid-State Circuits*, vol. 41, no. 3, pp. 540–551, 2006.
- [107] A. Brown and B. Wolt, “Digital L-band receiver architecture with direct RF sampling,” in *Position Location and Navigation Symposium, 1994., IEEE.* IEEE, 1994, pp. 209–216.
- [108] G. Lennen and H. Falk, “Architecture for power consumption reduction in GNSS receivers,” May 22 2018, US Patent 9,977,132.
- [109] T. Kadoyama, N. Suzuki, N. Sasho, H. Iizuka, I. Nagase, H. Usukubo, and M. Katakura, “A complete single-chip GPS receiver with 1.6-V 24-mW radio

- in 0.18- $\mu\text{m}$  CMOS,” *IEEE Journal of Solid-State Circuits*, vol. 39, no. 4, pp. 562–568, 2004.
- [110] D. Sahu, A. Das, Y. Darwhekar, S. Ganesan, G. Rajendran, R. Kumar, B. Chandrashekar, A. Ghosh, A. Gaurav, T. Krishnaswamy *et al.*, “A 90nm CMOS single-chip GPS receiver with 5dBm out-of-band IIP3 2.0 dB NF,” in *Solid-State Circuits Conference, 2005. Digest of Technical Papers. ISSCC. 2005 IEEE International*. IEEE, 2005, pp. 308–600.
- [111] J. Ko, J. Kim, S. Cho, and K. Lee, “A 19-mW 2.6-mm<sup>2</sup>/L1/L2 dual-band CMOS GPS receiver,” *IEEE Journal of Solid-State Circuits*, vol. 40, no. 7, pp. 1414–1425, 2005.
- [112] D. M. Akos and J. B. Tsui, “Design and implementation of a direct digitization GPS receiver front end,” *IEEE Transactions on Microwave Theory and Techniques*, vol. 44, no. 12, pp. 2334–2339, 1996.
- [113] P. B. Kenington and L. Astier, “Power consumption of A/D converters for software radio applications,” *IEEE Transactions on Vehicular Technology*, vol. 49, no. 2, pp. 643–650, 2000.
- [114] D. Chen, W. Pan, P. Jiang, J. Jin, J. Wu, J. Tan, C. Lu, and J. Zhou, “Reconfigurable dual-channel tri-mode all-band RF receiver for next generation GNSS,” in *Solid State Circuits Conference (A-SSCC), 2010 IEEE Asian*. IEEE, 2010, pp. 1–4.
- [115] N. Qi, Y. Xu, B. Chi, X. Yu, X. Zhang, N. Xu, P. Chiang, W. Rhee, and Z. Wang, “A dual-channel compass/GPS/GLONASS/Galileo reconfigurable gnss receiver in 65 nm CMOS with on-chip I/Q calibration,” *IEEE Transactions on Circuits and Systems I: Regular Papers*, vol. 59, no. 8, pp. 1720–1732, 2012.
- [116] G. Wistuba, A. Vasylyev, S. Haas, J. Driesen, L. Dallüge, D. Peitscher, B. Kramer, C. Dohmen, and F. Henkel, “A highly integrated configurable GNSS receiver frontend design for high bandwidth operation on E1/L1 and



- E5a/L5,” in *2011 International Conference on Localization and GNSS (ICL-GNSS)*. IEEE, 2011, pp. 164–168.
- [117] S. S. Haykin, *Digital communications*. Wiley New York, 1988.
- [118] J. Bae and J. Park, “A searching algorithm for minimum bandpass sampling frequency in simultaneous down-conversion of multiple RF signals,” *Journal of Communications and Networks*, vol. 10, no. 1, pp. 55–62, 2008.
- [119] F. Nocedal, “Intermodulation in amplitude companded sideband systems.” *Dissertation Abstracts International Part B: Science and Engineering*, vol. 43, no. 8, 1983.
- [120] M. Valkama, L. Anttila, M. Renfors *et al.*, “Advanced digital signal processing techniques for compensation of nonlinear distortion in wideband multi-carrier radio receivers,” *IEEE Transactions on Microwave Theory and Techniques*, vol. 54, no. 6, pp. 2356–2366, 2006.
- [121] T. P. Weldon, “Methods and apparatus for substantially reducing third order intermodulation distortion and other nonlinear distortions,” Jun. 14 2005, US Patent 6,906,585.
- [122] W. Kester, “High speed sampling and high speed ADC,” *High speed design techniques*, Analog Devices Inc, 1996.